CALCITE DISSOLUTION KINETICS AND SOLUBILITY IN Na-Ca-Mg-Cl BRINES OF GEOLOGICALLY RELEVANT COMPOSITION AT 0.1 TO 1 BAR pCO_2 AND 25 TO 80 °C

A Dissertation

by

DWIGHT KUEHL GLEDHILL

Submitted to the Office of Graduate Studies of
Texas A&M University
in partial fulfillment of the requirements for the degree of

DOCTOR OF PHILOSOPHY

May 2005

Major Subject: Oceanography

CALCITE DISSOLUTION KINETICS AND SOLUBILITY IN Na-Ca-Mg-Cl BRINES OF GEOLOGICALLY RELEVANT COMPOSITION AT 0.1 TO 1 BAR pCO_2 AND 25 TO 80 °C

A Dissertation

by

DWIGHT KUEHL GLEDHILL

Submitted to Texas A&M University
in partial fulfillment of the requirements
for the degree of

DOCTOR OF PHILOSOPHY

Approved as to style and content by:

John W. Morse (Chair of Committee)	Niall Slowey (Member)
Ethan Grossman (Member)	Hongbin Zhan (Member)
Wilford Gardner (Head of Department)	

May 2005

Major Subject: Oceanography

ABSTRACT

Calcite Dissolution Kinetics and Solubility in Na-Ca-Mg-Cl Brines of Geologically Relevant Composition at 0.1 to 1 Bar pCO_2 and 25 to 80 °C. (May 2005)

Dwight Kuehl Gledhill, B.S., Eastern Connecticut State University;

M.S., Texas A&M University

Chair of Advisory Committee: Dr. John W. Morse

Sedimentary basins can contain close to 20% by volume pore fluids that are commonly classified as brines. These fluids can become undersaturated with respect to calcite as a result of processes such as migration, dispersive mixing, or anthropogenic injection of CO_2. This study measured calcite solubility and dissolution rates in geologically relevant Na-Ca-Mg-Cl synthetic brines (35 to 200 g L^{-1} TDS).

In brines < 50 g L^{-1} TDS, the EQPITZER calculated calcium carbonate ion activity product (IAP) at steady-state was in reasonable agreement (±10%) with the thermodynamic solubility constant for calcite (K_c). However, the IAP systematically exceeded K_c in more concentrated brines. The deviation was strongly correlated with calcium concentration and also was observed in magnesium-free solutions. This is interpreted as an uncertainty in the carbonate ion activity coefficient, and minor adjustment in stoichiometric association constants ($K^*_{M^{2+}CO_3^0}$) for the $CaCO_3^0$ or $MgCO_3^0$ ion pairs would correct for the error.

The dissolution rate dependency on brine composition, pCO_2 (0.1 to 1 bar), and temperature (25.0 to 82.5 °C) was modeled using the empirical rate equation

$$R = k(1-\Omega)^n$$

where R is the rate, k and n are empirical fitting terms, and Ω the degree of disequilibrium with respect to calcite. When Ω was defined relative to an apparent kinetic solubility, n could be assumed first-order over the range of Ω investigated (Ω = 0.2 to 1.0). Rates increased with increasing pCO_2 as did the sensitivity to brine concentration. At 0.1 bar, rates were nearly independent of concentration (k = 13.0 ±2.0 x 10^{-3} moles m^{-1} hr^{-1}). However, at higher CO_2 partial pressures rates became composition dependent and the rate constant, k, was shown to be a function of temperature, pCO_2, ionic strength, and calcium and magnesium activity. The rate constant (k) can be estimated from a multiple regression (MR) model of the form

$$k = \beta_0 + \beta_1(T) + \beta_2(pCO_2) + \beta_3(I) + \beta_4(a_{Ca^{2+}}) + \beta_5(a_{Mg^{2+}}).$$

A relatively high activation energy (E_a = 20 kJ mol^{-1}) was measured, along with a stirring rate independence suggesting the dissolution is dominated by surface controlled processes at saturation states $\Omega > 0.2$ in these calcium-rich brines. These findings offer important implications to reaction-transport models in carbonate-bearing saline reservoirs.

DEDICATION

This thesis is dedicated to my son, Avery Robert Gledhill, who has reminded me that perhaps there is hope for humanity after all, and that where there is wonder there is joy. He has redefined my life in accordance with what is truly important. Also, to my loving wife who has offered me unconditional patience, support, and the gift of my child. May I someday be able to repay her with the assurance of a better tomorrow.

ACKNOWLEDGMENTS

I would like to offer my sincere gratitude to Dr. John W. Morse for his generosity and extensive patience as well as my committee members for their careful insight: Dr. Ethan Grossman, Dr. Niall Slowey and Dr. Hongbin Zhan. I'd like to offer a special thanks to Dr. Rolf Ardvidson of Rice University who has been invaluable, providing practical aid in terms of the BET measurements as well as a profound source of both theoretical and philosophical guidance. Dr. Jay Pickney has been a vital source in the application of statistics. A great deal of assistance has been offered by the Texas A&M Department of Oceanography technical support staff, Eddie Webb and Rick O'Neill as well as the fine glass-blowing abilities of Bill Merka in the Department of Chemistry. This research was supported by the U.S. Department of Energy Grant DE-FG03-00ER-15033. In addition, thanks to the following: all of OGC with special regards to Andrew Hebert, JoJo Krako, Stealing Jin, Cerebus and 4.5 billion years of evolution.

TABLE OF CONTENTS

CHAPTER Page

LIST OF FIGURES

FIGURE Page

LIST OF TABLES

CHAPTER I

INTRODUCTION

1.1. General Considerations

Carbonate minerals constitute ~20% of Phanerozoic sedimentary rock, and at least 60% of the world's know petroleum reserves occur in carbonate reservoirs (Morse and Mackenzie, 1990). Because calcite is a reactive common mineral, its precipitation and dissolution are of great importance in the creation and destruction of secondary porosity in the subsurface.

Although the importance of carbonate mineral dissolution during sediment diagenesis has been known since at least the late 1800's (e.g., Murray and Renard, 1891), experimental determination of dissolution rates as a function of solution composition did not receive considerable attention until the 1960's (e.g., Weyl, 1958, 1967; Terjesen et al., 1961; Akin and Lagerwerff, 1965; Berner, 1967; Schmalz, 1967). Since that time, a large number of investigations have examined the influences of "foreign" ions, temperature, CO_2 partial pressure and other variables on calcite dissolution rates (see reviews of Plummer et al., 1979; Sjöberg and Rickard, 1985; Morse, 1983; Morse and Arvidson, 2002). Previous investigations sought to understand the behavior of calcite in solutions with ionic strengths that did not generally exceed that of seawater. Calcite reaction kinetics in concentrated solutions, typical of the

---

This dissertation follows the style and format of *Geochimica et Cosmochimica Acta*.

subsurface, have received relatively little attention. Although recent observations include precipitation rates in
high salinity waters (Zhang and Dawe, 1998), there are apparently no studies that have directly addressed dissolution kinetics in complex high ionic strength solutions.

Modeling carbonate mineral dissolution as a function of saturation state requires accurate calculations of the distribution of carbonic acid system species. However, accurate determination of the activities of these species in high ionic strength solutions continues to be problematic. Investigations of the solubility of calcite coupled with the Pitzer parameterizations of the carbonic acid system in synthetic brines (He and Morse, 1993) have made such calculations more reliable.

1.2. Historical Perspective

Previous investigations into the specific effects of calcium and magnesium on calcite kinetics have been conducted at many different saturation states and solution compositions using differing techniques. Consequently, the results are often contradictory and not readily comparable. Weyl (1967) and Berner (1967) noted that the presence of Mg^{2+} resulted in a marked inhibitory effect on calcite dissolution rates at neutral to basic pH, while Alkattan et al. (2002) found no Mg^{2+} inhibition at pH 1 and pH 3. Gutjahr et al. (1996b) also found no significant Mg^{2+} effect on the dissolution rate under neutral to basic conditions over a broad range of saturation states including near equilibrium. Sjöberg and Rickard (1985) found no effect of Ca^{2+} in acidic solutions whereas in neutral to basic solutions Ca^{2+} was found to decrease the rate of the transport reaction making the dissolution more transport-controlled. Buhmann and Dreybrodt

(1987) found that although the presence of Ca^{2+} and Mg^{2+} displace the calcite solution equilibria, the kinetics of the dissolution were hardly changed. Calcite dissolution experiments in these compositionally simple and generally dilute solutions were conducted under low pCO_2 and thus provide important insight into the kinetics from a "pure chemistry" standpoint but are of limited utility for subsurface waters where solutions are substantially more concentrated and high pCO_2 usually prevails (Coudrain-Ribstein et al., 1998).

1.3. Rate Equations Describing Calcite Dissolution

The dissolution of calcite in the case of surface reaction-controlled kinetics (e.g., relatively near equilibrium where transport processes are not dominating) has been described by empirical (Morse and Berner, 1972; Sjöberg, 1978) or semi-empirical rate equations (Plummer et al., 1978) and by more mechanistic models based on surface speciation (Van Cappellen et al., 1993; Arakaki and Mucci, 1995). In each case the models rely on the "principle of detailed balancing" (Lasaga, 1998, pp. 82-93). When a solid dissolves in a solution, the rate of the observed change in solution composition is a "net" rate that reflects both the forward (dissolution) and the back (precipitation) reaction rates.

When the observed rate is zero, it does not imply that no dissolution or precipitation is occurring. Instead, this kinetic equilibrium occurs when both the opposing rates are equal, provided that the following elementary reaction determines the rate of dissolution or precipitation:

$$CaCO_3 \underset{k_b}{\overset{k_f}{\rightleftharpoons}} Ca^{2+} + CO_3^{2-} \qquad (1\text{–}1)$$

where k_f and k_b are the forward and backward rate constants, the overall rate, R, is given by the sum of the forward (R_f) and backward (R_b) reaction rates:

$$R = R_f - R_b = k_f - k_b a_{Ca^{2+}} a_{CO_3^{2-}} \qquad (1\text{–}2)$$

where a_i are the activities of the calcium and carbonate ions in solution. If the reaction is reversible then the ratio k_f/k_b should be equivalent to the solubility product for calcite (K_c). The unidirectional rate (R) is generally dominant except very close to equilibrium where R_f and R_b are similar (Morse and Arvidson, 2002).

1.3.1. Empirical Models

The most commonly applied empirical model that describes the rate of calcite dissolution is the general rate equation (e.g., Morse and Berner, 1972):

$$R = -\frac{dm_{calcite}}{dt} = \left(\frac{A}{V}\right) k(1-\Omega)^n \qquad (1\text{–}3)$$

where t is time, A is the surface area of the solid, V is the volume of solution (or mass of solvent in cases where molal units are used), k is the rate constant and n is the "order" of the reaction. The saturation state (Ω) is the ratio of the ion activity product of calcium and carbonate (IAP) to K_c and the term ($1-\Omega$) describes the degree of disequilibrium. The rate equation describes the rate increase as the degree of disequilibrium increases. The relative linearity of the relation between the degree of disequilibrium and rate is described by the reaction "order" where a value of 1 denotes perfect linearity. With increasing values of n the function develops a hysteresis where the rate increases

exponentially far from equilibrium. In complex solutions, such as seawater, the value of *n* has typically been observed to be ~3. In these instances, it implies that equation 1–3 is an oversimplification and other elementary reactions become important. A similar, although not simply related, empirical model is given by Sjöberg (1978):

$$R = -\frac{dm_{calcite}}{dt} = \left(\frac{A}{V}\right) K_{sp}^{n} \left(1 - \Omega^{n}\right) \qquad (1\text{–}4)$$

where *n* was found to be 1/2 for calcite in a pure ionic media (also see Lasaga, 1998).

Plummer et al. (1979) described the dissolution by three simultaneous mechanisms:

$$CaCO_3 + H^+ \underset{k_b}{\overset{k_f}{\rightleftharpoons}} Ca^{2+} + HCO_3^- \qquad (1\text{–}5)$$

$$CaCO_3 + H_2CO_3^0 \underset{k_b}{\overset{k_f}{\rightleftharpoons}} Ca^{2+} + 2\,HCO_3^- \qquad (1\text{–}6)$$

$$CaCO_3 + H_2O \underset{k_b}{\overset{k_f}{\rightleftharpoons}} Ca^{2+} + HCO_3^- + OH^- \qquad (1\text{–}7)$$

in which the net rate of dissolution was given by the semi-empirical equation:

$$R = -\frac{dm_{calcite}}{dt} = k_1 a_{H^+} + k_2 a_{H_2CO_3^{0*}} + k_3 a_{H_2O} - k_4 a_{Ca^{2+}} a_{HCO_3^-} \qquad (1\text{–}8)$$

where k_1, k_2, and k_3 are the forward rate constants and k_4 is the back rate constant that is pCO_2 dependent.

1.3.2. Mechanistic Models

A more sophisticated mechanistic model, based on surface complexation theory, has recently been offered by Van Cappellen et al. (1993). It postulates the formation of the hydration species $>CO_3H^0$ and $>CaOH^0$ (where > denotes a surface bond) at the calcite surface that govern the reactivity of the carbonate-water interface. The model proposes the following surface species:

$$> CO_3H^0 \Leftrightarrow > CO_3^- + H^+ \quad (1\text{–}9)$$

$$> CO_3H^0 + Ca^{2+} \Leftrightarrow > CO_3Ca^+ + H^+ \quad (1\text{–}10)$$

$$> CaOH_2^+ \Leftrightarrow > CaOH^0 + H^+ \quad (1\text{–}11)$$

$$> CaOH^0 \Leftrightarrow > CaO^- + H^+ \quad (1\text{–}12)$$

$$> CaOH^0 + CO_2 \Leftrightarrow > CaHCO_3^0 \quad (1\text{–}13)$$

$$> CaOH^0 + CO_2 \Leftrightarrow > CaCO_3^- + H^+ \quad (1\text{–}14)$$

Arakaki and Mucci (1995) combined the semi-empirical model of Plummer et al. (1979) with the surface complexation model of Van Cappellen et al. (1993) to describe the dissolution of calcite in deionized water. This yielded an overall reaction rate given by:

$$R = -\frac{dm_{calcite}}{dt} = k_1(> CO_3^-)(a_{H^+})^2 + (k_2 - k_5)(> Ca^{2+})a_{H_2CO_3^{0*}} + k_4 - (k_6 - k_3)(> CO_3H^0)a_{CaHCO_3^+} - k_7(> Ca^+)a_{H_2CO_3^*}a_{CaCO_3^0} - k_8 a_{CaCO_3^0} \quad (1\text{–}15)$$

Although these mechanistic models are perhaps intriguing, they are largely hypothetical resting on unverified correlations rather than direct observations of surface species and mechanisms. They require the use intrinsic stability constants for the surface

complexation reactions that are not currently available in complex solutions causing them to have no predictive utility to natural waters.

1.4. EQPITZER Software

In this dissertation common use will be made of the EQPITZER software developed by He and Morse (1993). Using experimentally determined interaction parameters between the carbonic acid species ($CO_{2(aq)}$, HCO_3^-, and CO_3^{2-}) and the major ions Na^+, K^+, Ca^{2+}, Mg^{2+}, Cl^-, and SO_4^{2-}, the EQPITZER software makes calculations based on the Pitzer equation for electrolytes (Pitzer, 1973; Pitzer and Mayorga, 1973; Pitzer and Mayorga, 1974). This allows the determination of activity coefficients, not only for the major ion species, but also for the carbonic acid system in complex electrolyte solutions. The software incorporates into the model experimentally determined stoichiometric Henry's law constants (K_H^*) and dissociation constants (K_1^* and K_2^*) for the carbonic acid system appropriate to a wide range of high ionic strength solutions. It also includes the thermodynamic association constants of Reardon and Langmuir (1974) for the important ion pairs $CaCO_3^0$, $MgCO_3^0$, and $MgOH^+$. The program has been applied in this dissertation to provide a *complete* description of the carbonic acid system (at constant temperature and pressure) using at least two fundamental CO_2 system parameters (alkalinity, total inorganic carbon, pCO_2 and pH) and a solutions major ion composition. Typically, in this study total alkalinity (TA) and total inorganic carbon (TCO_2) will be coupled to calculate solution pH and pCO_2.

1.5. Saline Fluids in the Subsurface

Most sedimentary rocks are comprised of ~20% pore water that ranges in salinity by approximately five orders of magnitude (Hanor, 1994a), from dilute meteoric waters, to waters with greater than 600 g L^{-1} of dissolved salts (Case, 1945). The geochemistry of these waters imparts a significant influence on processes affecting the development of secondary porosity, reservoir permeability and mass transport in the subsurface. There has been considerable recent interest in the geochemistry of formation waters as reservoirs are being developed as possible repositories for waste gases and fluids. The mineral-brine-waste interactions in these repositories are of considerable interest with regards to reservoir management. Presented in the following discussion is a brief description of the general distribution and diagenetic origin of the major elements that comprise subsurface waters. Much of this discussion is based on review papers by Hanor (1994a) and Kharaka and Hanor (2004).

1.5.1. Nomenclature

In this dissertation I have adopted the terminology of Kharaka and Hanor (2004) when describing subsurface waters. This will include the use of *salinity* being synonymous with *total dissolved solids* (TDS), generally reported in milligrams per liter (mg L^{-1}) or grams per liter (g L^{-1}). Notice, however, that although this is a prevalent unit used by the petroleum industry, TDS is a mass-volume convention that makes it less than ideal for rigorous chemical treatment. Many of the "field" measurements are reported in TDS without any consideration for the considerable volume change that must have transpired as a result of the temperature-pressure differential between the

subsurface and the surface. In using liters, I recognize that there is a growing trend for usage of dm^3 for volume, however, virtually all literature data are currently reported in L.

Formation water has no genetic or age significance but typically refers to the pore water present in a formation prior to anthropogenic alteration. These waters typically experience post-burial diagenetic alteration differentiating them from *connate water*. The term *brine* will refer to water containing a higher salinity than that of seawater (35 g L^{-1} TDS). The *type* of brine will be described using the classification scheme whereby the cations followed by the anions are listed in order of decreasing concentrations and charges are omitted (e.g., a Na-Ca-Mg-Cl brine).

1.5.2. Chemical Composition of Subsurface Waters

1.5.2.1. Major Cations

The most dominant cation in formation waters is typically sodium, constituting 70% to > 90% of the total cation mass. With increasing salinity however, its relative proportion decreases and the proportions of K, Mg and Ca increase. Calcium is typically the second most important cation and can even exceed Na on a mass basis when salinities exceed 300 g L^{-1} TDS. It is usually found in greater abundance than magnesium. This is an important distinction from seawater where magnesium exceeds calcium by 5:1, at least in modern oceans.

1.5.2.2. Major Anions

Chloride is by far the most dominant anion in subsurface brines (>35 g L^{-1}), comprising > 95% by mass of the anions. The principle source of chloride is seawater, which may have been concentrated by subaerial evaporation prior to burial, and additional chloride contributed by mineral dissolution (primarily halite). Bromide can also be present, though it is minor relative to chloride. Sulfate can be quite prominent in relatively dilute waters and occurs in seawater at concentrations of about 2.7 g L^{-1}. In contrast, most brines contain relatively minor amounts of sulfate rarely exceeding 1 g L^{-1}. In waters having salinities greater than 30 g L^{-1}, and where the system is calcium carbonate-buffered, the inorganic carbon species, HCO_3^- and CO_3^{2-}, are generally less than a few hundred milligrams per liter.

Reactive organic species dissolved in subsurface waters can play an important role in mineral diagenesis (for discussion and references see Kharaka and Hanor, 2004). They serve as proton donors, pH and Eh buffering agents, and can form complexes with metals. In subsurface waters < 80 °C the concentration of monocarboxylic acid anions are typically < 0.5 g L^{-1} with propionate exceeding acetate. At reservoir temperatures between 80 and 120 °C they can exceed 10 g L^{-1} and acetate typically exceeds propionate. At higher temperatures thermal decarboxylation is responsible for conversion of acid anions to CO_2. The data for the concentrations of dicarboxylic acid anions such as oxalate is much more limited. The range of reported vales is 0–2.6 g L^{-1}. The low solubility of calcium oxalate and calcium malonate along with their rapid rate of thermal decomposition probably limits their concentration.

1.5.3. Origin and Controls of Saline Fluid in the Subsurface

Spatial variability in salinity in formation waters can be accounted for by several physical processes related to transport. Diffusive transport and dispersive mixing of waters of varying composition can produce formation waters with a wide range in salinity. In addition, large-scale fluid advection has been found capable of transporting subsurface waters on the scale of hundreds of kilometers. Perhaps the only generally observed trend in salinity is that it often tends to increase with increasing basin depth where deep bedded salt or brines derived from subaerial evaporation of seawater are present. However, there are notable exceptions such as the south Louisiana Gulf Coast (Hanor, 1994a).

Superimposed on the transport related controls of formation water salinity, a first-order effect may be metastable thermodynamic buffering by mineral assemblages as suggested by Hanor (1994b). Hanor (1994b) found a simultaneous and systematic variation in dissolved Na, K, Mg, Ca and alkalinity with chloride consistent with buffering by silicate-carbonate mineral assemblages in southwest Louisiana Gulf Coast reservoirs. In general a 1:1 covariance in monovalent cation concentration was observed on log-log plots while a 2:1 covariance was observed for divalent cations. Probably the most important water-rock reaction controlling cation concentrations is the dissolution of halite, which is responsible for the increased sodium in basins where evaporites are present. In addition, dissolution and precipitation of carbonate minerals impart a strong control on the concentration of the divalent cations calcium and magnesium. The generally lower magnesium concentrations relative to that of evaporated seawater can

result from diagenetic processes such as dolomitization and the formation of chlorite. Also, calcium can be contributed from $CaSO_4$ associated with evaporites. Generally most associated sulfate is lost to bacterial reduction.

1.6. Objectives of This Investigation

This research aims to investigate the rates of calcite dissolution reactions in carbon-dioxide-rich brines. In this study the solubility and dissolution kinetics of calcite have been determined in saline waters with a range in solution compositions approximating those in typical subsurface formation waters composed of Na-Ca-Mg-Cl brines. Results have important applications to predictive chemical process models in carbonate cemented reservoirs and for carbon sequestration strategies.

Because of the natural variability in subsurface waters with regards to composition, temperature and pCO_2, it would be impractical to perform experiments for all the possible permutations. Therefore, this study has centered around three primary objectives: (1) examine the solubility and change in reaction kinetics as a function of increasing brine concentration. In this instance, with increasing salinity the chemistry of the brines are modified such that they exhibit a covariance of Ca^{2+}, Mg^{2+}, and ionic strength as predicted in "real" subsurface brines. (2) Determine the independent effects of composition (Ca^{2+}, Mg^{2+} and ionic strength), temperature (25–82 ºC), and pCO_2 (0.1–1.0 bar) on the dissolution kinetics. (3) Examine the potential impact of a natural inhibitor commonly present in natural waters; SO_4^{2-}.

The results of these experiments have then been used to provide a purely empirical statistical model that describes the kinetics using the general rate equation.

The model has then been applied to offer a first-order geochemical constraint on $CaCO_3$ transport in the calcium-rich brines.

CHAPTER II

CALCITE SOLUBILITY IN GEOLOGICALLY RELEVANT BRINES

The principle of detailed balancing states that at equilibrium, the forward and reverse rates of every elementary reaction are equal. Therefore, equilibrium represents a state of dynamic balance at which the measured concentrations of products and reactants remain constant. In subsequent chapters, the kinetics of calcite dissolution in complex brines will be empirically modeled relative to this condition. The objective of this chapter is to evaluate the predictive capability of the EQPITZER program (He and Morse, 1993) with regards to the thermodynamic solubility of calcite in synthetic Na-Ca-Mg-Cl brines.

2.1. Materials and Their Preparation

2.1.1. Aqueous Solutions

Hanor (1994b) found that, for subsurface brines containing between 18 and 250 g L^{-1} Cl^-, the concentration of Cl^- can be predicted from TDS content. The variation in the other major dissolved species (Na^+, Ca^{2+}, Mg^{2+}, and Cl^-) can then, subsequently, be accounted for statistically as a function of Cl^- concentration. Using these relations, Morse et al. (1997) applied a series of fourth order polynomial equations to empirically fit the major solutes and the equations yielded a generally high degree of correlation (Table 2–1).

Table 2–1. Coefficients for the calculation of brine composition. Based on the equation C (mg L^{-1}) = a + bX + cX^2 + dX^3 + eX^4, where X is TDS (mg L^{-1}) for calculation of Cl^- (mg L^{-1}) and Cl^- is used for calculation of the other ion concentrations. The values have been reproduced from Morse et al. (1997).

Ion	a	b x 10^3	c x 10^6	d x 10^{12}	e x 10^{18}	r^2
Na^+	2199.1	494.43	0.18625	-0.7038	-25.175	0.74
Ca^{2+}	-2602.3	171.94	-1.4869	9.5377	0	0.87
Mg^{2+}	-689.3	50.27	-0.39096	1.6454	0	0.68
Cl^-	1652.8	602.35	0	0	0	0.99

The synthetic brines prepared for this study were based on these equations and ranged in salinity from 50to 195 g L^{-1}. Because potassium and bromide have not been shown to play an important role in carbonate mineral kinetics, for simplicity they have been omitted from these synthetic brines and the resulting deficiency in ionic strength has been balanced with additional NaCl. In selected brines, Mg^{2+} was deliberately omitted as well, and similarly the charge was balanced with NaCl. Each brine was prepared gravimetrically on the molal scale (m) from separate concentrated stock solutions of A.C.S. reagent grade NaCl, $CaCl_2 \bullet 2H_2O$ and $MgCl_2 \bullet 6H_2O$. The concentrations of the Ca^{2+} and Mg^{2+} in the stock solutions were verified by $AgNO_3$ titration as described in section 2.3.1.

2.1.2. Solids

Calcite rhombs (Iceland spar) obtained from Ward's Scientific Inc. were crushed into powder and wet sieved into >125 μm, 125–63 μm and 63–32 μm size fractions. The mineralogy was verified by powder X-ray diffraction as being >99% calcite. To relieve surface strain and to clean the grains of ultra-fine particles which can enhance solubility, the fractions were sonicated in methanol for one hour, re-sieved, briefly washed with milliQ® (18.1 μΩ) water and freeze dried. Figure 2–1 shows SEM micrographs of the 63–32 μm calcite fraction before (A, B) and after (C, D) sonication in methanol. Based on the SEM micrographs, the average grain size of the 63–32 μm fraction was 26 ±16 μm. In subsequent chapters where kinetics are addressed, the specific surface area will be more fully characterized and discussed.

2.1.3. Gases

Commercially purified high-grade CO_2 and ultra-high purity N_2 were precisely mixed and their flow rate controlled using dual MKS® Type 1479A mass-flow regulators that were controlled by specially developed LabVIEW® software. In order to minimize evaporation of experimental solutions, the gas was bubbled through as series of humidifiers. The humidifiers contained 90 ml of sodium chloride solutions having ionic strengths that were matched with the experimental solutions. The humidifiers also served as gas mixing chambers.

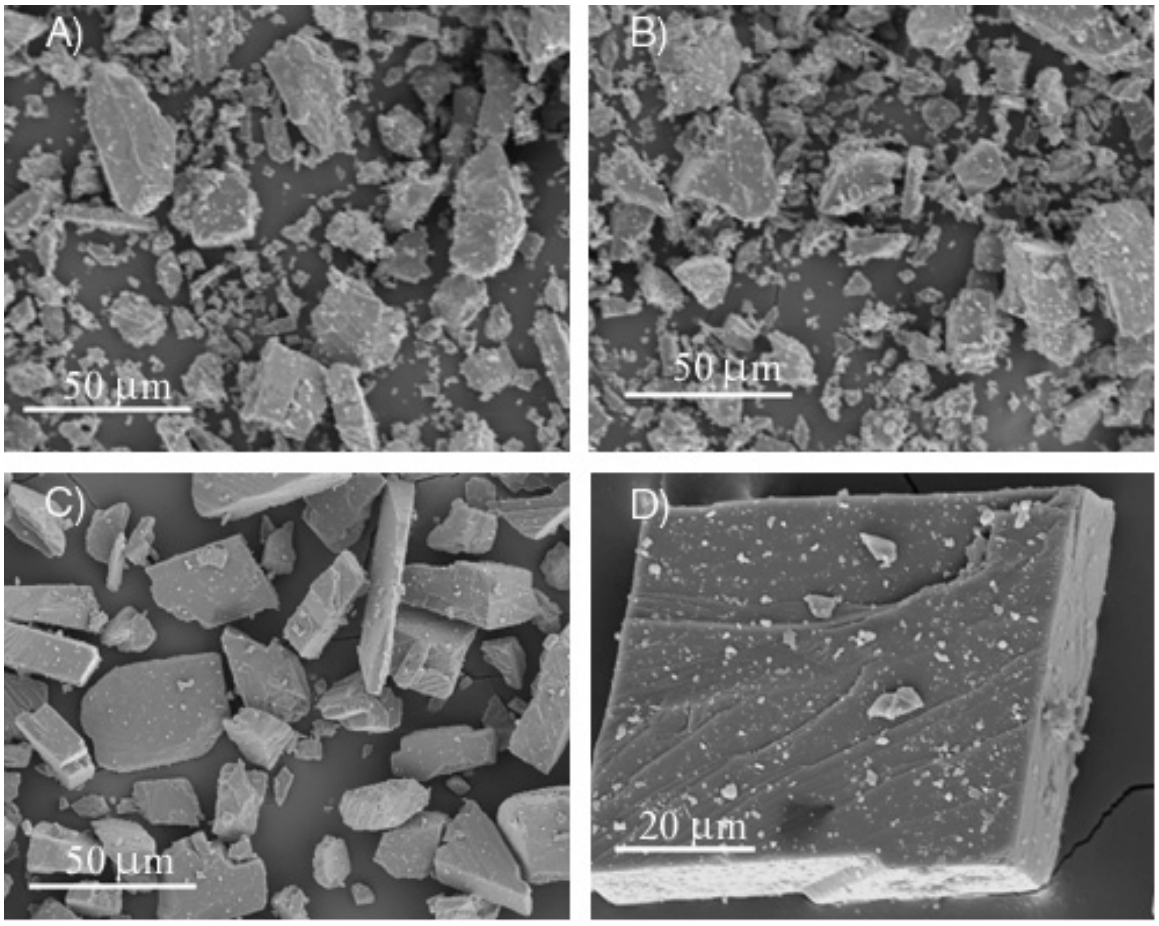

Figure 2–1. Scanning electron micrographs of crushed Iceland Spar calcite 32–63 μm size fraction used in solubility experiments. Prior to treatment (A, B) the calcite powder was highly irregular and inhomogeneous containing a considerable amount of ultra-fine particles. Scale bar = 50 μm. Following sonication in methanol (C, D), most of the ultra-fine material was eliminated and the powder exhibited a more uniform size distribution. Scale bar = 50 μm (C) and 20 μm (D).

2.2. Solubility Reactor

The solubility reactor consisted of four specially modified glass 125 ml serum bottles. Approximately 100 ml of brine was added to each serum bottle that accommodated a pipette tip and small vent. A CO_2-N_2 gas mixture was then gently bubbled into the solution through the pipette tip. In early experiments (i.e. Mg^{2+}-free solutions) pure CO_2 was used while in later experiments the gas mixture was approximately 50/50. The 0.5 bar pCO_2 system promoted a higher CO_3^{2-}:TCO_2 ratio for a given Ca^{2+} concentration allowing more robust measurements to be made. The serum bottles were then inserted into water-jacketed vessels that were maintained at constant temperature (25 ±0.01 ºC) using a Neslab® RTE-8DD circulating bath.

Following equilibration with the gas phase, 2 ml of concentrated primary standard grade Na_2CO_3 was added sufficient to establish approximately 20% saturation with respect to calcite. This was necessary to minimize the amount of calcite dissolution so as to limit changes in the solution Ca^{2+} concentration. Since a precise knowledge of the equilibrium concentrations was not initially known, the amount of sodium carbonate to be added could only be approximated based on EQPITZER predictions. After several attempts, much better estimates could be applied from trial and error. In the final experiments varying amounts of sodium carbonate were added to each of the four serum bottles so as to allow for a small range in final Ca^{2+} concentrations.

The solution was then allowed to reestablish equilibrium with the gas phase prior to the addition of approximately 1 g of the 63–32 μm calcite. Since the grinding action of magnetic stirrers has been known to produce enhanced solubility, the solutions were instead mixed by mounting the reactors on a Lab-line Instruments® orbit shaker which

was oscillated continuously at 250 RPM. The calcite was allowed to react under the constant pCO_2 gas mixture for 7 h. This reaction time generally brought the solution to within a few percent of equilibrium and consequently subsequent changes in pCO_2 were minor. The gas feed was then removed and the serum bottles sealed with a septum top. The calcite suspension was then permitted to react with the brine in the closed system for one week. The closed system eliminated evaporation of the brine for the duration of the experiment.

2.3. Post-Equilibration Analysis

At the experiment completion, a nitrogen gas feed was inserted into the serum bottle septum. A minimal amount of nitrogen was use to displace fluid which was passed though a second syringe needle equipped with an in-line 0.45 μm Acrodisk® filter. The filtered sample was collected into a 20-ml gas tight syringe. This method avoided any atmospheric exchange with the carbonic acid system.

2.3.1. Determination of Salts

Solution chloride concentrations were determined from a 1:10 gravimetric dilution of sample in milliQ® (18.1 μΩ) water. Determination was made by $AgNO_3$ titration using an Accumet silver ion selective electrode interfaced via an Orion 720A potentiometer. Endpoint detection was facilitated by a specifically developed computer software package. The $AgNO_3$ titrant was calibrated monthly against calibration curves using weighed amounts of IAPSO standard seawater. Based on the calibration curves

the precision of the titration was better than 1.5% and replication was typically unnecessary.

Calcium and total hardness ($Ca^{2+} + Mg^{2+}$) concentrations were determined from a 1:11 gravimetric dilution of sample in 0.01 N HCl. Calcium was analyzed by EGTA titration with the calcium indicator Cal/Ver II® using a NaOH buffer to precipitate out the Mg^{2+}. Total hardness concentrations were determined by EDTA titration with Eriochrome Black T (EBT) using an NH_3OH buffer. Endpoint detection was facilitated using a Brinkmann PC 800 colorimeter interfaced with a Brinkmann 682 titroprocessor. Fresh standards were prepared specific for each experiment that closely bracketed the anticipated concentration range. The standards were prepared gravimetrically from GFS® primary standard calcium carbonate dissolved in 0.01 N HCl and from a $MgCl_2 \bullet 6H_2O$ solution calibrated by $AgNO_3$ titration. The presence of Mg^{2+} in the standard was necessary for proper functioning of the indicators. Four point calibration curves were generated against weighed amounts of standard for each experiment. Precision was within 2% in most cases and triplicates of each sample were measured.

The concentrations of Mg^{2+} and Na^+ were calculated from mass and charge balance as given by,

$$Mg^{2+} = Hardness - Ca^{2+} \qquad (2\text{–}1)$$

and,

$$Na^+ = \left(Cl^- - 2 \times Ca^{2+} - 2 \times Mg^{2+}\right) + 2 \times Na_2CO_3 \qquad (2\text{–}2)$$

where Na_2CO_3 is the amount based on the primary standard grade sodium carbonate added at the initiation of the experiment.

2.3.2. Analytical Parameters in the Carbonic Acid System

The species distribution of the carbonic acid system was evaluated by coupling TA and TCO_2. These parameters were chosen over pH and pCO_2 for two reasons: (1) the pH of the solution could not be directly measured without disruption to the closed system, and (2) the pCO_2 could not be assumed from the gas mixture since once the system was closed a continued dissolution would result in a draw down of pCO_2.

TCO_2 was immediately determined on the samples according to the method of Dickson and Goyet (1994) with a UIC Inc. Model 5011 CO_2 coulometer. Precision was better than 100 μmoles kg^{-1}.

TA was determined by a Gran-type titration (Gran, 1952) using a Metrohm 655 Dosimat and an Orion 720A pH meter interfaced with a computer. Apparent sample pH was measured using a Corning Inc. semi-micro combination pH electrode calibrated using NBS 4 and 7 buffers. Computer software was used to evaluate the apparent inflection point. An HCl titrant and solutions of primary standard Na_2CO_3 were made in NaCl solutions at ionic strengths specific to each of the brines. The Na_2CO_3 standards were prepared gravimetrically under a nitrogen environment and their concentrations verified by coulometeric measurement of their TCO_2 concentrations. Four point calibration curves were made using weighted standards versus the volume at which the apparent inflection point occurred. Precision was better than 0.1 meq kg^{-1}. The titrations were conducted at 25 ±0.1 ºC in a water-jacketed open cell into which CO_2 was continuously bubbled. The bubbling of CO_2 into the cell served to facilitate gas exchange and prevent the solution from becoming oversaturated with respect to calcite as a result of degassing prior to the addition of the HCl titrant.

2.4. Results and Discussion

2.4.1. Solubility Calculations

The analytical results for the solubility experiments are presented in Table 2–2, where concentrations are those measured at the terminus of the experiment.

The saturation state with respect to calcite (Ω) is defined simply as the ratio of the measured ion activity product (IAP) to the thermodynamic solubility constant for calcite (K_c), as given by

$$\Omega = \frac{IAP}{K_c} \tag{2–3}$$

and

$$IAP = a_{Ca^{2+}} a_{CO_3^{2-}} = \gamma_{Ca^{2+}} m_{Ca^{2+}} \gamma_{CO_3^{2-}} m_{CO_3^{2-}} . \tag{2–4}$$

If Ω = 1, then the solution is in equilibrium with respect to calcite; if Ω < 1 the solution is undersaturated; and if Ω > 1 the solution is supersaturated. The only value that was directly measured is $m_{Ca^{2+}}$; the remaining values had to be derived using the EQPITZER software based on the solution compositions given in Table 2–2. Since the non-carbonic acid system contributions to TA are negligible in these synthetic brines, the carbonate alkalinity (A_C) can be approximated by

$$A_C \approx TA - m_{OH^-} + m_{H^+} . \tag{2–5}$$

The carbonate ion concentration, $m_{CO_3^{2-}}$, can then be calculated from TA and TCO_2 according to the equation

$$m_{CO_3^{2-}} = \frac{A_C\left(\frac{K_1^*}{K_2^*} - 4\right) - TCO_2\left(\frac{K_1^*}{K_2^*}\right) + \sqrt{\left(TCO_2\left(\frac{K_1^*}{K_2^*}\right)\right)^2 - A_C\left(\frac{K_1^*}{K_2^*}\right)\left(\frac{K_1^*}{K_2^*} - 4\right)\left(2TCO_2 - A_C\right)}}{2\left(\frac{K_1^*}{K_2^*} - 4\right)}$$

(2–6)

The stoichiometric first and second dissociation constants (K_1^* and K_2^*) of the carbonic acid system used by EQPITZER were experimentally determined in aqueous solutions containing Na^+, K^+, Ca^{2+}, Mg^{2+}, SO_4^{2-}, and Cl^- by He and Morse (1993). The activity coefficients for the aqueous species were also calculated with EQPITZER, which uses the Pitzer ion-interaction model parameterized for the carbonic acid system that accommodates the associated species of $CaCO_3^0$ and $MgCO_3^0$. The complete output of the EQPITZER model calculations for the solubility experiments are presented in Appendix I. Calculated saturation states are presented in Figure 2–2 along with values calculated from data reported in relevant literature.

Although the EQPITZER-calculated IAP was in reasonable agreement (±10%) with K_c in relatively low Ca^{2+} concentration brines, increasing brine Ca^{2+} concentration resulted in a systematic increase in the calculated equilibrium IAP. Consequently, calculated Ω values were considerably greater than 1 at high Ca^{2+} concentrations, suggesting an apparent supersaturation with respect to calcite. Solubility experiments performed in Mg^{2+}-free solutions exhibited the same behavior (solid circles in Figure 2–2) implying that this is not due to the formation of a more soluble Mg^{2+}-rich surface phase. Nor is it specifically related to ionic strength, since in the Mg^{2+}-free solubility experiments the ionic strength of the solutions was fixed (I = 3 m) by balancing with NaCl. It should also be noted that in these solutions the Mg:Ca ratio was always <0.5.

This is much lower than in seawater where a ~8 % Mg-calcite forms at a Mg:Ca ratio of ~5 (Mucci and Morse, 1984).

Table 2–2. Analytical results for the solubility experiments. Units are molal except for total alkalinity (TA) and total carbon dioxide content (TCO_2), which are in meq kg^{-1} H_2O and mmol kg^{-1} H_2O respectively.

EXPT ID	Na^+	Ca^{2+}	Mg^{2+}	Cl^-	TA	TCO_2
KSP_Brine1_1	0.745	0.043	0.021	0.859	13.76	28.52
KSP_Brine1_2	0.744	0.044	0.021	0.858	15.83	32.05
KSP_Brine1_3	0.742	0.043	0.023	0.856	16.08	33.38
KSP_Brine1_4	0.731	0.042	0.022	0.844	16.30	32.65
KSP_Brine2_1	1.800	0.160	0.068	2.252	9.02	20.03
KSP_Brine2_2	1.804	0.159	0.066	2.250	8.96	19.51
KSP_Brine2_3	1.801	0.160	0.066	2.248	8.83	18.59
KSP_Brine2_4	1.800	0.159	0.064	2.241	9.09	20.27
KSP_Brine3_1	2.670	0.365	0.117	3.627	5.58	14.40
KSP_Brine3_2	2.670	0.362	0.117	3.626	5.66	14.50
KSP_Brine3_3	2.684	0.364	0.116	3.646	5.65	14.57
KSP_Brine3_4	2.665	0.362	0.116	3.620	5.51	14.60
MgFree_1	3.022	0.023	0.000	3.043	24.72	41.19
MgFree_2	2.583	0.154	0.000	2.881	10.76	28.50
MgFree_3	0.237	0.912	0.000	2.053	7.08	28.49
MgFree_4	3.022	0.023	0.000	3.043	25.51	41.80
MgFree_5	2.583	0.154	0.000	2.881	10.40	28.49

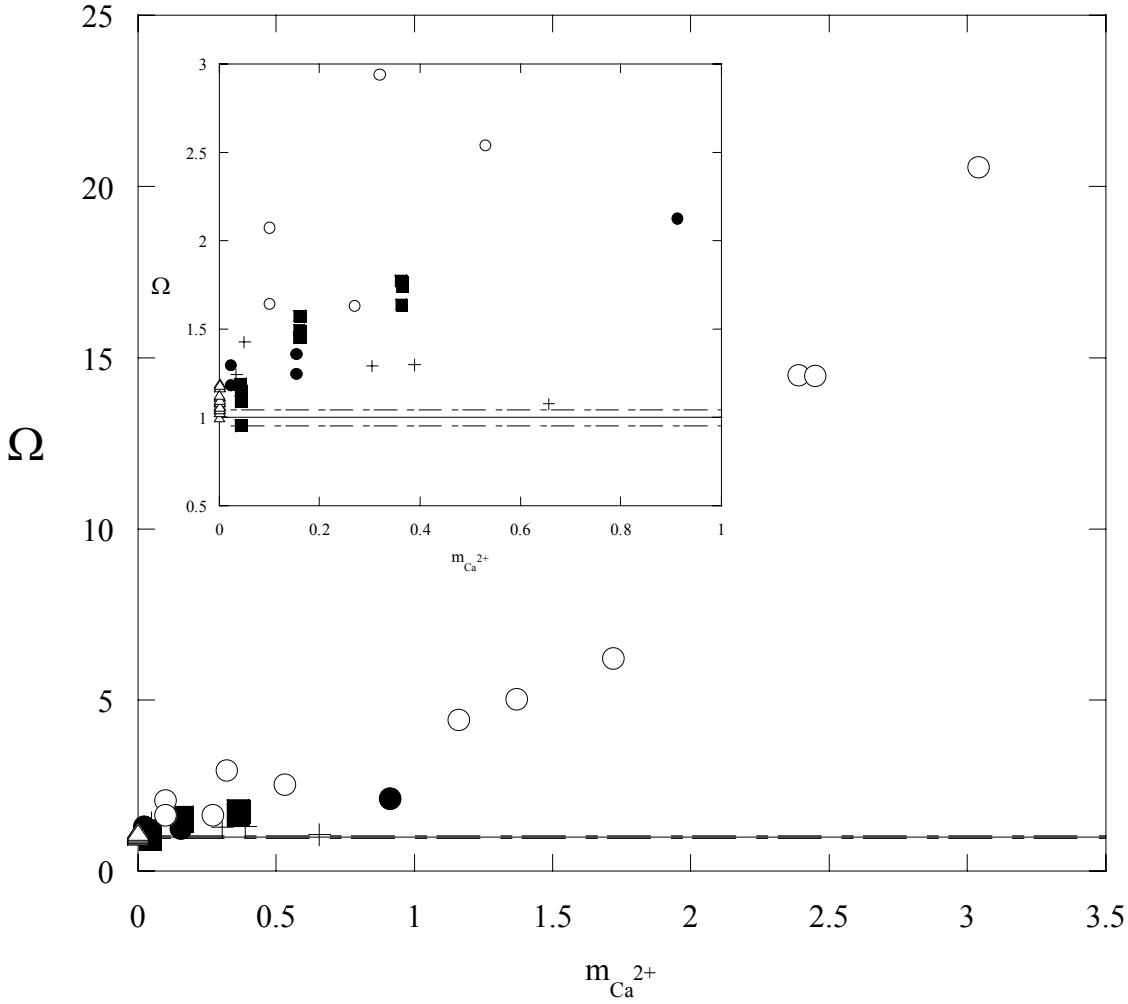

Figure 2–2. The Ω values calculated using EQPITZER from the analytical results of this study compared with values calculated from literature data. Solid scatter points are experimental data from this study. Solid squares were measured in Na-Ca-Mg-Cl brines, while solid circles were measured in Mg^{2+}-free brines. Crosses are from He (1992). Open triangles are from Millero et al. (1984). Open circles are from Wolf et al. (1989). The inset figure expands the region investigated in this study. The solid line represents thermodynamic equilibrium within the uncertainty depicted by the dashed lines (Plummer and Busenberg, 1982).

Millero et al. (1984) measured the solubility of calcite in NaCl solutions up to 6 m. In these experiments the m_{Ca}^{2+} did not exceed 0.6 mmol kg^{-1} H_2O. Based on the reported solution compositions and coupling TA and TCO_2 to solve for the carbonic acid system, analogous to the approach used with the analytical data from this study, the derived Ω values using EQPITZER closely approximated 1. The same approach was applied to the data reported by Wolf et al. (1989) in which calcite dissolution was measured in highly concentrated $CaCl_2$ solutions (up to 3 m Ca^{2+}). In this case a near exponential deviation with increasing m_{Ca}^{2+} was observed with an apparent supersaturation in excess of 20 times for the most concentrated case. Even the data sets for solubility experiments performed in complex brines reported by He et al. (1993) yield apparent $\Omega > 1$. However, no systematic error is seen in He et al.'s data and it is unclear what the preferred coupling should be since he reported all four parameters of the carbonic acid system. Applying different combinations of each of the parameters yielded widely differing results. Coupling pCO_2 and TA yielded the best agreement with the other data sets.

2.4.2. Indeterminate Error Contribution to the Calculated Ω Value

In order to evaluate if the systematic deviations from unity in the calculated Ω values in these solutions are significant, we must first consider the magnitude of the indeterminate analytical error. The error associated with m_{Ca}^{2+} in equation 2–4 is 2%, as reported previously in section 2.3.1. Only an estimate of the error in $m_{CO_3^{2-}}$ can be calculated since the error associated with the regression analysis used to derive the stoichiometric dissociation constants (K_1^* and K_2^*) is not reported (He and Morse, 1983).

Based on equation 2–5 we can estimate the error contributed by analytical uncertainty in TA and TCO_2 measurements to the calculated $m_{CO_3^{2-}}$ to between 1.0% and 2.5%.

Error associated with the activity coefficients is harder to evaluate as these are derived values based on model calculations. The uncertainty of the analytical data used as input for the model, however, is only accurate to within approximately ±2%. How this error propagates through the model is complex, but as a conservative approximation, if we assume that the derived activity coefficients yield an uncertainty of similar relative magnitude, the net uncertainty in the calculated IAP is roughly 4%. This is in close agreement with the observed reproducibility between replicate experiments (see error bars in Figure 2–3). This is comparable to the relative uncertainty reported by Plummer and Busenberg (1982) for K_c. At 25 °C it is valid only to within ±4.6%.

The analytical error is significantly less than observed systematic deviation of Ω from unity (Figure 2–3). Therefore, the error is probably an artifact of the model's predictive capability for the activity coefficients in these solutions. A possible source of this systematic error will be further examined in the following section.

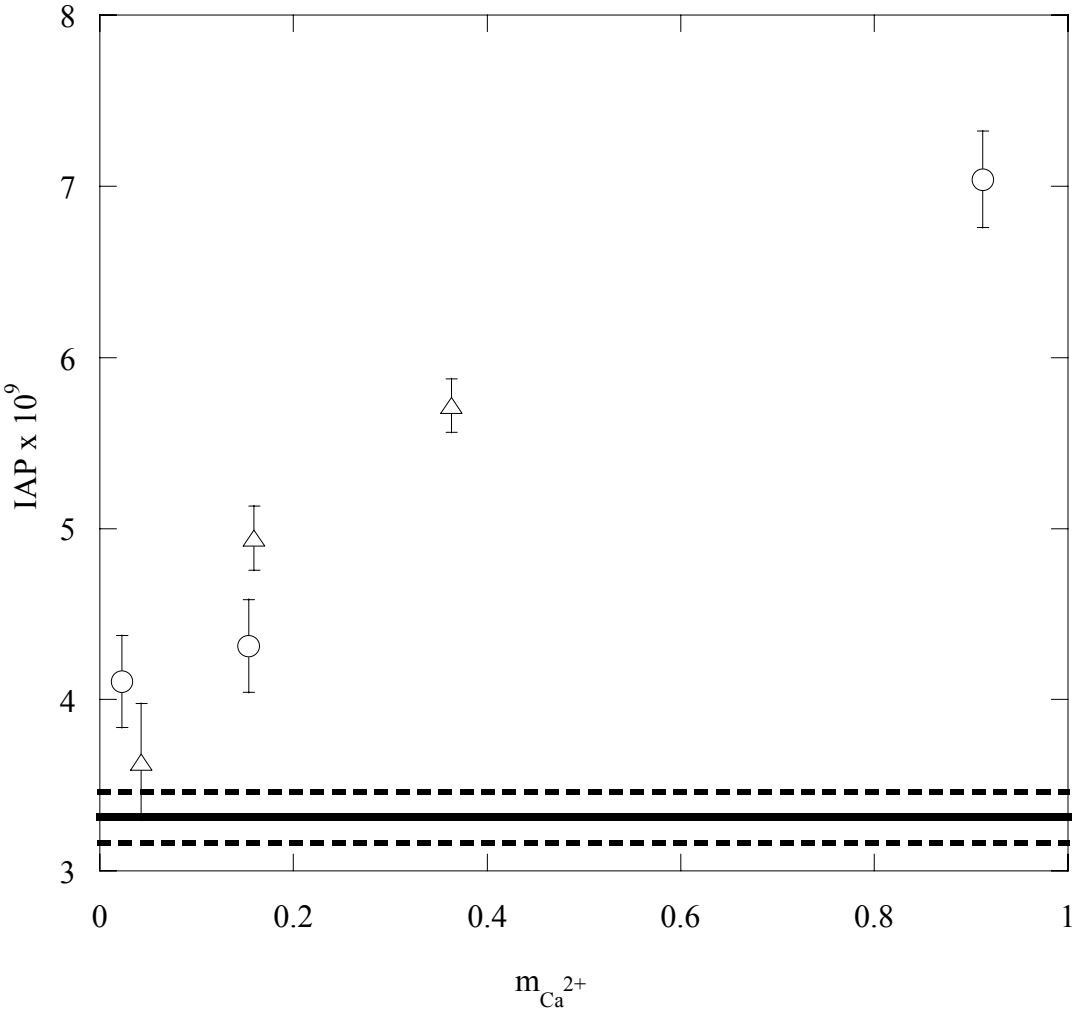

Figure 2–3. Experimental uncertainty of the calculated ion activity product (IAP) for the calcite solubility experiments. Scatter points are experimental data from this study and error bars represent 1 standard deviation amongst replicate experiments. Open triangles are Na-Ca-Mg-Cl brines exhibiting a range of ionic strengths (I = 0.9 to 4.1 m) and open circles are from Mg-free solutions at a fixed ionic strength (I = 3.0 m). The solid line is the thermodynamic equilibrium constant for calcite (K_C) within the uncertainty depicted by the dashed lines (Plummer and Busenberg, 1982).

2.4.3. The Effect of Ion Pairing on EQPITZER Total Activity Coefficients for the Carbonate Ion

He et al. (1993) applied the criteria offered by the Harvie et al. (1984) evaluation of the ion interaction model with and without the addition of ion pairs when considering which ion pairs to include in the EQPITZER model. From this, the 2-2 type ion pairs with thermodynamic association constants (K_A) greater than 500 where chosen to be included. For the Na-K-Ca-Mg-HCO_3-CO_3 system the important ion pairs, $CaCO_3^0$ and $MgCO_3^0$, were defined using the $K_{CaCO_3^0}$ and $K_{MgCO_3^0}$ values of Plummer and Busenberg (1982). In order to maintain internal consistency with the Pitzer parameters for the carbonic acid system, He et al. elected to assign unity activity coefficients to these ion pairs. However, there is evidence that this assumption may not be valid. Although Millero and Schreiber (1982) felt that in most cases the activity coefficient for neutral species formed between divalent cations and most anions could be assigned the value of 1.0, for pairs formed with CO_3^{2-} it could be considerably less. For seawater (I = 0.7 m) they calculated a $\gamma = 0.7 \pm 0.2$ where the error is related to uncertainties in K_A.

The effect of the $CaCO_3^0$ ion pair on the activity coefficient for Ca^{2+} would be negligible since in these solutions the free-Ca^{2+}: total-$Ca^{2+} \approx 1.0$. However, in the case of CO_3^{2-} ion, the fraction of free-CO_3^{2-} ions can be considerably less than one. The free carbonate ion concentration ($m_{CO_{3,F}^{2-}}$) can be calculated from the relation given by Millero and Schreiber (1982):

$$m_{CO_{3,F}^{2-}} = \left(\frac{\gamma_{CO_{3,T}^{2-}}}{\gamma_{CO_{3,F}^{2-}}} \right) m_{CO_{3,T}^{2-}} \qquad (2\text{–}7)$$

where the subscripts F and T refer to the free and total concentration respectively. The total concentrations and activity coefficients for each of the experimental brines are given in Table 2–3. EQPITZER can also be used to calculate the carbonate ion activity coefficients for hypothetical solutions containing only KCl at concentrations equivalent to the ionic strengths of each of the experimental brines. In these cases, the carbonate ion activity coefficient can be considered equivalent to $\gamma_{CO_{3,F}^{2-}}$ since a pure KCl solution doesn't contain any significant ion pairing. This assumes that the free activity coefficient can be approximately assumed to be solely dependent on ionic strength (Lewis and Randall, 1921). The free carbonate ion concentrations can then be estimated from equation 2–7 (Table 2–3).

In all cases less than 40% of the carbonate ion is free (Table 2–3). As a result, the calculated Ω values become increasing sensitive to errors in the total carbonate ion activity coefficient ($\gamma_{CO_{3,T}^{2-}}$) with increasing calcium concentration. We can calculate the correction to $\gamma_{CO_{3,T}^{2-}}$ required to correct the Ω values to unity. At equilibrium,

$$\Omega = 1 = \frac{a_{Ca^{2+}}\left(\gamma_{CO_{3,T}^{2-}} + \Delta\gamma\right)m_{CO_{3,T}^{2-}}}{K_C}, \qquad (2\text{–}8)$$

where activities and concentrations refer to their steady-state values, $a_{Ca^{2+}}$ is calcium activity, $\gamma_{CO_{3,T}^{2-}}$ is the EQPITZER-calculated carbonate ion activity coefficient, and Δγ is the empirical correction factor. Rearrangement to solve for the empirical correction factor (Δγ) yields,

$$\Delta\gamma = \frac{K_C}{\left(a_{Ca^{2+}}\right)m_{CO_{3,T}^{2-}}} - \gamma_{CO_{3,T}^{2-}}. \qquad (2\text{–}9)$$

The EQPITZER predicted $\gamma_{CO_{3,T}^{2-}}$ values are compared with their empirically corrected values ($\gamma'_{CO_{3,T}^{2-}}$) in Table 2–3, where $\gamma'_{CO_{3,T}^{2-}} = \gamma_{CO_{3,T}^{2-}} + \Delta\gamma$. In all cases the necessary correction is relatively minor.

Using these corrected activity coefficients we can demonstrate the sensitivity of the calculated IAP to ion pairing by first deriving an apparent stoichiometric association constant (K^*_A) for the $CaCO_3^0$ ion pair. From the EQPITZER model output (Appendix I) we can extract an apparent $K^*_{CaCO_3^0}$ by applying the equations offered by Millero and Schreiber (1982) which state that for the complex,

$$Ca^{2+} + CO_3^{2-} \rightarrow CaCO_3^0, \qquad (2\text{–}10)$$

the fraction of free CO_3^{2-} ion can be related to the stoichiometric association constants for the ion pairs in which it appears by

$$\frac{m_{CO_{3,F}^{2-}}}{m_{CO_{3,T}^{2-}}} = \left(1 + K^*_{CaCO_3^0} m_{Ca_F^{2+}} + K^*_{MgCO_3^0} m_{Mg_F^{2+}} + K^*_{NaCO_3^-} m_{Na_F^+} \ldots\right)^{-1} \qquad (2\text{–}11)$$

where K_i^* are the appropriate stoichiometric association constants. We assume that the predominate ion pairs are $CaCO_3^0$, $MgCO_3^0$ and $NaCO_3^-$. Typically, the relative magnitude of the stoichiometric association constants have been found to be: $K^*_{CaCO_3^0} > K^*_{MgCO_3^0} >> K^*_{NaCO_3^-}$. In seawater, for example, Millero and Schreiber (1982) measured values of $K^*_{CaCO_3^0} = 126 \pm 26$, $K^*_{MgCO_3^0} = 87 \pm 11$ and $K^*_{NaCO_3^-} = 2.6 \pm 0.5$. Considering the high cation concentrations relative to the carbonate ion, we have assumed that $m_{M_F^{Z+}} \approx m_{M_T^{z+}}$, where M^{z+} refers to the metal cation. Therefore, rearranging

equation 2–11 and applying these simplifying assumptions we can estimate $K^*_{CaCO_3^0}$ and $K^*_{MgCO_3^0}$ from:

$$K^*_{M_xCO_3^0} \approx \frac{1}{m_{M_x^{2+}}}\left(\frac{m_{CO_{3,F}^{2-}}}{m_{CO_{3,T}^{2-}}} - 1\right) - K^*_{M_yCO_3^0} m_{M_y^{2+}} - K^*_{NaCO_3^0} m_{Na^+} \qquad (2\text{–}12)$$

where M_x is initially $m_{Ca^{2+}}$ and M_y is $m_{Mg^{2+}}$. The values are then exchanged and the solution is derived in an iterative fashion. In the case of the Mg-free solutions, the magnesium terms were omitted. The value for $K^*_{NaCO_3^-}$ was taken to be that measured by Millero and Schreiber (1982) for seawater ($\log K^*_{NaCO_3^-} = 0.41$). Although this is unlikely to be strictly true, provided $K^*_{M^{2+}CO_3^0} m_{M^{2+}} > K^*_{NaCO_3^0} m_{Na^+}$, it is a reasonable assumption in these solution and should suffice for purposes sought here.

The average $\log K^*_{CaCO_3^0}$ values derived from these calculations is 1.53 ±0.16 (Table 2–4). For seawater, reported values for $\log K^*_{CaCO_3^0}$ range from 1.51 (Hansson, 1973) to 2.21 (Pytkowicz and Hawley, 1974), but Millero and Schreiber (1982) offer perhaps the most reliable value of 2.1 ±0.1. As expected, the $\log K^*_{CaCO_3^0}$ values for these more concentrated brines are lower than this; but more importantly, the range in literature values give some indication of the magnitude of precision that is to be anticipated (±0.7 log units).

Next we can calculate what the required $K^*_{CaCO_3^0}$ values would have to be to account for $\Delta\gamma$ such that Ω is corrected to unity at steady-state. Combining equations 2–8 and 2–12, a corrected $K^*_{CaCO_3^0}$ can be approximated by:

$$K^*_{M_x^{2+}CO_3^0} = \frac{1}{m_{M_x^{2+}}}\left(\frac{a_{Ca^{2+}} m^2_{CO^{2-}_{3,T}} \gamma_{CO^{2-}_{3,T}}}{K_C m_{CO^{2-}_{3,F}}} - 1\right) - K^*_{M_y^{2+}CO_3^0} m_{M_y^{2+}} - K^*_{NaCO_3^0} m_{Na^+} \quad (2\text{–}13)$$

The results are given in Table 2–4 and show that the difference required to account for the error is within ±0.2 log units in most cases; far less than the observed uncertainty in the literature values. We can go further by using the relationship between $K^*_{CaCO_3^0}$ and the thermodynamic association constant ($K_{CaCO_3^0}$) to estimate the $\gamma_{CaCO_3^0}$ value needed to account for this error. Millero and Schreiber (1982) describe how $\gamma_{CaCO_3^0}$ can be derived from $K^*_{CaCO_3^0}$ relation to the $K_{CaCO_3^0}$ by

$$\gamma_{CaCO_3^0} = \frac{\gamma_{Ca_F^{2+}} \gamma_{CO^{2-}_{3,F}} K_{CaCO_3^0}}{K^*_{CaCO_3^0}} \quad (2\text{–}14)$$

where we again assume that calcium is sufficiently buffered given its high concentration so that $\gamma_{Ca_F^{2+}} \approx \gamma_{Ca_T^{2+}}$. Substituting equation 2–14 into 2–13 yields

$$\gamma_{CaCO_3^0} \approx \frac{\gamma_{Ca^{2+}}\left(\frac{m_{CO^{2-}_{3,T}}}{m_{CO^{2-}_{3,F}}} \gamma'_{CO^{2-}_{3,T}}\right) K_{CaCO_3^0}}{K^*_{CaCO_3^0}}. \quad (2\text{–}15)$$

The average $\gamma_{CaCO_3^0}$ required to correct Ω to unity in these brines is 0.7 ±0.1 (Table 2–4).

Table 2–3. The total versus free carbonate ion activity. The free carbonate ion molal concentration ($m_{CO_3^{2-}}$, free) was calculated from estimates of the free carbonate ion activity coefficient ($\gamma_{CO_3^{2-}}$, free) calculated in hypothetical pure KCl solutions. The error in the total carbonate ion activity coefficient ($\gamma_{CO_3^{2-}}$, total) necessary to correct the equilibrium IAP's to unity is relatively minor ($\gamma_{CO_3^{2-}}$, corrected).

	$m_{CO_3^{2-}}$			$\gamma_{CO_3^{2-}}$		
Experiment ID	Free	Total	% Free	Free	Total	corrected
KSP_Brine1_1	2.8E-06	9.8E-06	29%	0.123	0.036	0.037
KSP_Brine1_2	3.4E-06	1.2E-05	29%	0.123	0.036	0.031
KSP_Brine1_3	3.3E-06	1.2E-05	29%	0.123	0.035	0.033
KSP_Brine1_4	3.6E-06	1.2E-05	29%	0.124	0.036	0.030
KSP_Brine2_1	1.7E-06	1.3E-05	13%	0.074	0.010	0.007
KSP_Brine2_2	1.8E-06	1.3E-05	13%	0.074	0.010	0.007
KSP_Brine2_3	1.8E-06	1.4E-05	13%	0.074	0.010	0.006
KSP_Brine2_4	1.7E-06	1.3E-05	13%	0.074	0.010	0.007
KSP_Brine3_1	7.4E-07	1.3E-05	6%	0.060	0.003	0.002
KSP_Brine3_2	7.5E-07	1.3E-05	6%	0.060	0.003	0.002
KSP_Brine3_3	7.5E-07	1.3E-05	6%	0.060	0.003	0.002
KSP_Brine3_4	7.2E-07	1.2E-05	6%	0.060	0.004	0.002
MgFree_1	7.1E-06	1.7E-05	40%	0.067	0.027	0.023
MgFree_2	1.4E-06	9.2E-06	15%	0.067	0.010	0.007
MgFree_3	8.7E-07	1.6E-05	5%	0.068	0.004	0.002
MgFree_4	7.6E-06	1.9E-05	40%	0.067	0.027	0.021
MgFree_5	1.3E-06	8.5E-06	15%	0.067	0.010	0.008

Table 2–4. The sensitivity of carbonate ion activity to ion pairing. The free carbonate ion molal concentration ($m_{CO_3^{2-}}$, free) was calculated from estimates of the free carbonate ion activity coefficient ($\gamma_{CO_3^{2-}}$, free) calculated in hypothetical pure KCl solutions. The error in the total carbonate ion activity coefficient ($\gamma_{CO_3^{2-}}$, total) necessary to correct the equilibrium IAP's to unity is relatively minor ($\gamma_{CO_3^{2-}}$, corrected). The discrepancy could be easily explained by a minor error in the stoichiometric association constant for the $CaCO_3^0$ ion pair ($K^*_{CaCO_3^0}$).

	Log $K^*_{CaCO_3^0}$		$\gamma_{CaCO_3^0}$	Log $K^*_{MgCO_3^0}$	
Experiment ID	EQPITZER	corrected	corrected	EQPITZER	corrected
KSP_Brine1_1	1.72	1.68	0.9	2.05	2.19
KSP_Brine1_2	1.72	1.80	0.7	2.05	2.26
KSP_Brine1_3	1.73	1.78	0.7	2.02	2.21
KSP_Brine1_4	1.73	1.83	0.7	2.03	2.26
KSP_Brine2_1	1.48	1.68	0.7	1.94	2.17
KSP_Brine2_2	1.48	1.69	0.7	1.94	2.19
KSP_Brine2_3	1.48	1.72	0.6	1.95	2.22
KSP_Brine2_4	1.48	1.67	0.7	1.96	2.19
KSP_Brine3_1	1.38	1.66	0.9	2.10	2.38
KSP_Brine3_2	1.39	1.68	0.8	2.10	2.38
KSP_Brine3_3	1.38	1.68	0.8	2.10	2.39
KSP_Brine3_4	1.37	1.63	0.9	2.09	2.35
MgFree_1	1.75	1.88	0.6	-	-
MgFree_2	1.47	1.65	0.9	-	-
MgFree_3	1.26	1.61	0.4	-	-
MgFree_4	1.75	1.94	0.6	-	-
MgFree_5	1.47	1.60	0.9	-	-

2.5. Conclusion

Although the EQPITZER model reasonably predicted equilibrium (±10%) with respect to calcite in relatively low concentration brines (< 50 g L^- TDS), with increasing brine concentration a systematic increase in the calculated saturation state was observed, yielding at steady-state an apparent 2-fold supersaturation in the most-calcium rich brine. The error was not specifically related to magnesium concentration suggesting that it is not the result of the formation of an enhanced solubility Mg-rich phase. Instead, it was strongly correlated with increases in calcium concentration. We can not be certain that the apparent increase in steady-state IAP is not related to a complex interaction between the calcite surface and these highly concentrated brines, but perhaps the simplest explanation is that the apparent IAP increase represents minor uncertainty in the carbonate ion activity coefficient. A minor adjustment in stoichiometric association constants ($K^*_{M^{2+}CO_3^0}$) for the $CaCO_3^0$ or $MgCO_3^0$ ion pairs could correct for the error. Alternatively, if the neutral species ion activity coefficient (i.e., $\gamma_{CaCO_3^0}$) were permitted to deviate slightly from unity, the error could also be resolved. Although this minor error would have little consequence in many geochemical context such as in the case of mineral mass transport, it can impart significant error to kinetic rate models that empirically describe the rate of dissolution as a function of the degree of disequilibrium (1-Ω). Jeschke and Dreybrodt (2002) showed that when rates are modeled by linear fits of log R versus log (1-Ω), small uncertainties in Ω can have a pronounced effect on the interpreted reaction order (n) and rate constant (k). Small errors can create nonlinearity in log-log plots. Such effects are particularly important under near equilibrium conditions such as those that will be considered in the subsequent chapters.

CHAPTER III

CALCITE DISSOLUTION KINETICS IN BRINES UP TO 1 MOLAL CALCIUM

A series of classical pH-free-drift batch reactor experiments were used to measure the rate of calcite dissolution at a temperature of 25 °C and pressure of 1 atm (0.5 MPa) in a range of Na-Ca-Mg-Cl synthetic brines. The free-drift method allows for rapid determination of dissolution rates over a broad range of saturation states. An open system method was employed in which the rate of $CaCO_3$ dissolution was determined by monitoring changes in solution pH as a function of time at a constant pCO_2. The rate of change in pH was subsequently converted to changes in alkalinity using the program EQPITZER (He and Morse, 1993) which could then be directly related to a dissolution rate. Experiments examined the combined affects of a broad range of major ion concentrations and ionic strength (I) on the net rate of dissolution. The calcium concentration in the brines reached a maximum of nearly 1 m at an ionic strength in excess of 4 m. The compositions are representative of the high levels of calcium that can be found in Gulf Coast basin formation waters (Moldovanyi and Walter, 1992). These experiments served as a foundation for later experiments presented in subsequent chapters where the specific effects were determined.

3.1. Materials and Methods

3.1.1. Aqueous Solutions

Brines prepared for these experiments ranged in concentration that from pseudo-seawater (I = 0.7 m) to nearly I = 4.5 m. The most concentrated brines contained calcium and magnesium concentrations similar to those of Smackover Formation waters of the southwest Arkansas shelf (Gulf Coast basin) (Moldovanyi and Walter, 1992). Each solution was prepared in the same manner as described in Chapter II. Their initial chemical compositions are presented in Table 3–1.

Table 3–1. Initial solution compositions of synthetic brines and pseudo-seawater (psw).

Brine ID	~TDS *(g L^{-1})*	Ionic Strength *(molal)*	Ca^{2+} *(molal)*	Mg^{2+} *(molal)*	Na^{+} *(molal)*	Cl^{-} *(molal)*
psw_a	35	0.73	0.0116	0.0593	0.5164	0.6426
psw_b	35	0.75	0.0112	0.0742	0.5076	0.6329
brine 1	49	0.99	0.0795	0.0795	0.5360	0.0809
brine 2	56	1.14	0.0914	0.0456	0.7295	0.9971
brine 3	77	1.60	0.1475	0.0532	0.9995	1.3960
brine 4	105	2.13	0.2624	0.0858	1.1740	1.6880
brine 5a	134	2.96	0.4275	0.0817	1.4349	2.4496
brine 5b	134	2.99	0.4366	0.0903	1.4070	2.4580
brine 6	158	3.70	0.6408	0.1112	1.4400	2.9410
brine 7a	179	4.35	0.9045	0.1266	1.2595	3.3204
brine 7b	179	4.43	0.9356	0.1624	1.1360	3.3300

3.1.2. Solids

A.C.S. reagent grade calcite (Fisher Scientific) was pretreated with dilute (0.1 N) HCl according to the methods of Sass et al. (1983). Mineralogy was verified as >99% calcite by X-ray diffraction. A JEOL JSM-6400 scanning electron microscope was used to characterize grain size and distribution (Figure 3–1). Using scanning electron

micrograph (SEM) images calibrated to an SRM 2090 SEM magnification standard, precise measurements of 250 individual grain edge lengths were obtained. These were then used to calculate the geometric specific surface area (A_{GEO}, $m^2\ g^{-1}$) using the following equations:

$$A_{GEO} = \sum_j A_j m_f \tag{3–1}$$

$$A_j = \frac{6\ell^2}{\rho\ell^3} = \frac{6}{\rho}\ell^{-1} \times 10^{-4} \tag{3–2}$$

$$m_f = \frac{m_j}{m_T} \tag{3–3}$$

$$m_j = \rho\ell^3 \tag{3–4}$$

$$m_T = \sum_j m_j \tag{3–5}$$

where, assuming cubic geometry, A_j is the surface area per gram of grain j ($m^2\ g^{-1}$), ℓ is its edge length (cm), m_f is its mass fraction, and m_j is its mass (g), and ρ = calcite bulk density (2.71 g cm^{-3}). The geometric surface area calculated from these equations (0.91 $m^2\ g^{-1}$) was in excellent agreement with a separate determination by N_2-BET gas absorption (0.95 $m^2\ g^{-1}$) (Brunauer et al., 1938).

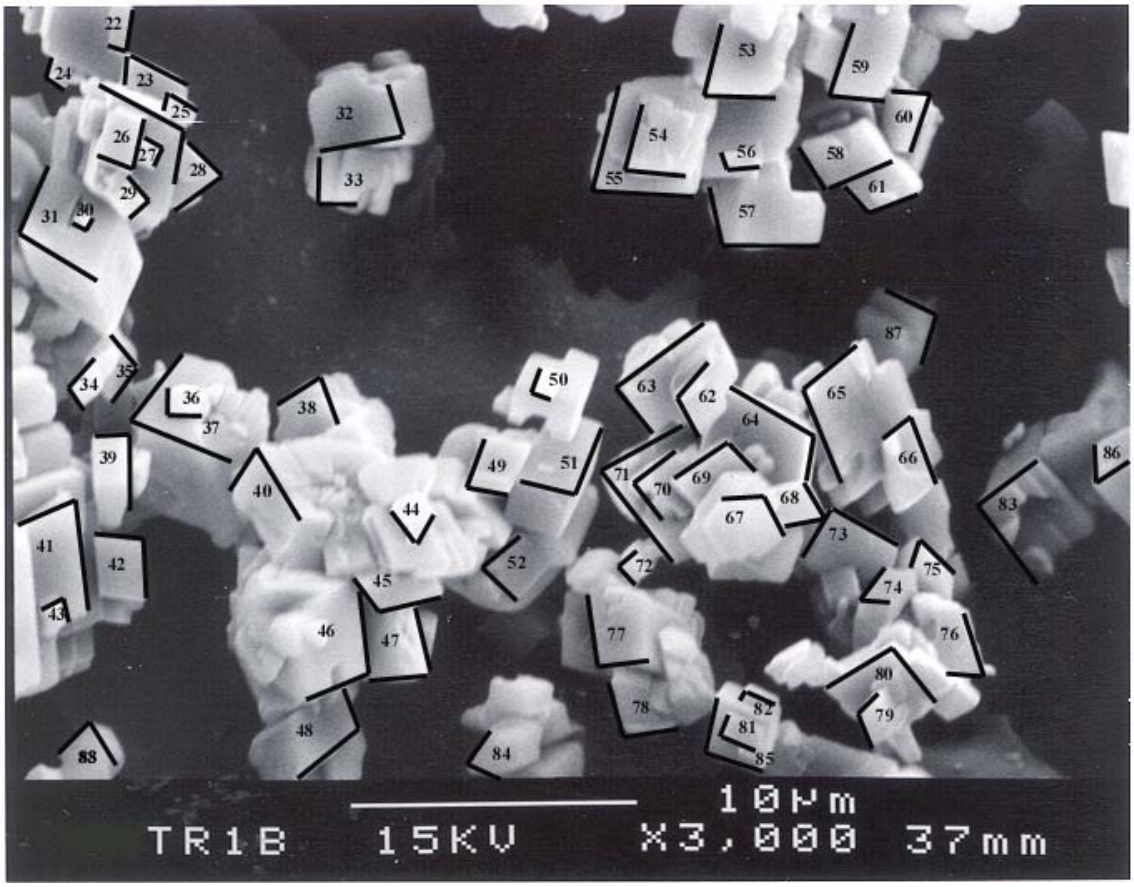

Figure 3–1. Scanning electron micrograph of acid treated A.C.S. reagent powder calcite. Magnification is x3000 and scale bar = 10 μm. Geometric surface area was estimated from the average of two edge lengths of each grain (black lines).

There were two reasons why this fine grain size, high specific surface area powdered calcite was specifically chosen in these early experiments. First, when contending with an open system it can be difficult to precisely balance the water vapor flux of the reactor. Over extended periods, a small imbalance can result in dilution or enrichment of the reacting solution thereby complicating the interpretation of the rate of dissolution. A high specific surface area assured that the reaction could be followed through to near equilibrium in a relatively short time (< 3 hours) thus mitigating this effect. Second, if the particle radius is <10 μm, then the velocity of the crystal relative to the surrounding fluid is low making convection negligible (Nielsen and Toft, 1984), and thus simplifying the hydrodynamics of the system and eliminating a potential stirring rate dependence on the reaction rate.

3.1.3. Solution Chemistry

Solution chemistry was determined using the methods described in Chapter II. These included the analysis of the salts (Ca^{2+}, total hardness and Cl^-) and the carbonic acid parameters TA and TCO_2. In addition, solution pH was measured with an Orion 720A potentiometer using the modified approach of Knauss et al. (1990). The method seeks to avoid the problems associated with pH measurement in high ionic strength solutions by referencing the H^+-selective electrode to a solid state Cl^- ion selective electrode, thereby avoiding a liquid junction potential.

While calibration of pH electrodes is commonly made with respect to NBS buffers, this approach is generally accurate only in dilute solutions. Since standard buffers are not readily available for solutions exhibiting the high ionic strengths used in

this study, the electrodes were calibrated directly to the EQPITZER software from measurements of the initial and final TA and TCO_2 of the experimental solutions. Coupling these two carbonic acid system parameters with the solution composition, a "Pitzer scale" pH could be calculated using EQPITZER at the start and terminus of each experiment. The electrode response slope (S_x) could then be established using a two-point calibration from:

$$S_x = \frac{E_f - E_i}{pH_i - pH_f} \qquad (3–6)$$

where E is the emf and pH is the calculated "Pitzer pH", initial (*i*) and final (*f*). Electrode response in the brines was typically within 10% of the ideal Nernst value (Table 3–2). The Knauss method is internally consistent with the EQPITZER software since it was used in the CO_2-system Pitzer parameter determinations of He and Morse (1993).

3.2. Experimental

The 550 ml water-jacketed reaction vessel accommodated a gas feed, two electrodes, vent, temperature probe, and sampling port (Figure 3–2). The solution was stirred at constant rate with a propeller shaft that passed through the top of the reaction vessel. Temperature (25 ±0.1 °C) and pCO_2 were maintained in the same manner as that described in Chapter II and similarly included the use of gas humidifiers.

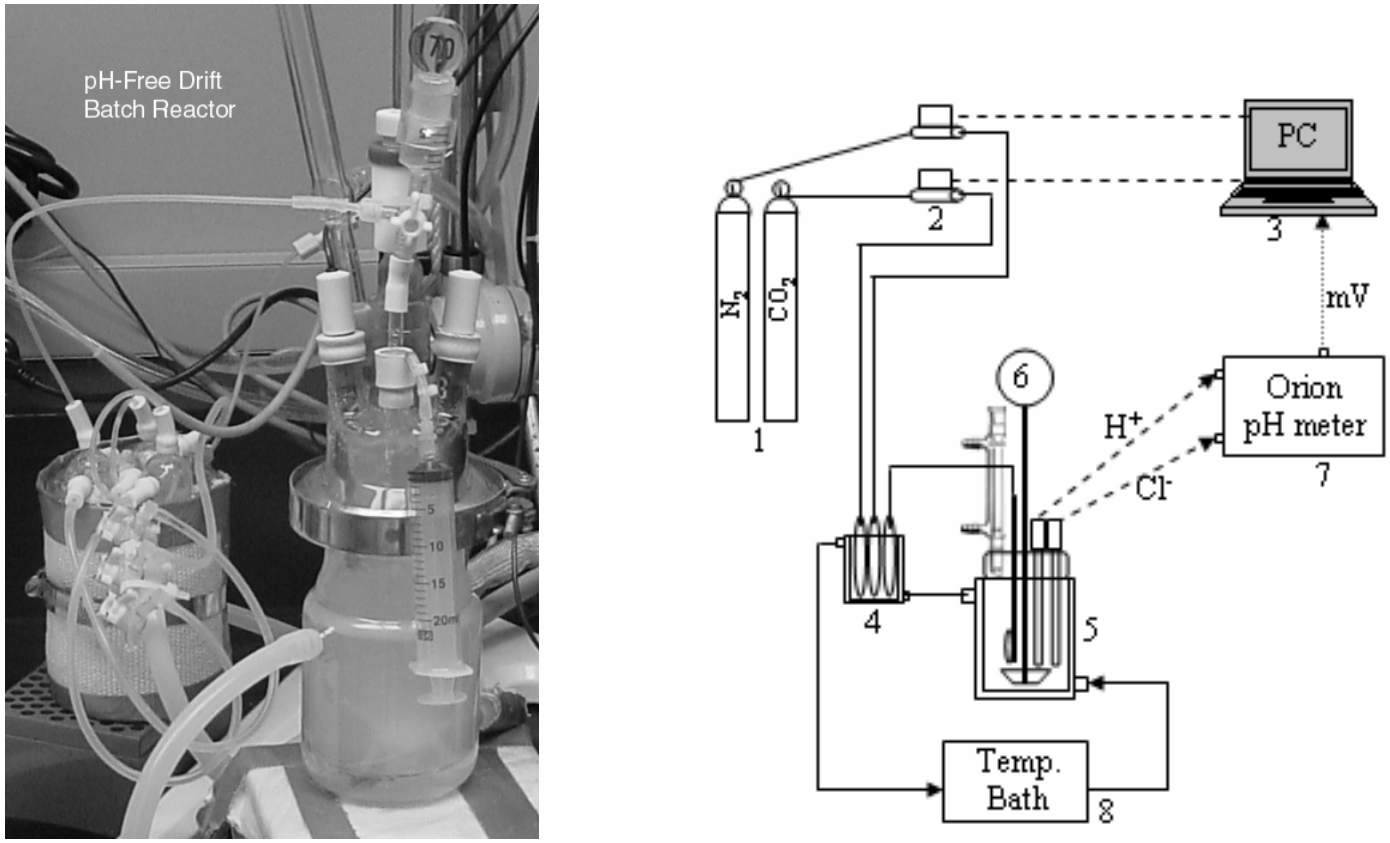

Figure 3–2. Open system pH-free-drift batch reactor used to measure calcite dissolution rates in concentrated synthetic brines. Photo image shows the reactor (foreground) and gas humidifier. The elements of the experimental setup are illustrated in the schematic: 1) high grade nitrogen and carbon dioxide gas; 2) dual MKS® Type 1479A mass-flow regulators; 3) computer; 4) gas humidifier; 5) batch reactor; 6) stir motor; 7) Orion® 720A pH meter; 8) Neslab® RTE-8DD circulating bath.

The initial conditions of the brines prior to calcite addition were established by bubbling with a pure CO_2 gas stream at a flow rate of 2 L min^{-1} followed by addition of a concentrated primary standard grade Na_2CO_3 solution sufficient to establish the $CaCO_3$ saturation state (Ω) at approximately 0.2. The solution was then equilibrated with the gas phase for several hours and the electrodes were allowed to stabilize. The emf was recorded, and a 10 ml aliquot was drawn for the initial determination of key parameters (Cl^-, Ca^{2+}, Mg^{2+}, TA and TCO_2). Powdered calcite was then added to the reaction vessel at 200 mg in excess of its predicted consumption, and changes in solution emf were measured with reaction time.

After 1 hour, the rate of change was typically too slow to resolve from electrode "noise". A final emf value was then recorded and a second aliquot drawn and filtered through a Millipore 0.45 μm syringe filter for determination of final Pitzer-scale pH for electrode calibration. The change in solution composition continued to be monitored by hourly sampling until, within experimental error, steady-state was achieved. The system typically achieved steady-state within 2 hours.

3.3. Results

Table 3–2 lists the CO_2-related parameters at the start of each experiment and the mean steady-state values. Figure 3–3 shows the raw pH data as a function of time. Calculated pH values from direct sample analysis illustrate the stability of the system at steady-state.

Table 3–2. Initial ($_i$) and steady-state ($_{ss}$) carbonic acid system parameters for the synthetic brines and pseudo-seawater (psw). Electrode response is reported as percent Nernstian. The pCO_2 was derived using EQPITZER from coupling TA and TCO_2 and the value reported is the mean of the initial and final conditions.

Brine ID	pH_i	pH_{ss}	electrode response	TA_i *(meq $kg^{-1}H_2O$)*	TA_{ss} *(meq $kg^{-1}H_2O$)*	TCO_{2i} *(molal)*	TCO_{2ss} *(molal)*	pCO_2 *(bar)*
psw_a	5.794	6.059 ±0.015	88%	15.7	27.2 ±0.2	0.0443	0.0541 ±0.0007	0.98 ±0.00
psw_b	5.983	6.099 ±0.010	91%	22.1	28.4 ±0.2	0.0480	0.0539 ±0.0007	0.86 ±0.01
brine 1	5.409	5.776 ±0.009	83%	6.2	14.2 ±0.2	0.0319	0.0394 ±0.0008	0.88 ±0.01
brine 2	5.368	5.737 ±0.005	94%	6.0	13.5 ±0.1	0.0320	0.0385 ±0.0003	0.92 ±0.03
brine 3	5.297	5.646 ±0.001	96%	5.2	11.6 ±0.1	0.0290	0.0353 ±0.0005	0.91 ±0.02
brine 4	5.187	5.599 ±0.009	89%	3.8	9.7 ±0.1	0.0244	0.0298 ±0.0003	0.86 ±0.01
brine 5a	5.079	5.438 ±0.028	112%	3.2	7.3 ±0.1	0.0233	0.0274 ±0.0012	0.95 ±0.06
brine 5b	5.071	5.481 ±0.011	96%	2.8	7.6 ±0.1	0.0208	0.0264 ±0.0004	0.88 ±0.04
brine 6	5.054	5.433 ±0.008	106%	2.3	6.4 ±0.1	0.0170	0.0235 ±0.0002	0.83 ±0.09
brine 7a	4.790	5.429 ±0.003	86%	1.4	5.8 ±0.1	0.0181	0.0217 ±0.0001	0.98 ±0.00
brine 7b	4.733	5.399 ±0.006	86%	1.2	5.6 ±0.0	0.0176	0.0218 ±0.0001	0.90 ±0.00

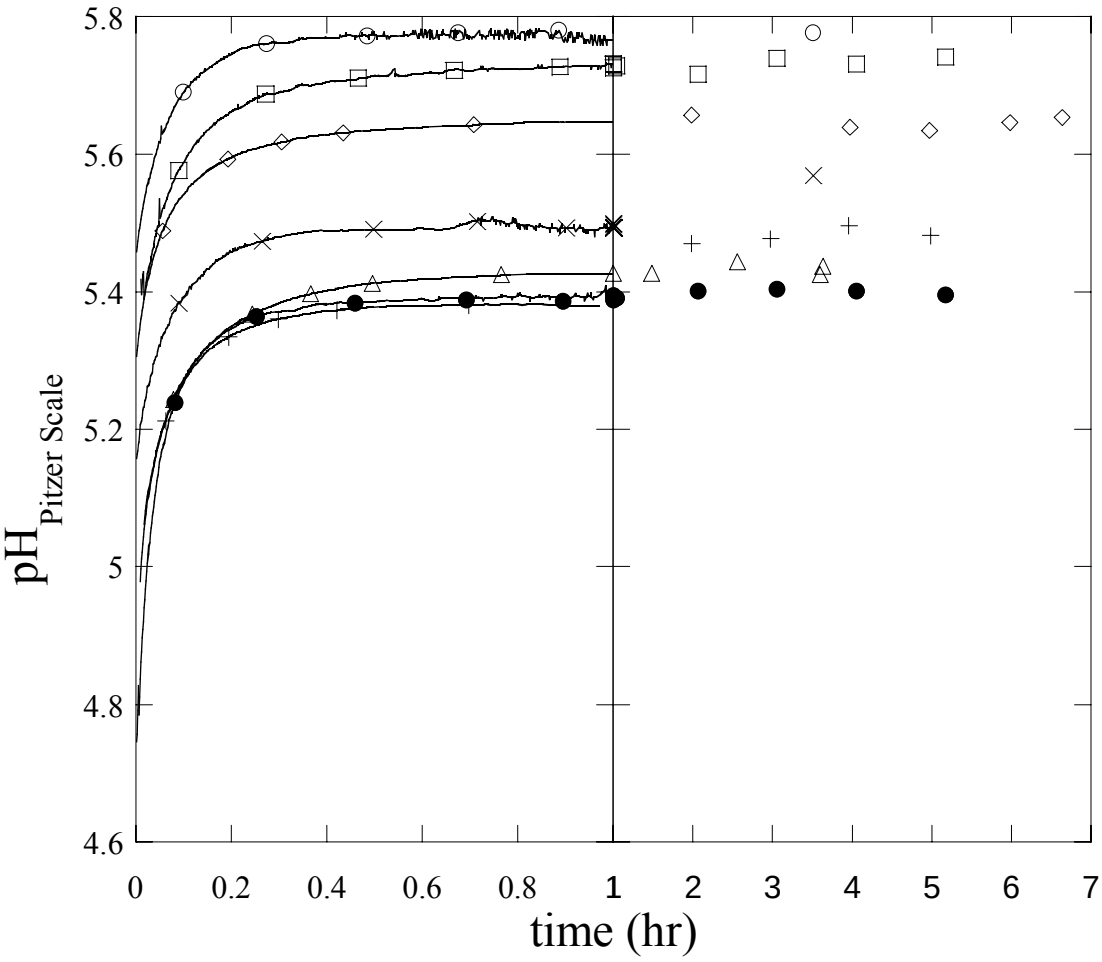

Figure 3–3. Pitzer-scale pH as a function of time as measured *in situ* from electrodes out to 1 hour (line trace) and then as calculated from direct sample analysis (values >1 hour). Brine 1 (open circle), brine 2 (open square), brine 3 (open diamond), brine 4 (x), brine 5 (+), brine 6 (open diamond), brine 7 (solid circle).

3.3.1. Calculation of Dissolution Rate

The dissolution of 1 mole of calcite contributes 2 moles of TA, as given by the overall reaction,

$$CaCO_3 + H_2O \Leftrightarrow Ca^{2+} + 2HCO_3^- . \quad (3–7)$$

Thus, the dissolution rate can be defined from the time dependent rate of change in TA:

$$\frac{dCaCO_3}{dt} = \frac{1}{2}\left(V\frac{dTA}{dt}\right) \quad (3–8)$$

where V is the mass of solvent since molal units are used. This requires that the pH-time data be converted to TA-time. Since pCO_2 remained near constant over the course of the reaction, TA can be determined using EQPITZER by coupling pCO_2 and pH. A 7^{th}-order polynomial equation was fit to the resulting TA-time data, and the first derivative of the fitted equation applied to equation 3–8. As a result of the poor asymptotic properties of high order polynomial equations, the $\frac{dTA}{dt}$ data had to be truncated near the terminus. To avoid this, several other empirical fits to the data were attempted. However, none provided as complete a fit to the data as the high order polynomial despite its limitations when applied to very slow rates such as those measured very near equilibrium ($\Omega > 0.98$).

3.3.2. Surface Area Correction

The rate of dissolution calculated in equation 3–8 must be normalized to the surface area of calcite. The decrease in calcite surface area as a function of reaction extent was included in the rate calculations. The available surface area within the reaction vessel ($A_{rxn,t}$, m^2) at a given time t was estimated from:

$$A_{rxn,t} = W_t A'_{GEO,t} \qquad (3\text{–}9)$$

Where the first term (W_t) accounts for the loss of calcite mass and the second term ($A'_{GEO,t}$) corrects for the change in specific surface area. The loss of calcite mass is calculated from changes in TA by:

$$W_t = W_i - \left(\frac{1}{2} V (F.W.)(TA_t - TA_i) \right), \qquad (3\text{–}10)$$

where W_i is the initial calcite mass (g), V is mass of solvent (kg), F.W. is the formula weight of calcite, and TA_t and TA_i are alkalinities at time t and t = 0.

The term $A'_{GEO,t}$ is the specific surface area ($m^2\ g^{-1}$) at time t, and is solved using an iterative procedure. The approach assumes cubic geometry for each $CaCO_3$ grain, and that the activity of each calcite grain is equivalent per unit surface area. As a result of dissolution, the volume of grain *j* at time t ($v_{j,t}$) can be expected to vary approximately as follows:

$$v_{j,t} = \left(\frac{A_{j,t-1}}{6} \right)^{\frac{3}{2}} - R_t (\Delta t) 6 v_{j,t-1} v_m, \qquad (3\text{–}11)$$

where $A_{j,t-1}$ is the specific surface area of grain *j* calculated at the previous time increment (t–1) using equation 3–2; R_t is the surface area normalized dissolution rate (moles $m^{-2}\ hr^{-1}$) at time t, Δt is the time interval (hours) over which $\frac{dCaCO_3}{dt}$ is numerically differentiated, and v_m is the molar volume of calcite ($3.693 \times 10^{-5}\ m^3\ mole^{-1}$). A corrected surface area for grain *j* ($A'_{j,t}$) is then calculated,

$$A'_{j,t} = 6 (v_{j,t})^{\frac{2}{3}}. \qquad (3\text{–}12)$$

The corrected grain dimension ($\ell'_{j,t}$) is calculated from rearrangement of equation 3–2 and $A'_{GEO,t}$ calculated from equations 3–1 through 3–5. The surface normalized rate is then recalculated and the process iterated several times. The available surface area within the reaction vessel at time t ($A_{rxn,t}$) is then calculated from equation 3–9.

The effect on the specific surface area was minor but the loss of calcite was significant in some cases (Figure 3–4). This issue was resolved in later experiments (see Chapter IV) where a coarser calcite was used. In terms of the effect on available surface area, the increase in specific surface area tended to partially offset loss of calcite mass. The total decrease in surface area over an experimental run was typically about 30%.

A MATLAB software program was developed that facilitated these rate calculations along with the model fitting that will described in following discussion. The program along with output for each of the experiments is presented in Appendix II.

3.4. Discussion

Rate data were modeled using the general rate equation (see Morse and Arvidson, 2002, for discussion of application of different types of rate equations to calcite dissolution). The general rate equation is (e.g., Morse and Berner, 1972):

$$R = -\frac{dm_{calcite}}{dt} = k(1-\Omega)^n \qquad (3\text{–}13)$$

where R is the rate (mole m^{-2} hr^{-1}), m is moles of calcite, t is time, k is the empirical rate constant, and n is the reaction order. The equation describes the

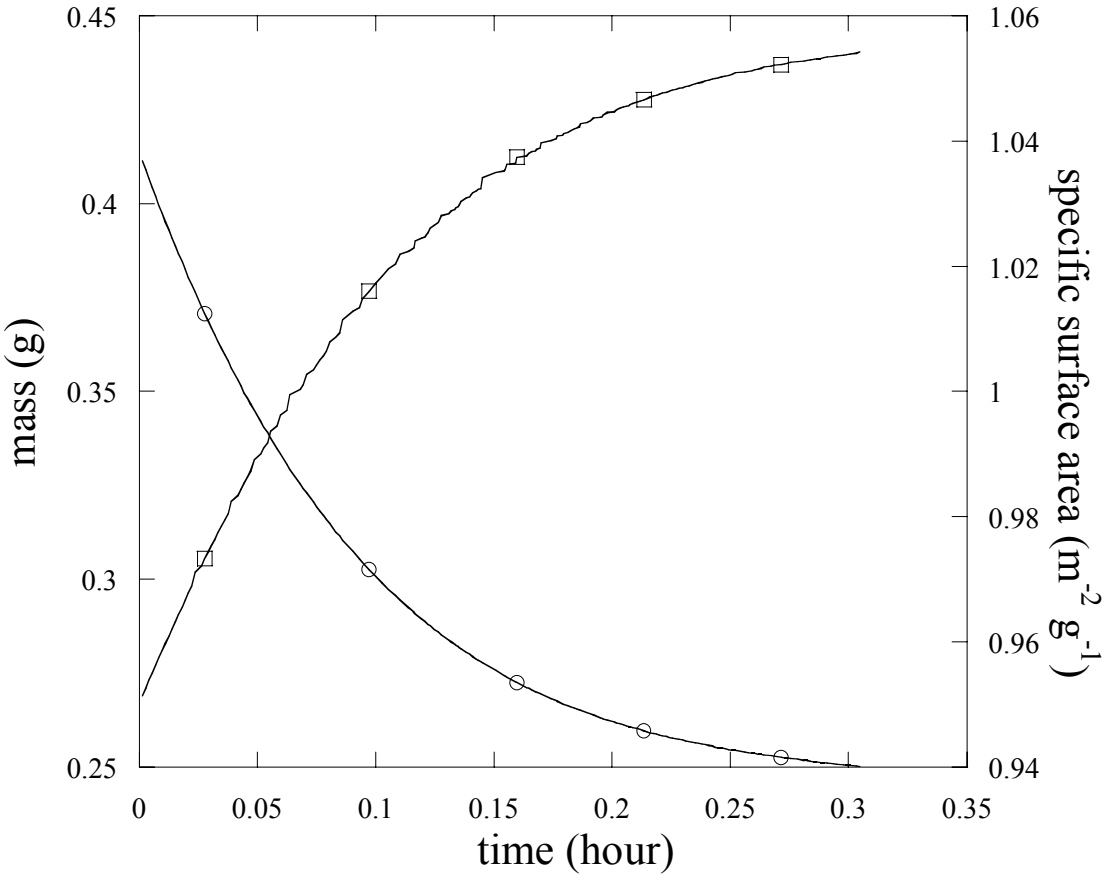

Figure 3–4. The change in calcite mass. The calculated change in calcite mass (open circle) and corresponding change in specific surface area (open square) as a result of dissolution for the brine 1 experiment.

rate as a function of saturation state (Ω) (see Chapter II, equation 2–3) where 1 - Ω represents the extent of disequilibrium. Jeschke and Dreybrodt (2002) showed that when rates are modeled using this equation, small uncertainties in the IAP_{ss} used to calculate Ω can have a pronounced effect on the interpreted reaction order (*n*) and rate constant (*k*). Such effects are particularly pronounced under near equilibrium conditions as is the case in these experiments.

As was established in Chapter II, EQPITZER failed to correctly predict equilibrium in these concentrated solutions yielding Ω > 1 at steady state. Furthermore, there was considerable variability amongst replicate solubility experiments. Therefore, to model the rate data, the Ω value in equation 3–13 was derived from an apparent kinetic equilibrium IAP specific to each rate experiment. The following discussion describes how this value was derived.

3.4.1. Apparent Kinetic Equilibrium

Figure 3–5 shows the change in carbonate ion activity as a function of dissolution rate for each of the synthetic brines. In all cases a near linear correlation was observed. The apparent carbonate ion activity ($a^*_{CO_3^{2-}}$) when the rate is zero was estimated from the intercept of a linear least square regression (Table 3–3). Given that in these calcium-rich solutions the calcium activity remains nearly constant, the apparent saturation state (Ω^*) could be closely approximated by

$$\Omega^* = \frac{a_{Ca^{2+}} a_{CO_3^{2-}}}{K^*_{eq}} \approx \frac{a_{CO_3^{2-}}}{a^*_{CO_3^{2-}}} \qquad (3\text{–}14)$$

where K^*_{eq} is the apparent IAP at equilibrium (IAP*) calculated as the product of $a^*_{CO_3^{2-}}$ and the average steady state calcium ion activity.

As shown in Figure 3–6, IAP* was generally in close agreement with the measured steady state IAP and exhibited a similar trend to that observed in the solubility experiments in which they systematically exceed K_c with increasing brine concentration. However, in most cases the kinetic experiments yielded somewhat lower steady state IAP's than observed in the solubility experiments. This may indicate that the steady state conditions observed in the kinetic experiments represent a metastable equilibrium and that given sufficient time the system reestablishes a new equilibrium. However, the predominant free energy driving the dissolution is clearly relative to this initial metastable phase.

When modeled with respect to the apparent saturation state, first-order kinetics (n = 1) were sufficient to provide an excellent fit to the rate data. Reported in Table 3–3 are the k values (mmole m^2 hr^{-1}) along with the correlation coefficients. In general the rates decrease with increasing brine concentration although the relation is complex and will be further examined in Chapter IV. It is remarkable that given the extreme variability in brine concentration, the rate constants agree to within 20% (51.5 ±8.4 mmole m^2 hr^{-1}).

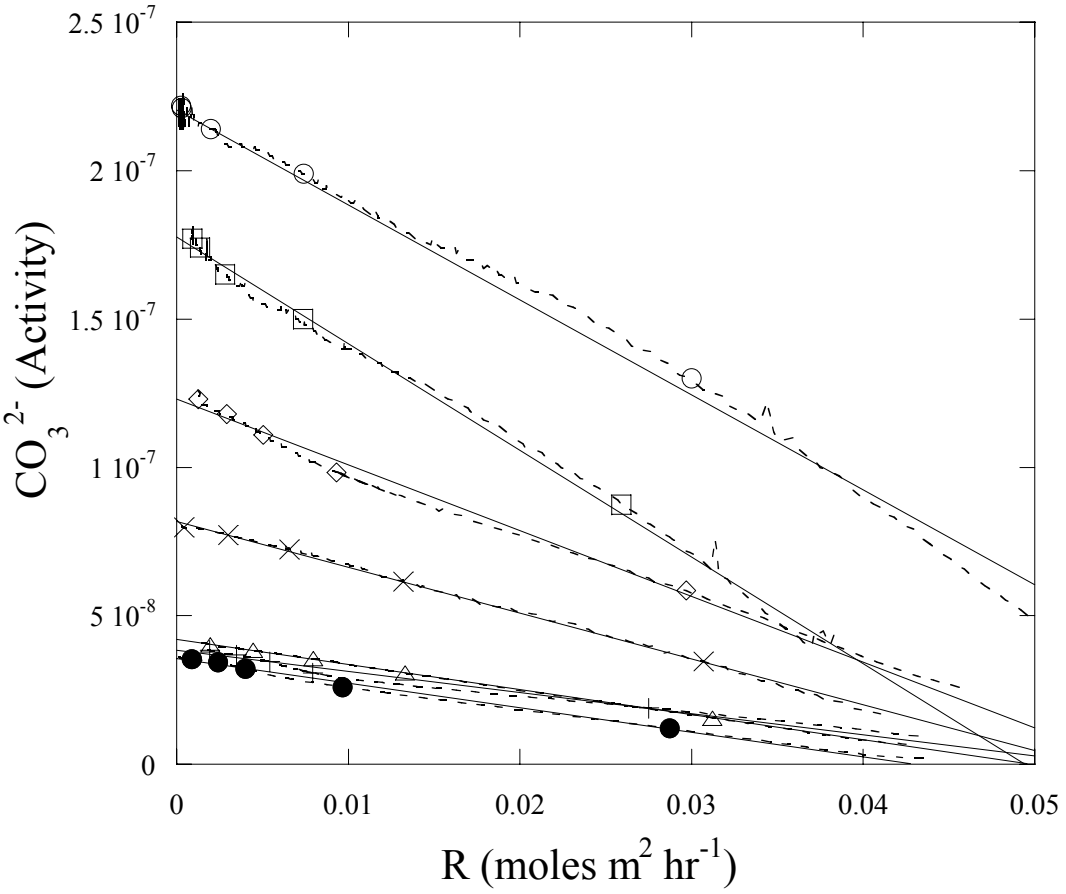

Figure 3–5. The apparent carbonate ion activity as calculated from the experimental data using EQPITZER as a function of dissolution rate (dashed lines). Solid lines are linear least square regression fits of the experimental data. Brine 1 (open circle), brine 2 (open square), brine 3 (open diamond), brine 4 (x), brine 5_a (+), brine 6 (open diamond), brine 7_a (solid circle).

Table 3–3. The apparent carbonate ion activity at equilibrium ($a^*_{CO_3^{2-}}$) predicted from regression analysis in Figure 3–5. The rate constant (k, mmole m^2 hr^{-1}) for the general rate equation in which n = 1 yielded and excellent fit of rate data when modeled as a function of Ω^*.

Brine ID	$a^*_{CO_3^{2-}}$ x10^8	k	r^2
psw_a	84.8	55.9	0.986
psw_b	97.3	63.3	0.956
brine 1	22.3	66.6	0.993
brine 2	18.6	48.1	0.993
brine 3	12.7	54.7	0.991
brine 4	8.1	51.7	0.998
brine 5_a	4.8	52.5	0.973
brine 5_b	5.5	43.7	0.994
brine 6	4.3	48.2	1.000
brine 7_a	4.1	42.1	0.992
brine 7_b	3.6	39.6	0.987

In contrast to this study, the general rate equation has typically yielded reaction orders between 3 and 4 (e.g., Berner and Morse, 1974; Morse and Arvidson, 2002) when applied to calcite dissolution in complex natural waters (e.g., seawater). However, first-order kinetics for calcite dissolution is not unprecedented. When Arakaki and Mucci (1995) measured calcite dissolution rates in solutions near saturation ($0.1 < \Omega < 0.8$) they found that their mechanistic dissolution model predicted first-order dissolution kinetics. Furthermore, when Hales and Emerson (1997) reexamined experimental data of the dissolution rate of reagent grade calcite in seawater, they found that their original conclusion of a rate law with 4.5-order dependence was very sensitive to uncertainties in the Ω with respect to calcite. When they applied an apparent kinetic solubility product, the dissolution rate could be adequately described by first-order kinetics.

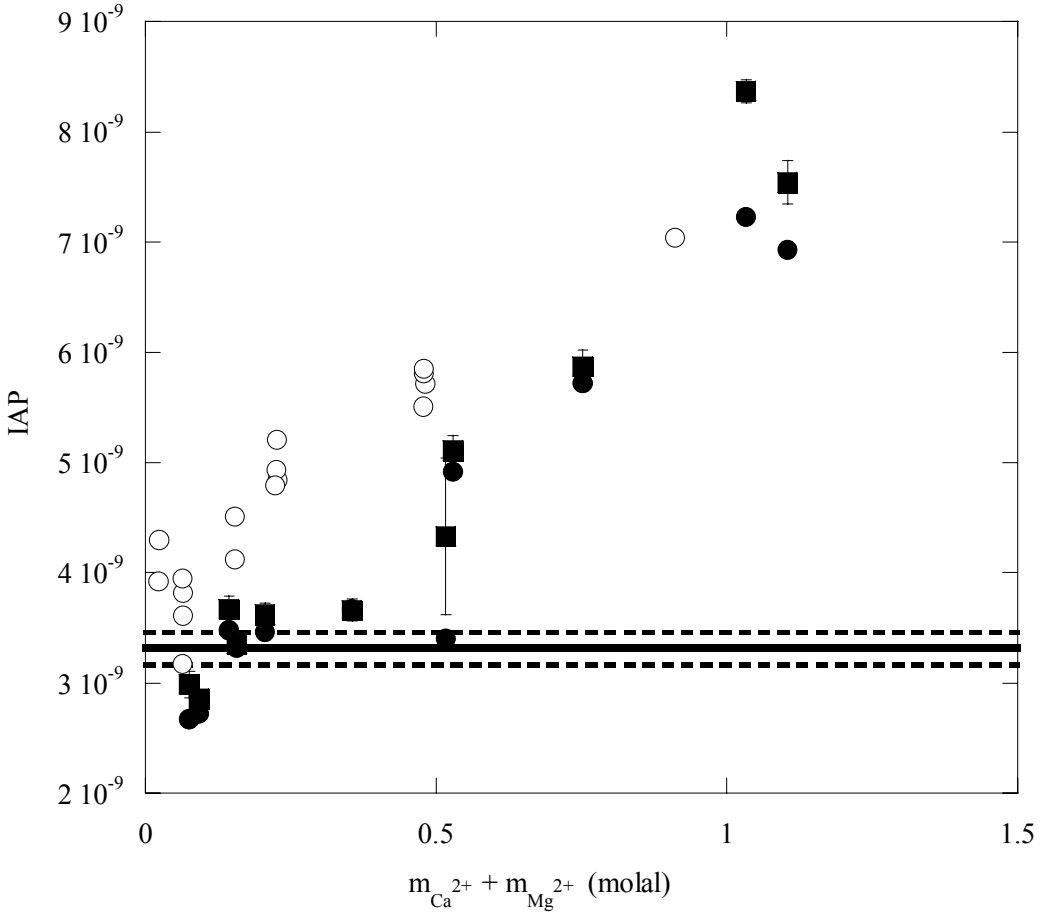

Figure 3–6. The apparent kinetic equilibrium IAP (solid circle) was in close agreement in most cases with the measured steady state IAP (solid square). Values systematically exceeded K_c (lines) with increasing brine concentration similar to that observed in the solubility experiments (open circle), although to a lesser extent.

Another consideration is that the pseudo-seawater used in this study was phosphate-free unlike natural seawater. Morse (1974) demonstrated that although phosphate contributes a minor change on the rate constant, it can have a pronounced effect on the reaction order. Its absence in these solutions may explain the linear dependence on undersaturation. Sjöberg (1978) reported a reaction order close to 2 for a pseudo-seawater prepared in a similar fashion to the one used here but containing sulfate. Gutjahr et al. (1996b) examined the effect of modest amounts of calcium on the dissolution kinetics of calcite and also reported values close to first-order.

3.4.2. Surface versus Diffusion Controlled Processes

Calcite dissolution can proceed by both surface reaction and mass transport processes. Which of the two processes exhibits a dominant control on the observed rates can be determined by comparing the theoretical diffusion-controlled rate (R_D) to the measured rate (R). A similar approach, using the control index (q_D) of Nielsen and Toft (1984), was employed by Zhang and Dawe (1998) to evaluate the controlling mechanism of calcite growth in high salinity water. They defined the equation;

$$q_D = \frac{R}{R_D}. \qquad (3\text{–}15)$$

When $q_D \leq 0.1$, surface reactions dominate the dissolution, and when $q_D \geq 0.9$, diffusion dominates. Values between $0.1 < q_D < 0.9$ indicate a mixed kinetic regime where rates show intermediate behavior (Morse and Arvidson, 2002). The theoretical diffusion-controlled rate (R_D) was estimated using the method of Morse and Berner (1972):

$$R_D = \frac{DA}{r}\left[\left(\overline{m}_{HCO_3^-} - m_{HCO_3^-}\right) + \left(\overline{m}_{CO_3^{2-}} - m_{CO_3^{2-}}\right)\right], \qquad (3\text{–}16)$$

where D is the diffusion coefficient (assumed 3.6×10^{-5} m^2 hr^{-1}), A is the surface area of the calcite, r is the crystal particle radius (~3.5 μm), and $\overline{m}_j$ and m_j denote the concentration of the j^{th} species in the solution layer adjacent to the crystal surface and in the bulk solution respectively. The thickness of the stagnant boundary layer was not considered because the particle radius was <10 μm and the low velocity of the crystal relative to the surrounding fluid makes convection negligible (Nielsen and Toft, 1984).

As a first-order approximation it was assumed that $m_i = \overline{m}_i$. While this will produce an overestimation for R_D, the approximation is sufficient in this case since, for all experiments, experimental rates (R) are two to three orders of magnitude less than theoretical diffusion rates (R_D) (Figure 3–7). Since $q_D << 1$ across the range of modeled saturation states, the dissolution is dominated by surface controlled processes. This is to be expected provided the near saturation region over which these rates were measured (e.g., Plummer et al., 1979; Busenberg and Plummer 1986; Morse and Arvidson, 2002; Brantley, 2004) R_D rates tended to decrease with increasing brine concentration. These slower diffusional rates are a consequence of the proportional decrease in equilibrium carbonate ion concentration with increasing calcium, thus resulting in smaller concentration gradients.

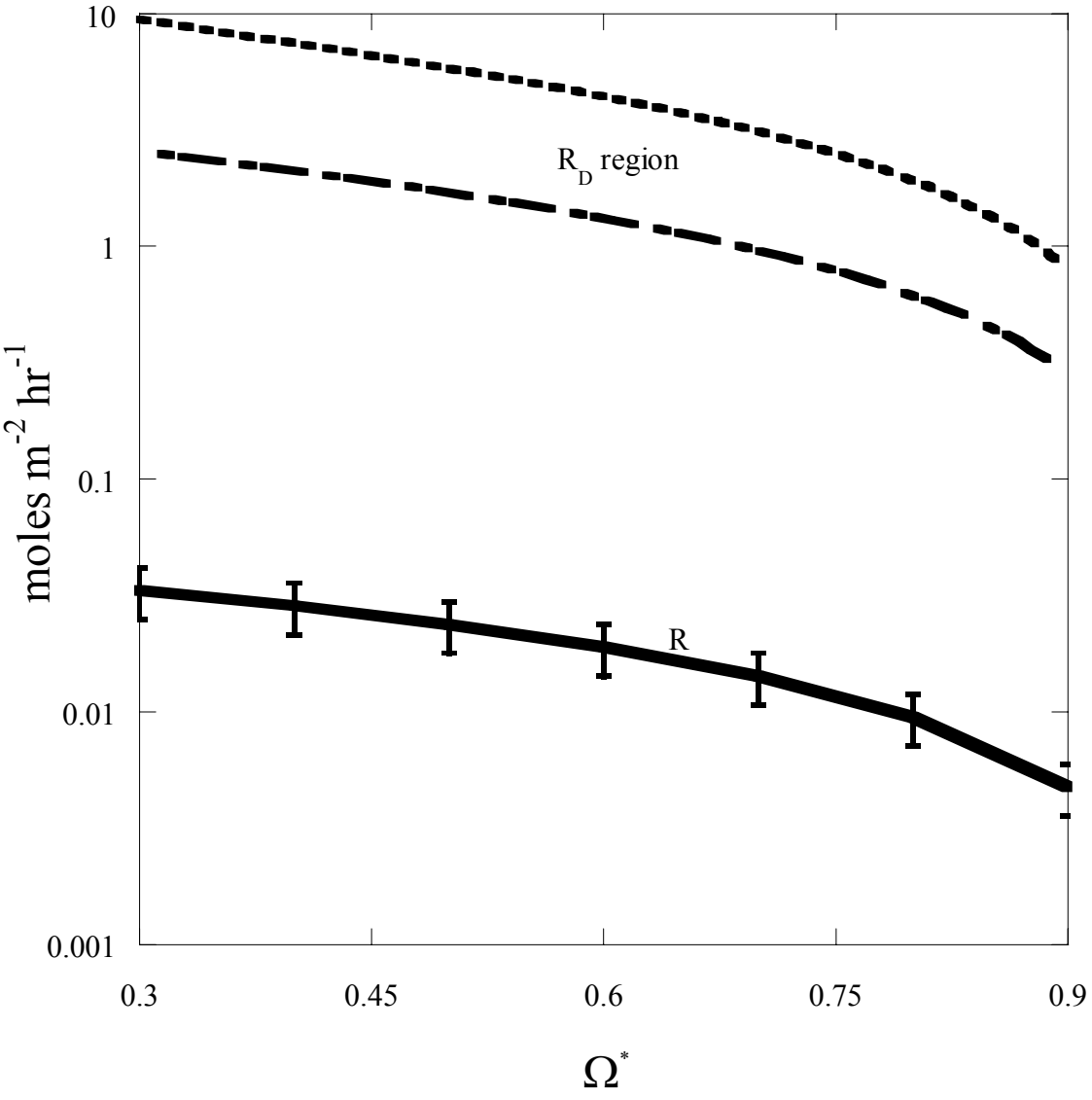

Figure 3–7. Theoretical versus measured diffusion rates. Theoretical diffusion rates for dissolution (R_D) are 2 to 3 orders of magnitude greater than the experimental rates (R) indicating surface controlled kinetics. The upper limit of the range in the R_D is bounded by the pseudo-seawater R_D while the lower limit is bonded by the most concentrated brine (brine 7). Thus, the rate of theoretical diffusion decreases with increasing brine concentration.

3.5. Conclusion

An open-system pH-free-drift technique was employed to measure calcite dissolution rates in synthetic brines at 1 bar pCO_2 for brines ranging in concentration from simple seawater (35 g L^{-1}) to 179 g L^{-1}. Dissolution rates were modeled using the general equation ($R = k(1-\Omega)^n$). Observed rates were two to three orders of magnitude smaller than theoretical diffusional rates, over the range of saturation states modeled. Rates generally decreased with increasing brine concentration, but despite the large compositional range of the brines, rates varied by only about 20%. The mean rate constant (k) is 51.5 ±8 mmole m^2 $hr^{-1}$and the reaction order (n) could be assumed unity (n = 1). These rates are in good agreement with previous studies under high pCO_2 conditions.

CHAPTER IV

CALCITE DISSOLUTION KINETICS IN GEOLOGICALLY RELEVANT BRINES

This chapter presents the findings from experiments similar to those conducted in Chapter III, but with important refinements made to the experimental methods that allowed for investigations over a broader range of conditions including lower pCO_2 and higher temperature. This series of experiments sought to determine the specific effects of temperature, pCO_2, and solution composition on the rate of calcite dissolution for a broad range of geologically relevant brines. Dissolution rates were measured at 25, 52.5 and 80 ºC and near 1, 0.5 and 0.1 bar pCO_2. The dissolution experiments were performed in synthetic brines at ionic strengths and calcium and magnesium concentrations more typical of worldwide subsurface brines than those explored in the previous chapter. In addition to examining the combined effect of covarying calcium, magnesium and ionic strength in a geologically meaningful way, the specific effects of each of these solution parameters was investigated. Finally, the effect of a common natural inhibitor which has a highly variable concentration in natural brines, SO_4^{2-}, was also investigated. Multiple regression analysis was used to produce an empirical model capable of predicting the rate of dissolution in solutions typical of many subsurface formation waters.

4.1. Materials and Methods

4.1.1. Aqueous Solutions

The composition of the synthetic brines prepared for these experiments was based on the relation between total dissolved solids (TDS, g L^{-1}) and the major dissolved species observed by Hanor (1994b). Figure 4–1 shows the calcium, magnesium concentrations, and ionic strength that are predicted from TDS content based on those relations.

Three 'model' brines were prepared with calcium, magnesium and ionic strength equivalent to subsurface brines exhibiting approximate TDS values of 50, 125 and 200 g L^{-1}. Although these solutions were similar in both magnesium concentration and ionic strength to those investigated in Chapter III, they exhibited only about half the calcium enrichment with increasing TDS (Figure 4–1). This lower calcium enrichment is both more typical of most subsurface brines and also resulted in a higher carbonate carrying capacity, making the observed change in solution chemistry as a result of calcite dissolution more pronounced. This made it considerably easier to make robust rate measurements in comparison with the earlier experiments.

The preparation of each brine was done in the same manner described in Chapter II. In addition, phosphate measurements were made on the concentrated stock solutions from which the brines were prepared according to the methods of Murphy and Riley (1962) and in all cases were found to be below our detection limit (< 1 μM). The initial chemical compositions are presented in Table 4–1.

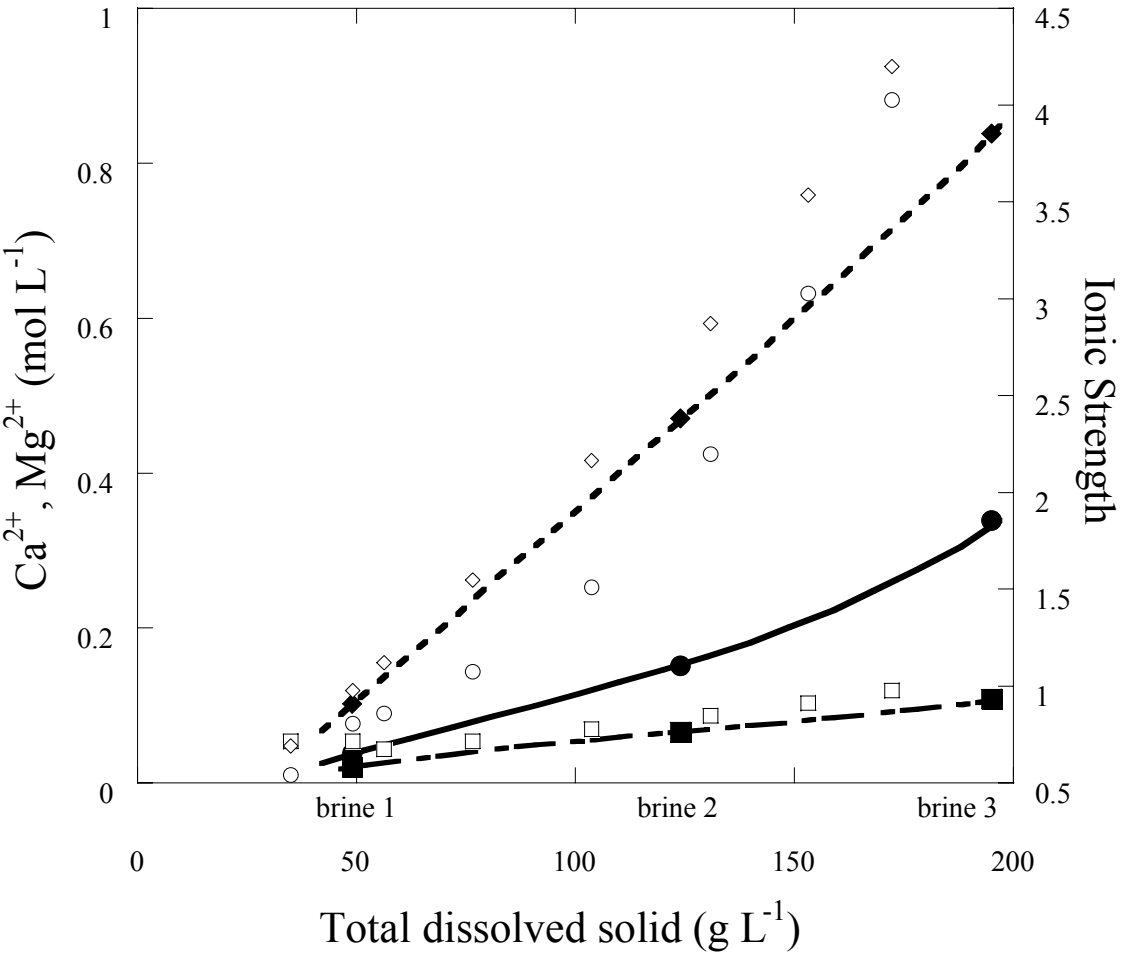

Figure 4–1. The chemistry of the 'model' brines. The brines prepared for these experiments were based on the relation between TDS and major dissolved species concentration observed by Hanor (1994b). Three brines were prepared whose calcium (solid circle), magnesium (solid square) and ionic strength (solid diamond) were equivalent to subsurface brines exhibiting approximate TDS concentrations of 50, 125 and 200 g L^{-1}. For comparison, the brine compositions of the Chapter III solutions are also shown (open scatter points). Note the differences in scale of the two ordinate axes.

Table 4–1. Initial solution concentration and experimental conditions. For each experiment concentration (molal), gas composition is X_{CO2}, temperature (ºC), and reactor stirring rate (RPM) are given. The gas mixture was balanced with nitrogen.

Brine	Experiment	Ca^{2+}	Mg^{2+}	Na^{+}	Cl^{-}	SO_4^{2-}	I	X_{CO2}	ºC	RPM
1	PCO2_01	0.0387	0.0229	0.7390	0.8504	0.0000	0.9235	1.0	25.0	300
2	PCO2_02	0.1574	0.0651	1.8210	2.2610	0.0000	2.4889	1.0	25.0	300
3	PCO2_03	0.3472	0.1223	2.7310	3.6670	0.0000	4.1395	1.0	25.0	300
1	PCO2_04	0.0391	0.0217	0.7351	0.8485	0.0000	0.9175	0.5	25.0	300
2	PCO2_05a	0.1622	0.0677	1.8270	2.2830	0.0000	2.5169	0.5	25.0	300
2	PCO2_05b	0.1543	0.0703	1.7660	2.2110	0.0000	2.4399	0.5	25.0	500
2	PCO2_05c	0.1557	0.0656	1.6980	2.1360	0.0000	2.3611	0.5	25.0	700
3	PCO2_06	0.3509	0.1234	2.7270	3.6740	0.0000	4.1501	0.5	25.0	300
1	PCO2_07	0.0388	0.0228	0.7398	0.8592	0.0000	0.9247	0.1	25.0	300
2	PCO2_08	0.1549	0.0660	1.7690	2.2090	0.0000	2.4312	0.1	25.0	300
3	PCO2_09	0.3572	0.1177	2.6560	3.6050	0.0000	4.0806	0.1	25.0	300
2	TEMP_03a	0.1586	0.0656	1.7640	2.2100	0.0000	2.4363	0.5	52.5	300
2	TEMP_04a	0.1531	0.0678	1.7740	2.2140	0.0000	2.4366	0.5	80.0	300
2	Ca_01a	0.0410	0.0705	2.2220	2.4340	0.0000	2.5549	0.5	25.0	300
2	Ca_02a	0.3579	0.0626	1.2200	2.0570	0.0000	2.4815	0.5	25.0	300
2	I_01a	0.1522	0.0701	0.2504	0.6903	0.0000	0.9172	0.5	25.0	300
2	I_02a	0.1613	0.0743	3.3700	3.8370	0.0000	4.0763	0.5	25.0	300
2	Mg_01a	0.1637	0.0172	1.9740	2.3320	0.0000	2.5165	0.5	25.0	300
2	Mg_02a	0.1577	0.1235	1.6870	2.2460	0.0000	2.5307	0.5	25.0	300
1	SO4_01a	0.0395	0.0237	0.7296	0.8215	0.0115	0.9303	1.0	25.0	300
2	SO4_02a	0.1537	0.0772	1.7770	2.2090	0.0117	2.4816	1.0	25.0	300
3	SO4_03a	0.3451	0.1292	2.6300	3.5490	0.0127	4.0656	1.0	25.0	300

4.1.2. Solids

Calcite rhombs (Iceland spar) obtained from Ward's Scientific Inc. were crushed into powder and wet sieved into >125 μm, 125–63 μm and 63–32 μm size fractions and treated as described in Chapter III. The geometric specific surface area (A_{GEO}) of the 125–63 μm and 32–63 μm size fractions was calculated from SEM micrographs as described in Chapter III. BET surface areas were obtained using krypton adsorption, which is more effective than nitrogen adsorption when contending with low surface area materials (Brantley, 2004).

The ratio of the specific surface area measured by gas adsorption to the geometric surface area defines the surface roughness (Helgeson, 1984), λ:

$$\lambda = \frac{A_{BET}}{A_{GEO}}. \qquad (4–1)$$

The mean grain size diameters and surface area parameters for all the calcite material used in this manuscript are summarized in Table 4–2. The 125–63 μm size fraction was used for these later rate experiments while the 63–32 μm fraction was chosen for the solubility experiments presented in Chapter III because its greater specific surface area allowed it to more rapidly achieve equilibrium.

Table 4–2. Grain size and surface area parameters.

Calcite	Sieve fraction (μm)	Mean grain diameter (μm)	A_{GEO} (m^2 g^{-1})	A_{BET} (m^2 g^{-1})	λ
Reagent Grade	powder	1.8	0.91	0.95	1.05
Iceland Spar	32–63	35.1	0.051	0.225	4.39
Iceland Spar	63–125	84.2	0.022	0.098	4.48

The higher roughness factors calculated for the crushed calcite may be attributed to complex microstructure resulting from grinding (Hodson, 1998) or from the presence of particulates (Brantley, 2004) not fully removed during the sonication. However, BET measurement of specific surface areas on laboratory-ground powders < 0.1 $m^2 g^{-1}$ has been found unreliable in many cases (Brantley and Mellott, 2000).

Furthermore, it may be more appropriate to use the geometric rather than the BET surface area when applied to mineral kinetics. Gas adsorption measures the total surface area that can include both external and internal surface area. Internal surface area includes cracks or connected pores that are deeper than they are wide and can develop during the grinding process (Jeschke and Dreybrodt, 2002). Advection can control transport to and away from external surfaces, while diffusion must control transport for internal areas (Hochella, 1988). This results in the net dissolution rate being dominated by the external surface area which is better approximated by geometric estimate.

For many silicate minerals, White et al., (1996) found a mean roughness factor of about 7 for a wide assortment of mineral particles. However, Walter and Morse (1984) calculated a surface roughness of close to 1 for crushed calcite rhombs of similar mean grain diameter to the 63–125 μm fraction. The disparity between the Walter and Morse (1984) study and the calcite used here may be a consequence of the BET measurement reliability and/or of calcite pretreatment. The custom-made BET apparatus used by them was specifically designed for very low specific surface area materials (Kanel and Morse, 1979) and is believed to have been considerably more sensitive than the commercial one used in this study. They also annealed their calcite after sonication

which may have helped to "heal" grinding induced fissures that would contribute to internal surface area. In any event, they too concluded that for texturally complex calcite the relative reactivity during dissolution may be more accurately estimated from surface geometry than from BET surface areas which can overestimate the amount of reactive surface area. Unless otherwise noted, the measured rates presented in this chapter are normalized to the geometric surface area. The appropriateness of this choice will be made clear in Section 4.4.4.

4.1.3. Solution Chemistry

The analysis of the salts (Ca^{2+}, total hardness, and Cl^-) and the carbonic acid system parameters TA and TCO_2, were performed using the methods described previously in Chapters II and III. The salt membrane of the chloride selective electrode used as a reference electrode for pH measurement in the earlier experiments was compromised by the corrosive nature of these concentrated brines. This resulted in electrode instability and poor and erratic electrode response that was considerably exacerbated at the elevated temperature of some experiments. Many of the latter experiments performed in Chapter III had to be discarded as a result of electrode failure.

For the experiments presented here, the H^+ selective electrode was referenced to a Single Refex® solid-state reference electrode. The Refex® reference electrode uses an ionically conductive hard-non-porous salt loaded polymeric matrix. The matrix acts as an immobilized electrolyte thus avoiding a porous liquid-junction. The calibration of the electrodes to "Pitzer scale" pH was performed in accordance to the methods detailed in Chapter III. The electrode response was considerably more stable and consistent than in

the prior experiments and in most cases yielded good agreement (90 ±5%) with the ideal Nernst value even at high temperature.

4.2. Experimental

The reaction vessel used in these experiments was a modified version of the one used in Chapter III. These experiments included high temperature and low pCO_2 conditions requiring that a water cooled condenser be adopted and improvements made to the gas dispersion. Gas previously was dispersed only by means of a submerged glass pipette tip, but this method was inefficient at maintaining constant pCO_2 in the reaction vessel under low CO_2 partial pressures. Therefore, a specially developed ground glass gas dispersion tube was used. Because calcite has been reported to become lodged in ground glass (Morse, 1973), the gas dispersion tube was only fritted on the downstream side.

Common to open-system free-drift experiments, if the initial rate of dissolution is too rapid, gas phase disequilibrium can occur in which there is an excess consumption of CO_2 relative to supply in the solution (Arakaki and Mucci, 1995). This can be avoided by: 1) conducting the dissolutions at high pCO_2 where appropriate; 2) reducing the available surface area; and 3) not initiating the experiments at extreme degrees of disequilibrium. In most cases, experiments were conducted near 0.5 bar pCO_2 or greater, although three experiments were conducted at < 0.1 bar pCO_2. In contrast to the Chapter III experiments, calcite of roughly an order of magnitude lower specific surface area was used. This produced considerably slower initial rates and meant that considerably more calcite could be added, reducing the change in surface area during the

experiments. Finally, as with the previous experiments, a concentrated primary standard grade Na_2CO_3 solution was added sufficient to establish the $CaCO_3$ saturation state (Ω) at approximately 0.2.

The initial conditions of the brines prior to calcite addition were established by bubbling with an ultra high purity nitrogen-CO_2 gas mixture appropriate for the desired experimental conditions (Table 4–1). The approximate mole fraction (X_{CO2}) was estimated from the ratio of the CO_2 flow rate (R_j) to the total gas flow rate,

$$X_{CO2} \approx R_{CO_2} / \left(R_{CO_2} + R_{N_2} \right). \qquad (4\text{–}2)$$

The total flow rate was fixed at 2 L min^{-1} for all experiments. The stirring rate was maintained at 300 rpm except where otherwise noted and the solution was equilibrated for several hours allowing the electrodes to stabilize. The initial emf was noted and a 20 ml aliquot drawn for solution analysis (Cl^-, Ca^{2+}, Mg^{2+}, TA and TCO_2).

Unlike the previous experiments, in which the calcite added varied, in these experiments the volume of solution to surface area ratio was maintained to a near constant with two exceptions. In the first two experiments (PCO2_06a and PCO2_07a), 1 g of calcite was added (V:A = 2.3 cm), but this proved to generate a $\frac{dpH}{dt}$ that was too slow (< 5 mV h^{-1}). These slow changes in solution chemistry made numerical differentiation of the rate data problematic since the high order polynomial equations used to fit the data are prone to oscillations when slopes approach zero. Therefore, in the remaining experiments 2 g of calcite (V:A = 1.1 cm) were added.

The calcite was allowed to react with the solution and changes in solution emf were measured. Because of the enhanced stability of the Refex® electrode, the reactions

could be followed for extended periods encompassing the entire duration of the reaction. The experiments were terminated typically after 5 hours at which point steady-state was achieved within the precision of measurement. A final emf value was noted and triplicate 20 ml samples were drawn and filtered through a Millipore 0.45 μm syringe filter for solution analysis and the results averaged. The calcite remaining in solution was then collected by vacuum filtration and briefly rinsed with milliQ® (18.1 μΩ) water. The filtered material was freeze dried and stored in a vacuum desiccator for later SEM imaging.

4.3. Results

Table 4–3 lists the CO_2-related parameters at the start of each experiment and the mean steady-state values. Calcite dissolution rates as a function of Ω^* were calculated from the equations presented in Chapter III facilitated by the MATLAB program provided in Appendix II. The apparent carbonate ion activity at equilibrium as extrapolated from the kinetic data ($a^*_{CO_3^{2-}}$) were in close agreement with the measured steady-state values ($a^{ss}_{CO_3^{2-}}$) (Table 4–4). The rates were modeled using the empirical rate equation, $R = k(1-\Omega)^n$ with $n = 1$ (first-order), and the rate constants were normalized to both the geometric surface area (k_{GEO}) and the BET surface area (k_{BET}) (Table 4–4). The MATLAB outputs have been complied in Appendix II for each of the experiments.

Table 4–3. Initial ($_i$) and steady-state ($_{ss}$) carbonic acid system parameters. Electrode response is reported as percent Nernstian. The pCO_2 was derived using EQPITZER from coupling TA and TCO_2 and the value reported is the mean of the initial and final conditions.

Experiment ID	pH_i	pH_{ss}	electrode response	TA_i *(meq $kg^{-1}H_2O$)*	TA_{ss} *(meq $kg^{-1}H_2O$)*	TCO_{2i} *(molal)*	TCO_{2ss} *(molal)*	pCO_2 *(bar)*
PCO2_01	5.655	5.820 ±0.019	84%	11.6	167 ±0.1	0.0387	0.0432 ±0.0012	0.98 ±0.01
PCO2_02	5.312	5.624 ±0.015	90%	5.6	107 ±0.0	0.0255	0.0301 ±0.0004	0.89 ±0.04
PCO2_03	5.064	5.427 ±0.016	86%	3.3	67 ±0.2	0.0194	0.0222 ±0.0001	0.92 ±0.08
PCO2_04	5.823	6.039 ±0.028	90%	8.2	264 ±0.1	0.0212	0.0264 ±0.0005	0.45 ±0.00
PCO2_05a	5.448	5.769 ±0.006	94%	4.0	80 ±0.0	0.0143	0.0180 ±0.0000	0.47 ±0.01
PCO2_05b	5.448	5.769 ±0.004	97%	3.9	78 ±0.1	0.0140	0.0178 ±0.0001	0.46 ±0.01
PCO2_05c	5.442	5.785 ±0.010	91%	3.9	80 ±0.1	0.0145	0.0180 ±0.0002	0.46 ±0.02
PCO2_06	5.205	5.542 ±0.005	97%	3.4	46 ±0.1	0.0115	0.0127 ±0.0001	0.47 ±0.02
PCO2_07	6.222	6.45 ±0.002	85%	3.9	61 ±0.1	0.0063	0.0084 ±0.0001	0.08 ±0.00
PCO2_08	5.781	6.171 ±0.010	69%	1.7	35 ±0.0	0.0038	0.0053 ±0.0001	0.09 ±0.01
PCO2_09	5.583	5.959 ±0.005	83%	1.0	22 ±0.1	0.0026	0.0036 ±0.0001	0.09 ±0.01
TEMP_03a	5.431	5.754 ±0.006	93%	2.0	42 ±0.0	0.0072	0.0094 ±0.0001	0.37 ±0.01
TEMP_04a	5.399	5.731 ±0.003	99%	1.2	24 ±0.1	0.0048	0.0059 ±0.0001	0.33 ±0.01
Ca_01a	5.734	5.978 ±0.003	87%	7.8	127 ±0.0	0.0177	0.0222 ±0.0000	0.46 ±0.03
Ca_02a	5.438	5.671 ±0.002	93%	3.6	60 ±0.0	0.0142	0.0164 ±0.0001	0.46 ±0.01
I_01a	5.567	5.813 ±0.001	86%	4.7	81 ±0.0	0.0188	0.0220 ±0.0001	0.47 ±0.01
I_02a	5.340	5.664 ±0.008	88%	3.1	59 ±0.1	0.0105	0.0132 ±0.0001	0.44 ±0.03
Mg_01a	5.377	5.762 ±0.006	98%	3.3	76 ±0.0	0.0134	0.0175 ±0.0002	0.46 ±0.02
Mg_02a	5.386	5.749 ±0.004	92%	3.4	75 ±0.0	0.0137	0.0176 ±0.0001	0.46 ±0.02
SO4_01a	5.662	5.869 ±0.004	90%	11.2	179 ±0.1	0.0365	0.0432 ±0.0001	0.88 ±0.00
SO4_02a	5.353	5.620 ±0.002	90%	5.9	105 ±0.1	0.0252	0.0296 ±0.0002	0.87 ±0.03
SO4_03a	5.240	5.441 ±0.007	90%	4.4	66 ±0.1	0.0191	0.0212 ±0.0001	0.84 ±0.04
PCO2_01b	5.642	5.894 ±0.005	91%	10.8	190 ±0.1	0.0365	0.0445 ±0.0002	0.89 ±0.01
PCO2_01c	5.663	5.897 ±0.004	90%	11.4	189 ±0.1	0.0374	0.0440 ±0.0003	0.89 ±0.02
PCO2_03b	5.074	5.457 ±0.005	85%	3.1	68 ±0.1	0.0183	0.0216 ±0.0002	0.86 ±0.06
PCO2_03c	5.066	5.442 ±0.011	87%	3.1	66 ±0.0	0.0184	0.0211 ±0.0004	0.87 ±0.07

Table 4–4. The apparent carbonate ion activity at equilibrium as extrapolated from rate data ($a^{*}_{CO_3^{2-}}$) and measured at steady-state ($a^{ss}_{CO_3^{2-}}$). The rate constant in mmol m^{-2} hr^{-1} for the general rate equation in which n = 1, normalized to the BET (k_{BET}) and geometric (k_{GEO}) surface area. Experiments denoted with an MR superscript were included in the multiple regression analysis (see Section 4.4.4)

Experiment ID	$a^{*}_{CO_3^{2-}}$ x10^8	$a^{ss}_{CO_3^{2-}}$ x10^8	k_{BET}	k_{GEO}	r^2
PCO2_01^{MR}	28.8	28.7±1.2	16.3	72.8	1.00
PCO2_02^{MR}	10.0	10.4±0.4	10.8	48.6	0.99
PCO2_03^{MR}	3.7	3.9±0.2	7.6	33.9	0.99
PCO2_04^{MR}	39.8	38.4±3.0	10.0	44.8	1.00
PCO2_05a^{MR}	9.8	10.7±0.2	6.1	27.4	0.99
PCO2_05b	10.0	10.6±0.1	7.1	31.8	0.99
PCO2_05c	10.1	11.3±0.3	6.7	30.2	0.99
PCO2_06^{MR}	3.4	3.6±0.0	5.1	22.8	0.99
PCO2_07^{MR}	40.9	44.9±0.0	3.6	16.0	0.99
PCO2_08^{MR}	11.4	12.0±0.0	2.7	12.0	0.99
PCO2_09^{MR}	4.1	4.4±0.1	2.7	12.0	0.99
TEMP_03a^{MR}	6.6	7.5±0.2	13.0	58.1	0.99
TEMP_04a^{MR}	2.5	3.7±0.4	23.9	106.9	0.98
Ca_01a^{MR}	25.8	26.9±0.2	5.6	25.3	0.98
Ca_02a^{MR}	6.6	6.8±0.0	7.3	32.5	0.99
I_01a^{MR}	13.8	14.2±0.1	9.8	43.7	0.99
I_02a^{MR}	5.6	5.7±0.2	4.3	19.3	0.99
Mg_01a^{MR}	9.7	10.1±0.1	6.7	30.0	0.99
Mg_02a^{MR}	9.2	9.6±0.1	6.2	27.7	0.99
SO4_01a	34.4	34.5±0.5	11.1	49.6	0.99
SO4_02a	9.6	10.1±0.1	8.3	37.2	0.99
SO4_03a	3.5	4.0±0.1	5.1	22.8	0.98
PCO2_01b	38.0	38.9±0.5	19.5	85.7	0.99
PCO2_01c	37.6	39.1±0.4	32.8	32.8	0.99
PCO2_03b	3.8	4.3±0.1	9.9	44.2	0.99
PCO2_03c	3.9	4.0±0.1	2.7	12.3	0.93

4.4. Discussion

4.4.1. Calcite Dissolution in 'Model' Brines and the Effect of pCO_2

Although natural waters have a huge range in composition, the study of calcite reaction kinetics has largely been confined to dilute waters and seawater (e.g., for reviews see Plummer et al., 1979; Sjöberg, 1978; Morse, 1983; Burton, 1993; Morse and Arvidson, 2002). Even in seawater, both the dissolution and precipitation kinetics have been shown to be complex. Unlike seawater, however, the composition of subsurface formation waters varies considerably in the concentrations and ratios of the major dissolved species. Fortunately, this variably is not entirely random as Hanor (1994b) demonstrated. Instead, much of the variability can be explained by mineral-brine equilibration considerations. This constrains somewhat the concentration of the major dissolved species as a function of TDS. However, caution should be used in applying the results of this study to brines with compositions substantially different from those used here.

Dissolution rates measured in each of the model brines at three CO_2 partial pressures (X_{CO2} = 1.0, 0.5 and 0.1) are shown in Figure 4–2 and their corresponding rate constants are plotted in Figure 4–3 as a function of equivalent TDS. The EQPITZER calculated partial pressures as derived from TA and TCO_2 were 0.88 ±0.04, 0.45 ±0.01 and 0.08 ±0.00 bar respectively, reflecting the contribution of vapor pressure. As mentioned in Section 4.2, the lower surface area to solution volume ratios used in experiments PCO2_06a and PCO2_07a resulted in pH-time changes that were comparatively slower than in the other experiments, making their numerical differentiation problematic. These experiments represent brine 3 (full square) under

X_{CO2} = 0.5 and brine 1 (open square) under X_{CO2} = 0.1 in Figure 4–2 and are noticeably disparate. The numerical differentiation had to be truncated far from equilibrium and may have resulted in the rates being slightly overestimated.

Other investigators (e.g., Sjöberg, 1978; Busenberg and Plummer, 1986) have demonstrated a rate dependence on CO_2 for partial pressures above 0.1 bar and for pH ranges greater than about 4.5 when the rate is dominated by surface control reactions. A strong dependence on CO_2 partial pressure was also observed in this study. About a 5-fold decrease in the rate constant was measured when the partial pressure was reduced from near 1 to approximately 0.1 bar (Figure 4–3). Van Cappellen et al. (1993) attributed this CO_2 dependence to the formation of carbonate complexes with surface lattice calcium ions. According to his surface complexation model, the CO_2-promoted dissolution rate is directly proportional to the concentration of $>CaHCO_3^0$ sites (where > represents the mineral lattice) and is an example of ligand promoted dissolution in which the formation of the bicarbonate surface complex increases the rate of detachment of Ca^{2+} from surface positions.

The inhibitory effects of the salts also appear to exhibit CO_2 dependence. Rates become progressively more depressed with increasing brine concentration but the effect is more pronounced at the higher partial pressures and all but absent at 0.1 bar.

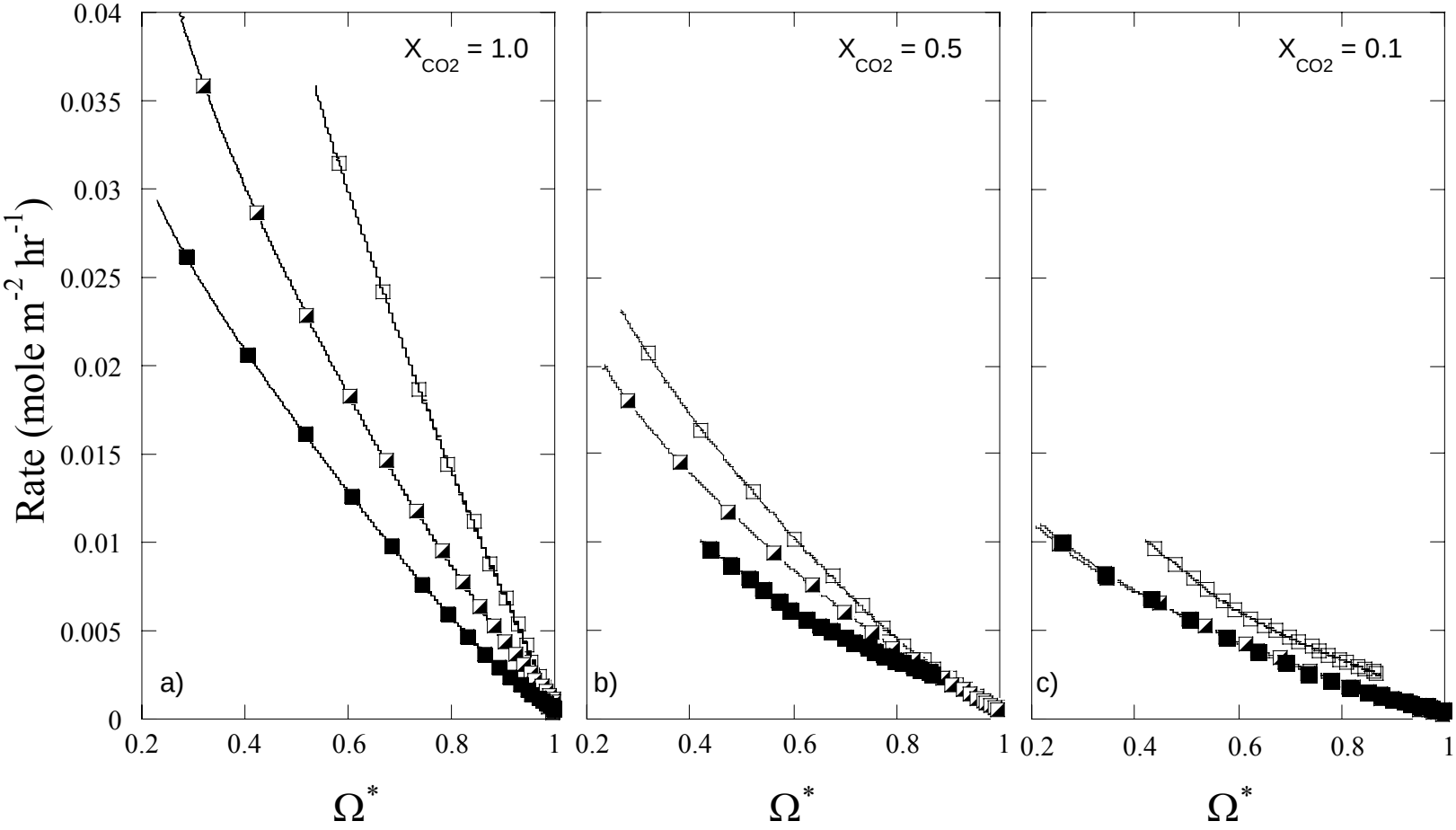

Figure 4–2. The pCO_2 effect on rates of calcite dissolution in model brines. Brine 1 (open square), 2 (half full square) and 3 (full square) emulated geologic brines exhibiting TDS concentrations of 50, 125 and 200 g L^{-1} respectively. The experiments were conducted at fixed pCO_2 by bubbling under continuous gas feeds of CO_2-N_2 mixtures where X_{CO2} = 1.0 (a) , 0.5 (b) and 0.1 (c).

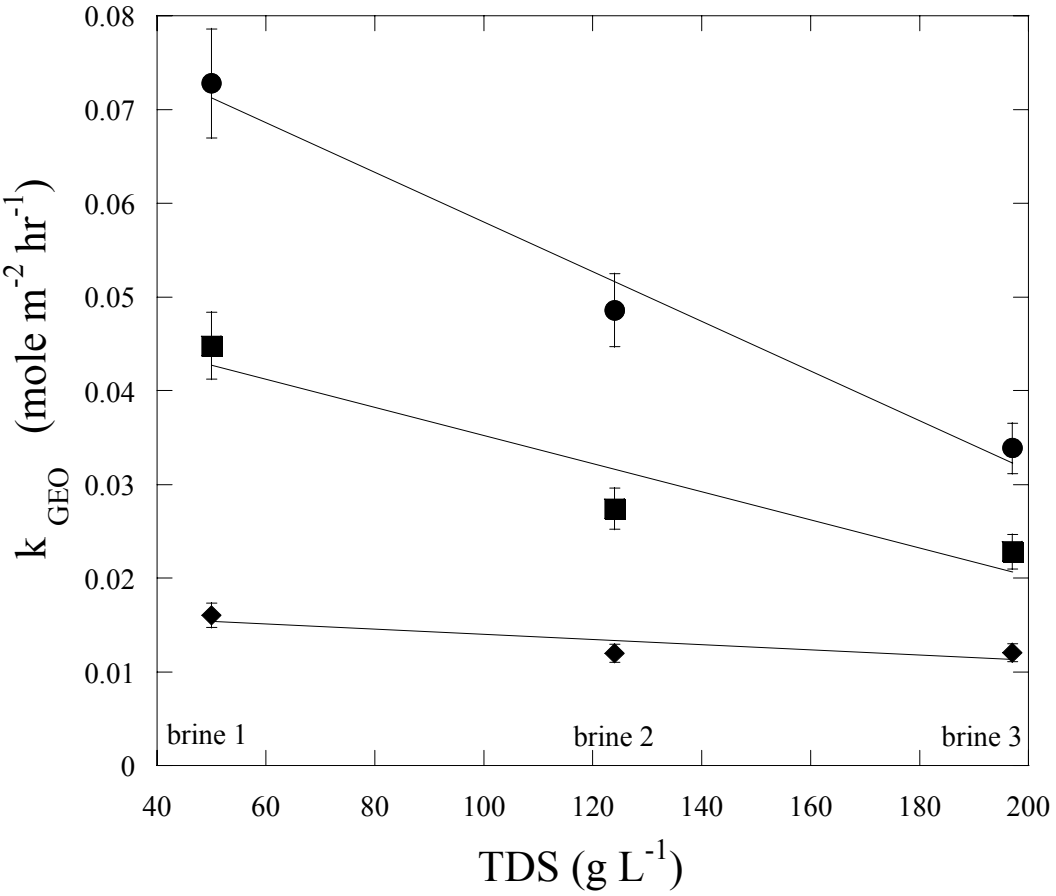

Figure 4–3. The rate constant (k_{GEO}) as a function of TDS (g L^{-1}). In general, with increasing brine concentration rates decrease, but this compositional effect is dependent on pCO_2. X_{CO2} = 1 (solid circle), 0.5 (solid square) and 0.1 (solid diamond). Error bars represent analytical uncertainty.

4.4.2. The Specific Effects of Ca^{2+}, Mg^{2+} and Ionic Strength

The independent effects of Ca^{2+}, Mg^{2+} and ionic strength were investigated by measuring the dissolution rate in solutions that were modifications of 'model' brine 2 (TDS = 125). In each case, one factor was varied while all other variables were held constant. For example, in the case of the Ca^{2+} effect experiments, two brines were prepared with Mg^{2+} concentration and ionic strength equivalent to brine 2, but with Ca^{2+} concentrations equivalent to brine 1 (Experiment Ca_01a) and brine 3 (Experiment Ca_02a) respectively. The experiments were performed under a $X_{CO2} = 0.5$ atmosphere at 25 ºC and the rates compared against experiment PCO2_05a. By using this approach the specific contribution to the net inhibition observed with increasing TDS (Figure 4–2 and 5–3) could be evaluated.

An interesting finding was that the greatest inhibition to the rate was attributed to increasing ionic strength (Figure 4–4a). There are relatively few studies that have examined the specific effect of ionic strength on calcite dissolution rates. Buhmann and Dreybrodt (1987) found that ionic strength was only of minor importance, but the study investigated very dilute solutions (< 2 mM) compared with those studied here. In contrast, Zhang and Dawe (1998) found that in high salinity waters (up to 2 mol kg^{-1}), the precipitation rate of calcite increased as a function of the square root of ionic strength. Similarly, Bischoff (1968) found that nucleation rates of calcite also increased proportional to the square root of ionic strength. In both cases, they suggested that with increased electrolyte concentrations, a stronger inter-particle attraction helps to catalyze calcite growth in a manner analogous to colloid flocculation.

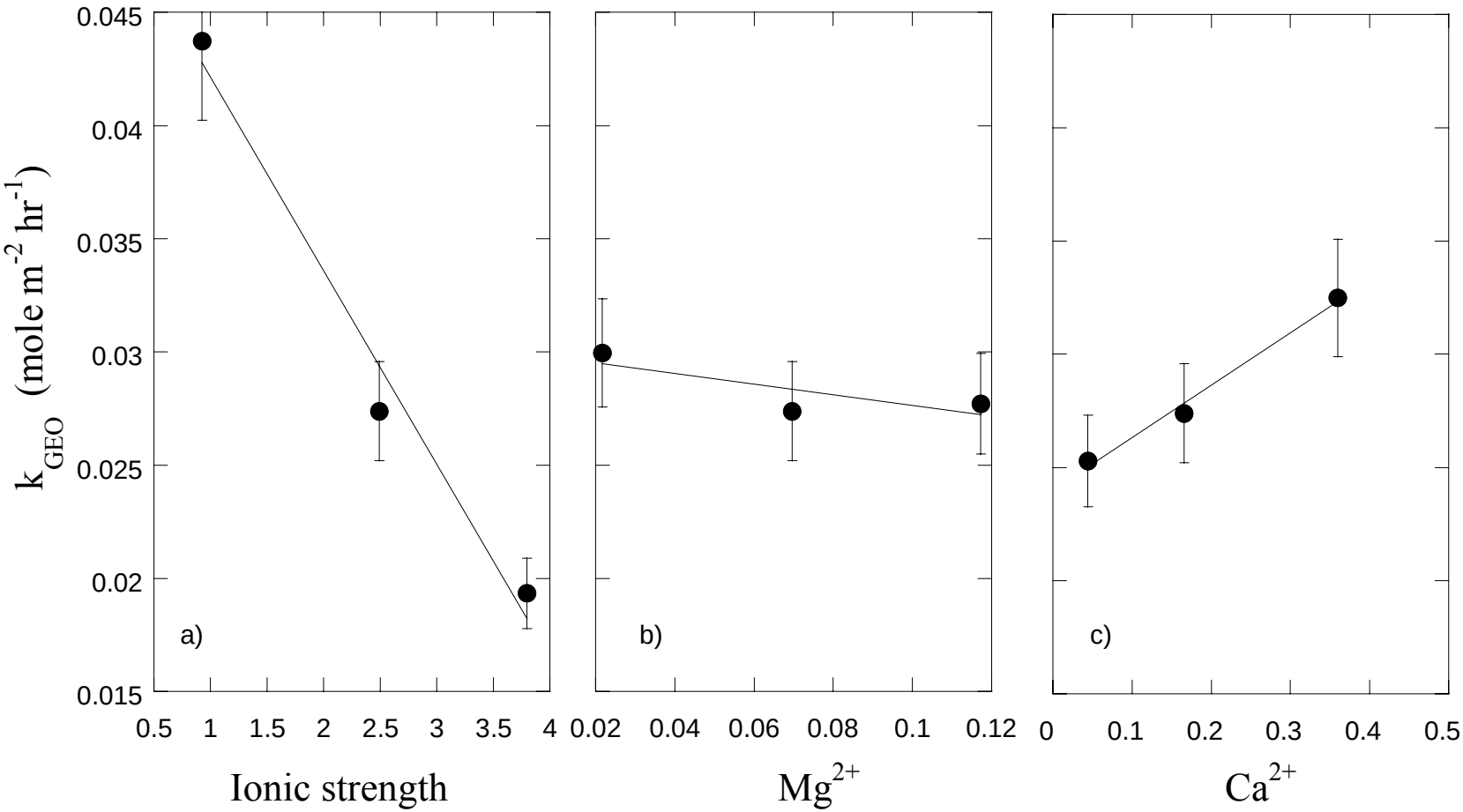

Figure 4–4. The specific effects of Ca^{2+}, Mg^{2+} and ionic strength. The rate constant (k_{GEO}) (moles m^{-2} hr^{-1}) as a function of the molal concentration of Ca^{2+} (a), Mg^{2+} (b) and ionic strength (c).

An alternative explanation that could account for both the increase precipitation rates observed in the prior studies, and the decreased dissolution rates measured in this study, is related to the effect water activity has on the hydration of metal ions. Consider that cation dehydration poses a fundamental energetic barrier to precipitation (Lippmann, 1973; Arvidson and Mackenzie, 1999). Conversely, the hydration of the calcium ion poses an energetic barrier to dissolution. In order for calcite to dissolve, the attractive interaction of water molecules most overcome the ionic attraction within the mineral lattice. If as a result of high ionic strength, the water activity is significantly diminished, one would expect the hydration efficiency of the calcium ion to be retarded. The rate constants shown in Figure 4–4a have been recast as a function of water activity in Figure 4–5.

There have been a considerable number of previous investigations regarding the effects of magnesium ion on calcite dissolution (Weyl, 1967; Berner, 1967; Sjöberg, 1978; Buhmann and Dreybrodt, 1987; Compton and Brown, 1994; Gutjahr et al., 1996b; Alkattan et al., 2002). While the magnesium ion has clearly been shown to strongly inhibit the rate of dissolution in neutral to basic solutions (e.g., Compton and Brown, pH 8–9), in acidic solutions the inhibition appears absent (Alkattan et al., 2002; pH 1–3). At intermediate pH such as those consistent with this study, the findings are often contradictory. Both Buhmann and Dreybrodt (1987) and Sjöberg (1978) report a strong inhibitory effect while Gutjahr et al. (1996b) found no effect.

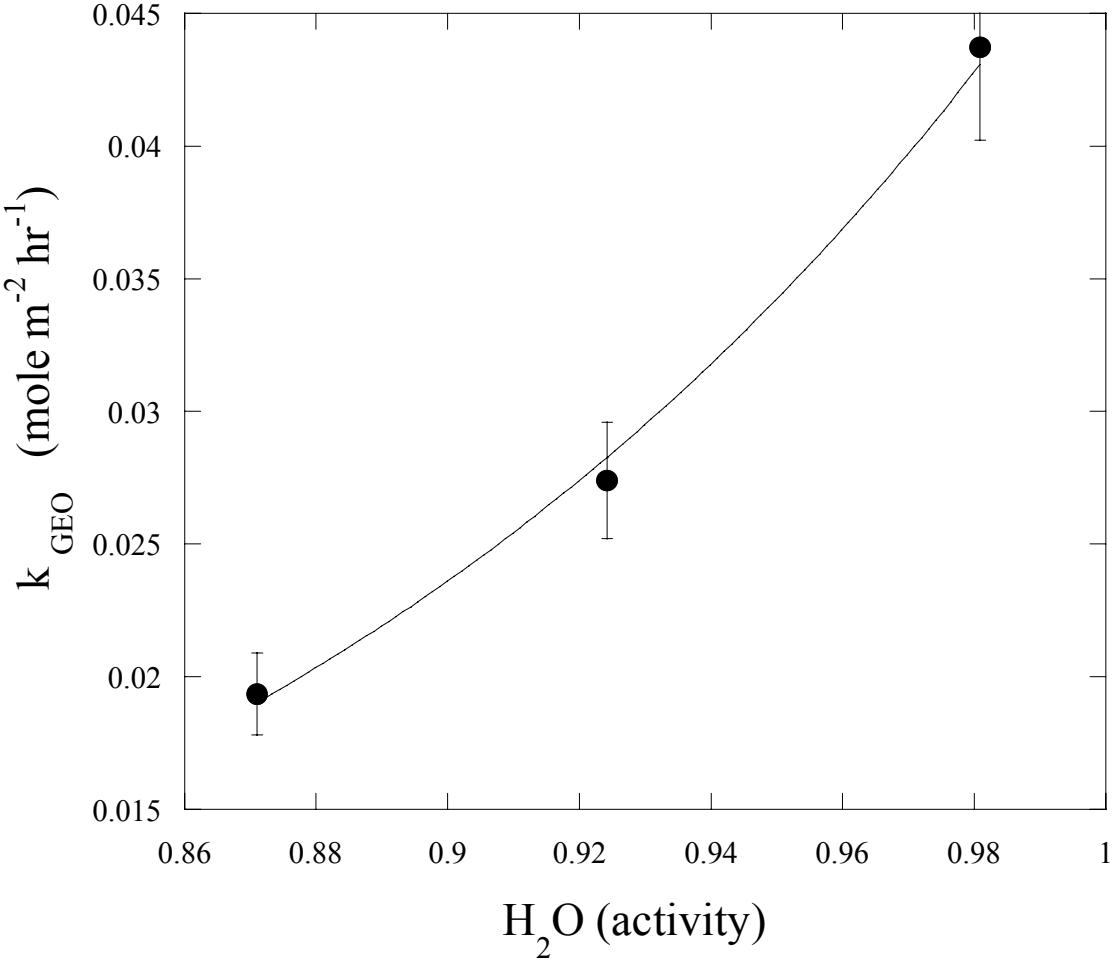

Figure 4–5. The rate constant (k_{GEO}) (moles m^{-2} hr^{-1}) as a function of water activity.

In this study only a modest inhibition was observed when magnesium was varied between 0.02 and 0.12 molal (Figure 4–4b). Sjöberg (1978) described the inhibition due to magnesium in solutions containing < 50 mM Mg^{2+} in terms of a Langmuir-type adsorption isotherm. The Langmuir-Volmer model would predict that beyond some inhibitor solution concentration the dissolution rate would become independent of the inhibitor concentration. It is possible that the absence of a strong effect observed in this study may suggest that the magnesium concentrations of these brines have exceeded this inhibition plateau. Although Compton and Brown (1994) did measure an inhibition effect in solutions containing up to 80 mM Mg^{2+}, their experimental solutions were at pH > 8, which may be above the pH of zero surface charge ($pH_{zpc} \approx 8.2$) (e.g., Hohl et al., 1980). Below the pH_{zpc} the effects of cationic inhibitors may be greatly diminished (Van Cappellen et al., 1993; Pokrovsky and Schott, 2002).

Several studies have also investigated the effect of the calcium ion on calcite dissolution (Sjöberg, 1978; Sjöberg and Rickard, 1985; Buhmann and Dreybrodt, 1987; Gutjahr 1996a, 1996b), often with contradictory results. Sjöberg (1978) found that the addition of Ca^{2+} in solutions ranging from 0 to 10 mM resulted in about a 17% decrease to the rate constant that he described in terms of a Langmuir-type adsorption isotherm similar to that of magnesium. Later Sjöberg and Rickard (1985) revisited the issue and concluded that due to surface adsorption, increasing Ca^{2+} resulted in a lower concentration gradient between the surface and the bulk solution thereby making the reaction more dependent on transport control. In contrast, Gutjahr (1996b) found that the rate constant actually increased by roughly 40% when Ca^{2+} concentrations were increased from 0.160 to 4.090 mM. The cause of the disparity between the different

studies is unclear since amongst these studies the pH, pCO_2 and degree of disequilibrium are relatively similar. In this study an increase in the measured rate constant was observed when calcium was increased from 0.04 to 0.36 molal (Figure 4–4c). The experimental conditions of the previous studies do differ considerably from this study, which was performed using moderately acidic (pH < 6.5) , high pCO_2, magnesium-bearing solutions.

An important consideration is the effect that calcium has on the carbonate carrying capacity of the solution. For a given degree of undersaturation, the relative amount of carbonate ion in solution is reduced when the initial calcium concentration is increased. The inhibiting effect of CO_3^{2-} has been demonstrated for dissolution far from equilibrium in the case of $ZnCO_3$ and $MnCO_3$ (Pokrovsky and Schott, 2002), dolomite and magnesite (Pokrovsky et al., 1999; Pokrovsky and Schott, 1999), and recently for calcite (Lea et al., 2001; Arvidson, personal communication). Whether such inhibition effects occur near equilibrium has not yet been established or if at this low CO_3^{2-} concentration they are significant, but they might contribute to the positive correlation between calcium and the rate constant measured here.

4.4.3. Temperature and Stirring Rate Dependence

Since a much coarser calcite was used in these experiments relative to those presented in Chapter III, the effects of temperature and stirring rate needed to be investigated to confirm that, under these experimental conditions (i.e., $\Omega > 0.2$), the reaction was still controlled by surface processes and not effected by hydrodynamic conditions. When experiment PCO2_05 (i.e., brine 2, $X_{CO2} = 0.5$, 25.0 ºC) was

replicated at 500 and 700 rpm, the rates varied less than 8%, probably within experimental error when compositional effects among the replicates is considered (see section 4.4.4). This confirms an independence on stirring rate as would be predicted for surface-controlled dissolution.

Temperature is one of the most important variables when considering reaction rate constants. Drastic variations in rates can occur owing to the exponential dependence of reaction rate on temperature, which is often assumed to follow the classic Arrhenius (1889) equation:

$$k = Ae^{-\left(\frac{E_a}{RT}\right)} \qquad (4\text{–}3)$$

where A is the pre-exponential factor, E_a is the activation energy, R is the gas constant (8.314×10^{-3} kJ mol^{-1}K^{-1}) and T is the temperature in degrees Kelvin. The apparent activation energy for the dissolution reaction can be calculated from the slope of a plot of log k versus the reciprocal absolute temperature since

$$\ln k = \left(\frac{-E_a}{RT}\right) + \ln A. \qquad (4\text{–}4)$$

A plot of ln k_{geo} against 1/T for dissolution experiments performed in brine 2 (equivalent TDS = 125 g L^{-1}) conducted under a $X_{CO2} = 0.5$ atmosphere at 25.0, 52.5 and 82.5 °C is shown in Figure 4–7. The apparent activation energy is calculated to be 21 ±1 kJ mol^{-1} for this reaction. There are a wide range of activation energies reported for calcite dissolution (about 8–60 kJ mol^{-1}; see Morse and Arvidson, 2002 for review). In dilute solutions far from equilibrium where diffusion-controlled processes dominate, most reported values are close to 10 kJ mol^{-1} (e.g., Plummer et al., 1978; Sjöberg, 1978; Salem, 1994). However, greater values are typically believed to be indicative of surface-

controlled processes (Lasaga, 1998). The value reported here is in excellent agreement with Alkattan et al. (1998) who determined an $E_a = 19 \pm 4$ kJ mol^{-1}.

4.4.4. Multiple Regression Analysis of the Dependence of k on Ca2+, Mg2+, Ionic Strength, Temperature and pCO2

The kinetics of calcite dissolution have typically been described in terms of empirical or semi-empirical rate equations (e.g., Morse, 1978; Sjöberg, 1978; Busenberg and Plummer, 1986), classical chemical kinetics (e.g., Plummer et al., 1978) or surface speciation (Van Cappellen et al., 1993; Arakaki and Mucci, 1995; Pokrovsky and Schott, 2002) models. With the exception of some empirical models applied to seawater, these models are only applicable to relatively dilute solutions since accurately quantifying many of the required species (e.g., surface complexes) in concentrated solutions (i.e., >1 m) is beyond current geochemical models.

A disadvantage of the general rate equation ($R = k(1-\Omega)^n$) is that it requires fitting parameters (k and n) specific to the solution composition of interest, where the major solute and inhibitor concentrations and environmental conditions (e.g., P, T and pCO_2) are known. The first-order kinetics observed in this study across a broad range of typical brine concentrations requires that only one term, k, be determined. This greatly simplifies the approach since conventional statistical methods can be applied to account for the variably in k as a function of the key factors investigated.

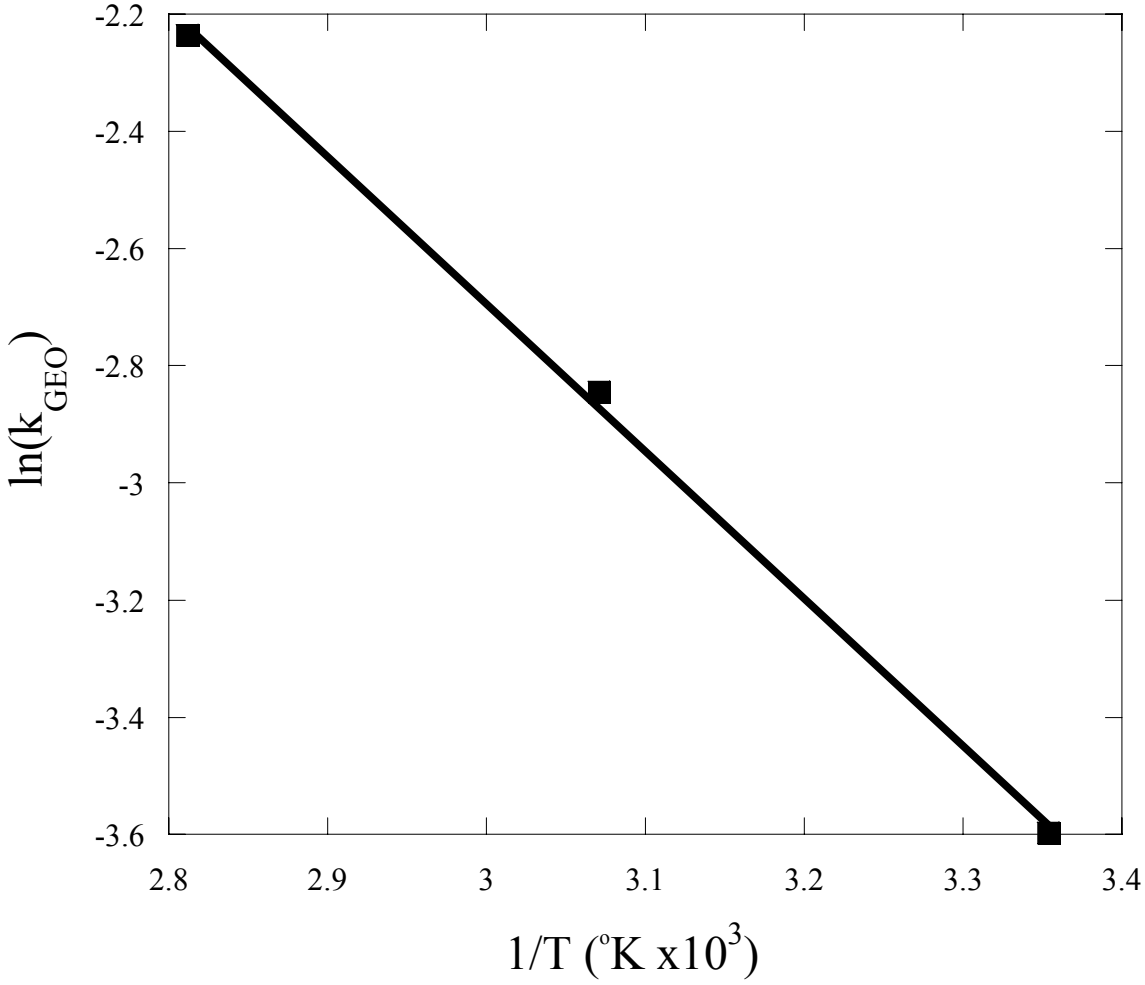

Figure 4–6. Arrhenius plot for apparent activation energy calculations for rates measured in brine 2 under a X_{CO2} = 0.5 atmosphere at 25.0, 52.5 and 82.5 °C. The apparent activation energy is 20.9 kJ mol^{-1} indicating a surface-controlled reaction.

A multiple regression analysis was used to evaluate to what extent the observed rate constant is dependent on each of the variables Ca^{2+}, Mg^{2+}, ionic strength, temperature and pCO_2. As with other regression models, multiple regressions (MR) may not be capable of yielding specific reaction mechanisms, but can estimate the relative strength of individual effects and thus be used to provide a predictive statistically-based empirical rate equation. The goal of this approach is to fully describe the observed rate data as a function of each of the investigated factors.

The MR analysis was performed using the statistical software SPSS® v. 11.0 for Windows. The regression was based on the final compositions of the solutions for the experiments denoted by a MR superscript in Table 4–4 (N = 17). The robustness of the model was evaluated from the coefficient of multiple determination (R^2) and by examination of the residuals. In addition, a colinearity diagnostic was determined. Colinearity is a common complication in MR that can occur when the effect of one independent variable on the dependent variable is contingent on the value of another independent variable (Philippi, 1993).

The greatest predictive capability (adjusted $R^2 = 0.953$, $P < 0.001$) was achieved when the data were left untransformed (i.e., linear regression) and activity was modeled rather than concentration in the cases of calcium and magnesium. The resulting regression yielded:

$$k = \beta_0 + \beta_1(T) + \beta_2(pCO_2) + \beta_3(I) + \beta_4(a_{Ca^{2+}}) + \beta_5(a_{Mg^{2+}}) \qquad (4\text{–}5)$$

where T is °C, pCO_2 is given in bars, I is ionic strength and a_i are activities of calcium and magnesium. The unstandardized coefficients are provided in Table 4–5 for solving

to the rate constant normalized to the geometric (k_{GEO}) and BET (k_{BET}) surface areas. The calculated condition numbers for colinearity for each of the predictors were less than 20 and the variance inflation factors (VIF) less than 10, indicating that severe colinearity was not a factor (Freund and Littell, 1986; Chatterjee and Price, 1991).

Since the predictors used in the model are measures in different units, the standardized coefficients (Beta, Table 4–5) are required for comparing the relative effects of each of the predictors. The relative effects are $T >> pCO_2 \approx I > a_{Ca^{2+}} >> a_{Mg^{2+}}$.

The results confirm that ionic strength strongly correlates with a reduction in rate, and that the inhibitory effect of magnesium is small in these solutions. It also shows that calcium is positively correlated with dissolution rate. Figure 4–8 illustrates the predictive capability of the model where the measured rate constants are plotted versus their predicted values.

Table 4–5. The coefficients derived from multiple regression analysis. These can be used to predict the rate constant from the predictors T °C, pCO_2, I, $a_{Ca^{2+}}$ and $a_{Mg^{2+}}$. The coefficients specific to the geometrically normalized (k_{GEO}) and BET normalized (k_{BET}) rate constants are given separately.

Predictor	Coefficient x10^3	Unstandardized geometric	BET	Standardized Beta
Constant	β_0	-6.07	-1.36	
T (°C)	β_1	1.42	0.32	0.879
pCO_2 (bar)	β_2	48.56	10.84	0.499
I (molal)	β_3	-10.97	-2.45	-0.475
$a_{Ca^{2+}}$	β_4	127.45	28.45	0.259
$a_{Mg^{2+}}$	β_5	-58.54	-13.07	-0.059

When we compare the dissolution rates measured using powered calcite in Chapter III versus these later experiments obtained using crushed rhombs, there are

apparent gross dissimilarities. Specifically, although powder rates generally decreased with increasing brine concentration, the net inhibition was relatively minor. In contrast, the crushed rhomb experiments reveal a stronger compositional effect at the same higher partial pressures. In addition, if the rate constants are normalized to the BET surface area as is the typical approach, then the dissolution rates of the powdered calcite appear roughly 5 times faster. However, Figure 4–8 reveals that when the rates are instead normalized to the geometric surface area, the MR model closely predicts the rates constants of the powdered calcite. It also shows that the limited inhibition that was measured in the powered calcite experiments is an artifact of how the brines were prepared.

The median Ca:I ratio in the Chapter III experimental brines are about twice that of the later experiments. Since the effects of calcium and ionic strength are inversely correlated, than the subdued compositional inhibition observed in the powdered calcite experiments can be accounted for as a result of the calcium effect partially compensating for the inhibitory effect associated with ionic strength.

4.4.5. The Inhibitory Effect of SO_4^{2-} *in Concentrated Brines*

A common inhibitor of calcite kinetics in natural waters is the divalent anion sulfate (Akin and Lagerwerff, 1965; Sjöberg, 1978; Buhmann and Dreybrodt, 1987; Mucci et al., 1989). Sulfate present at seawater concentration has been demonstrated to reduce the dissolution rate constant by 40% in phosphate-free pseudo seawater (Sjöberg, 1978). In subsurface formation waters sulfate is often, but not always, a relatively minor component rarely exceeding 1 g L^{-1} compared with 2.7 g L^{-1} in seawater. However,

Sjöberg (1978) found that the effect of sulfate increases with increasing calcium and magnesium concentration. Consequently, it could potentially be an even more potent inhibitor in brines. This could be related to the surface adsorption of calcium and magnesium, producing a more cationic surface that increases the adsorption of anions such as sulfate.

To test the effect, approximately 1 g L^{-1} (~0.01 m) of sulfate were added to each of the 'model' brines in the form of a concentrated Na_2SO_4 solution. The dissolution rates were measured in each solution at 25 °C and X_{CO2} = 1 and compared with its MR-model predicted rate. The higher CO_2 partial pressure was chosen since brines of this pCO_2 had the greatest compositional sensitivity. Figure 4–9 shows the increasing inhibitory effect of sulfate with increasing calcium and magnesium, consistent with Sjöberg's (1978) findings. The equation fit to the data is purely an empirical construct, but does suggest that in the absence of calcium and magnesium the inhibitory effect of 1 g L^{-1} SO_4^{2-} would only be about 20%. However, in brines containing a TDS of 200 g L^{-1} the inhibition would be similar to that observed in seawater.

4.5. Conclusion

The calcite dissolution rate near equilibrium ($\Omega > 0.2$) in concentrated Na-Ca-Mg-Cl brines, equivalent to subsurface formation waters ranging from TDS 50 to 200 g L^{-1}, have been measured. The rates can be described using first-order kinetics by the general rate equation: $R = k(1-\Omega)^n$, where n = 1 (first-order) and the rate constant k can be derived from the MR model:

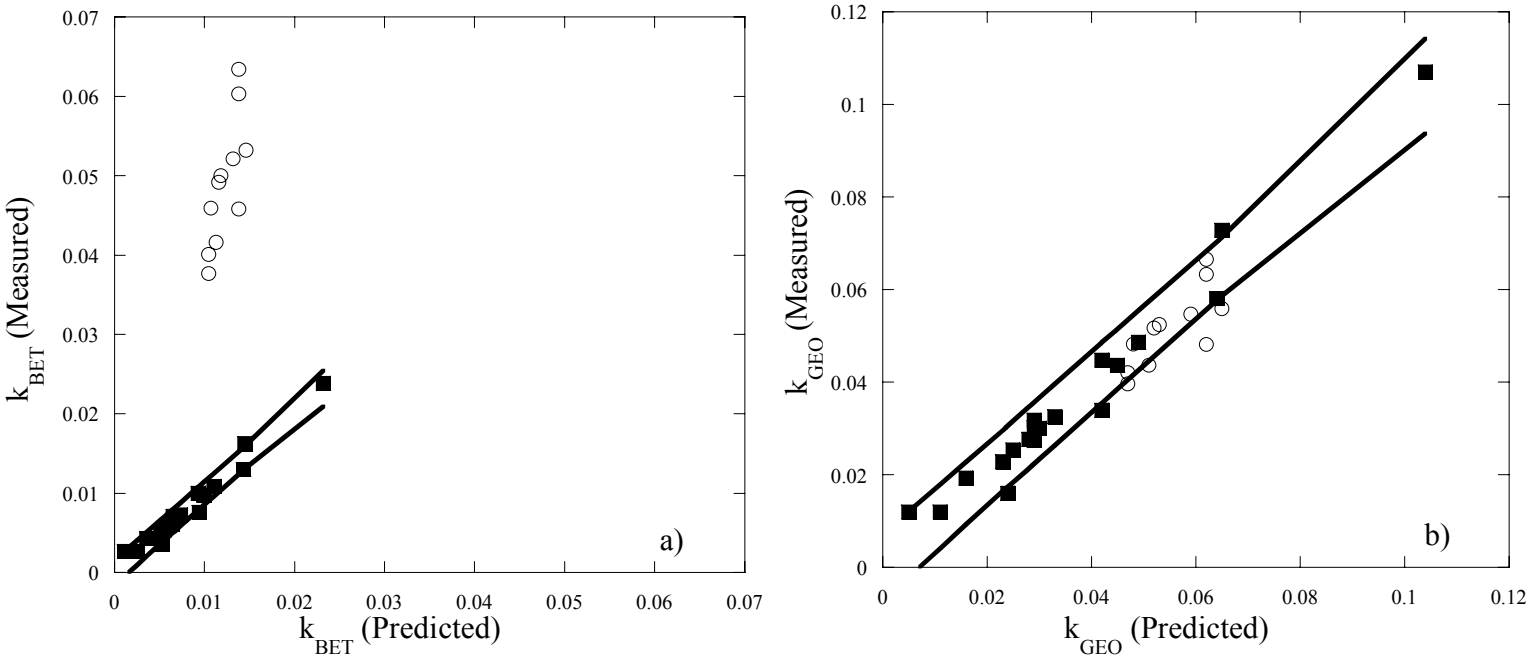

Figure 4–7. The measured rate constants versus the predicted values from equation 4–5. The lines represent the 95% confidence interval of the model prediction. The regression was fit to data obtained from dissolution rates using the rhombic calcite (solid square). When normalized to BET surface area, the previously measured rates obtained using powdered calcite (open circle) are shown to be considerably faster than the statistical model predicts (a). However, when the rates are instead normalized to the geometric surface area, the statistical model closely predicts the rates (b).

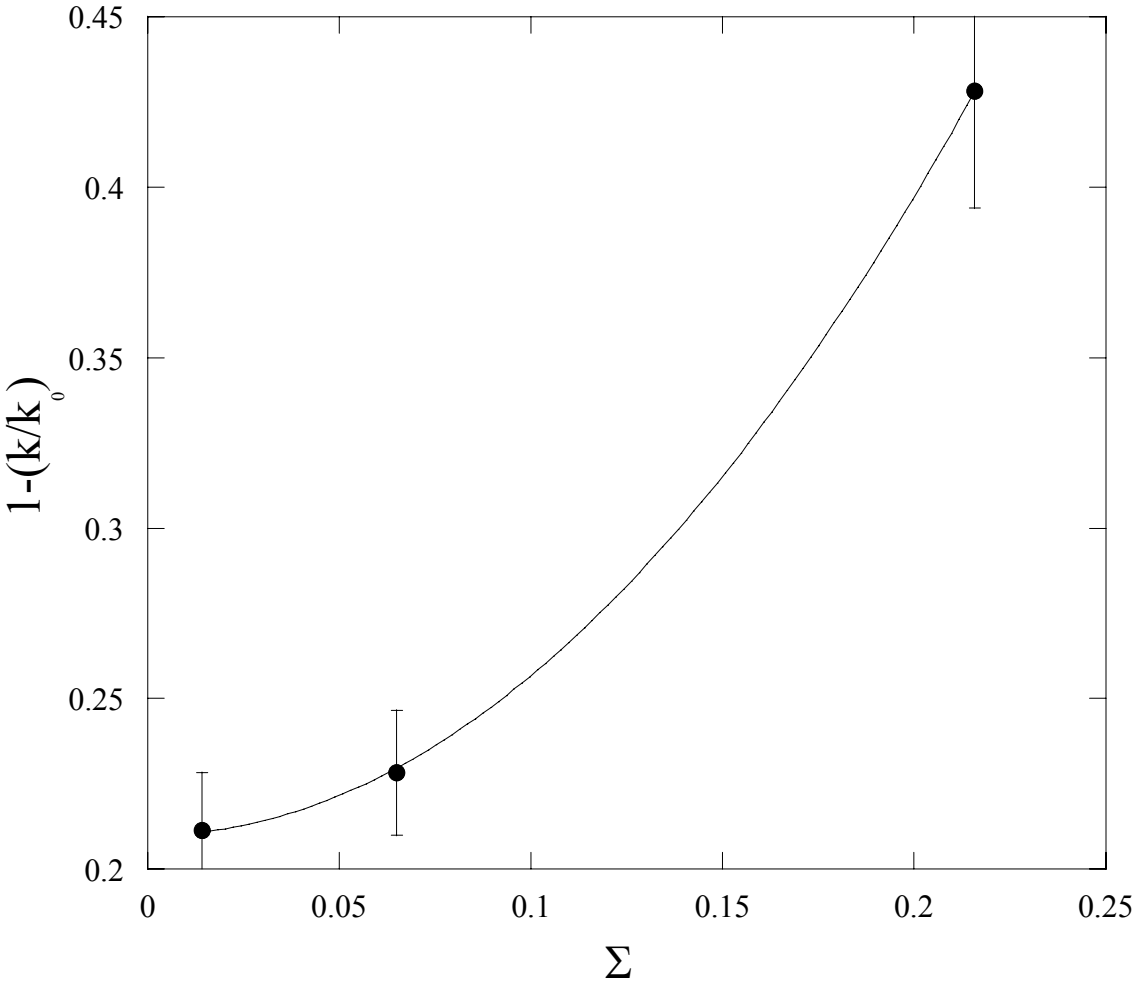

Figure 4–8. The inhibitory effect of 1 g L^{-1} sulfate in model brines at 25 °C at X_{CO2} = 1.0. The measured rate constant (k) relative to the MR-model prediction (k_0) show that with increasing calcium and magnesium activity ($\Sigma = a_{Ca^{2+}} + a_{Mg^{2+}}$) the sensitivity to sulfate increases. The equation of the line shown is:

$1-(k/k_0) = 0.20 + 4.68\left(a^2_{Ca^{2+}} + a^2_{Mg^{2+}}\right)$, $r^2 > 0.99$.

$$k = \beta_0 + \beta_1(T) + \beta_2(pCO_2) + \beta_3(I) + \beta_4(a_{Ca^{2+}}) + \beta_5(a_{Mg^{2+}}).$$

The strongest influence on the rate is not salt content but temperature and CO_2 partial pressure. Surprisingly, ionic strength strongly correlates with an inhibition of rate of dissolution beyond the specific effects of calcium and magnesium. Magnesium showed only a minor inhibitory effect while increasing calcium actually increased the rate constant.

When SO_4^{2-} is present at concentrations typical for subsurface formation waters there is a strong inhibition effect similar to that observed previously in seawater. Sulfate's effect is also strongly sensitive to the concentrations of calcium and magnesium. Due to this relation, even though sulfate concentrations in subsurface formation waters are generally less than that in seawater, at TDS concentrations greater than 200 g L^{-1}, its effect on the rate may be of similar magnitude.

When rates are normalized to geometric surface area rather than BET surface area, there appears to be no substrate effect on the rate. The rates obtained using reagent-grade powered calcite in Chapter III agree well with those obtained from crushed rhombs. The small variability in dissolution rate observed in the Chapter III experiments is an artifact of how the brines were prepared. In that case, the greater calcium concentrations of those earlier brines resulted in a rate increase that largely compensated for the inhibitory effect of ionic strength.

CHAPTER V

THE EFFECT OF CALCIUM-ENRICHED FORMATION WATERS ON REDUCING THE $CaCO_3$ REACTIVE TRANSPORT CAPACITY

5.1. Introduction

In order to stabilize atmospheric CO_2 concentrations, major emission reductions coupled with carbon mitigation must be implemented in the very near future. One mitigation strategy involves CO_2 removal from flue gasses at point-sources (e.g., coal or natural gas power stations) and injection into geological repositories. Although oil and gas reservoirs are an attractive choice because they are already equipped with the infrastructure necessary for the injection process and provide the cost benefit potential for field enhanced oil recovery (EOR or tertiary recovery), their overall storage capacity is rather limited (Bergman and Winter, 1995). The estimated world-wide storage capacity in natural gas fields is estimated at only 500 to 1100 Gtonnes CO_2 (Hendriks and Blok, 1993). By comparison, the storage capacity in non-potable saline (brine) aquifers may be as high as 10,000 Gtonnes (Hendriks and Blok, 1993).

Although brine aquifers lack the infrastructure available at the oil and gas fields, deep saline aquifers have the largest potential storage capacity because they are widespread (e.g., proximal to point sources) and may not require the special structural and stratigraphic trap geometries required for oil and gas reservoirs (Gunter et al., 1996). Instead, carbon dioxide can be stored hydrodynamically in the formation waters for tens of thousands of years or longer. In addition, oftentimes these formations contain dissolved hydrocarbons that are not concentrated enough to make them economically

attractive to conventional petroleum exploration. CO_2 flooding can liberate these dissolved hydrocarbons similar to the case with EOR (Koide et al., 1993; Koide et al., 1992), helping to make the sequestration cost effective.

Of major concern for carbon dioxide sequestration in saline aquifers is the impact of mineral-brine-CO_2 reactions on the storage capacity, permeability and integrity of the formation. Prior to this study, however, the actual kinetics of mineral-brine-CO_2 reactions remained poorly understood. Since fluid flow and fluid rock interactions are dynamic processes, rate kinetics is typically considered important to determining the localization of mineral dissolution.

5.2. The Reactive Front Along an Ideal Solution Channel

The effect of solution kinetics on a porous medium reacting with a calcium-rich brine will be examined by presenting the simplified case of an ideal solution channel. The approach used is based on Morse and Mackenzie (1993), where they explored geochemical constraints on carbonate transport in subsurface sedimentary environments. It was similar to the methods used by Dreybrodt (1981) and Buhmann and Dreybrodt (1985a, 1985b) when applied to calcite kinetics in developing a comprehensive model of karsification.

In this case, brine initially undersaturated with respect to calcite flows through an idealized cylindrical calcite pore of constant initial diameter. As the brine flows it reacts with the calcite in accordance with the reaction kinetics presented in the preceding chapters. The reactive front length, i.e. the length the solution travels over which it

experiences its most rapid change in saturation state, will be calculated for various brines and conditions.

In these examples, the composition of the brines will be reported in terms of TDS with their major ion composition calculated from Table 2–1. The first example considers a 50 g L^{-1} TDS brine, initially at equilibrium with respect to calcite at 25 °C, with an alkalinity of 11.7 meq Kg^{-1} H_2O (i.e. pCO_2 = 0.32 bar). Perhaps as a result of waste gas injection or from the mixing of subsurface waters (Morse et al., 1997; Dreybrodt, 1981), the pCO_2 increases to 1.0 bar causing the system to become undersaturated (Ω = 0.3) with respect to calcite, developing a renewed capacity for dissolving $CaCO_3$. The distance this newly undersaturated solution must travel to reestablish equilibrium will now be calculated.

The change in solution composition as a result of calcite dissolution is calculated for small incremental changes in travel distance (dx) assuming steady-state. For a closed-system the dissolution results in an increase in alkalinity (TA) and dissolved inorganic carbon (TCO_2) and a decrease in pCO_2. The following relations are utilized:

$$TCO_2 = TCO_{2(in)} + dm \qquad (5–1)$$

and

$$TA = TA_{(in)} + 2 \times dm \qquad (5–2)$$

where the subscript (in) refers to the initial concentration entering a discrete segment and *dm* refers to the moles of calcite dissolved.

The carbonate ion ($m_{CO_3^{2-}}$) at each segment is calculated from the TA and TCO_2 using equation 2–6 in Chapter II, where the stoichiometric dissociation constants (K_1^* and K_2^*) have been calculated for each brine using EQPITZER. For the 50 g L^{-1}

TDS brine used in this example, $K_H^* = \frac{m_{CO2}}{pCO_2} = 10^{-1.55}$, $K_1^* = \frac{m_{HCO_3^-} m_{H^+}}{m_{CO_{2(aq)}}} = 10^{-5.93}$ and

$K_2^* = \frac{m_{CO_3^{2-}} a_{H^+}}{m_{HCO_3^-}} = 10^{-9.08}$. The pCO_2 of each segment can then be calculated from TA, TCO_2 and $m_{CO_3^{2-}}$ from the relation:

$$pCO_2 = \left(\frac{m_{CO_3^{2-}}}{K_H^* K_1^* K_2^*} \right) \left(\frac{K_1^* \left(TCO_2 - TA - 3m_{CO_3^{2-}} \right)}{TA - 2m_{CO_3^{2-}}} \right)^2 \qquad (5\text{–}3)$$

The activity coefficients for the calcium and carbonate ions were calculated using EQPITZER. Given the extremely small change in solution composition that occurs, a good approximation is that the calcium activity and the activity coefficient of the carbonate ion remain constant. Therefore, the saturation state at each segment could be closely approximated by

$$\Omega^* = \frac{a_{Ca^{2+}} a_{CO_3^{2-}}}{K_{eq}^*} \approx \frac{a_{CO_3^{2-}}}{a_{CO_3^{2-}}^*} \qquad (5\text{–}4)$$

where K_{eq}^* and $a_{CO_3^{2-}}^*$ are the apparent equilibrium IAP and carbonate ion activities as defined in Chapter III. The rate of dissolution (mol m^{-2} hr^{-1}) can then be calculated at each segment as a function of degree of disequilibrium from the general rate equation $R = k(1-\Omega^*)^1$, where the rate constant (k) is calculated as a function of solution composition, temperature and pCO_2 based on the MR model presented in Chapter IV.

In order to calculate the moles of calcite dissolved at each segment (*dm*), the relationship between surface area (*A*) per unit volume of solvent (V) must be specified. Since concentration is given in molal, it is necessary to apply the conversion α (m^3 kg^{-1}

H_2O). In the case of the 50 g L^{-1} TDS brine, $\alpha = 9.8 \times 10^{-4}$ and the resulting equation that describes the rate in terms of concentration change in solution is:

$$\frac{dm}{dt} = \alpha\left(\frac{A}{V}\right)R. \qquad (5\text{–}5)$$

Surface area (A) of a cylinder is defined as

$$A = 2\pi r \times L \qquad (5\text{–}6)$$

where r is the cylinder diameter and L is the length. Cylinder volume (V) is given by

$$V = \pi r^2 \times L \qquad (5\text{–}7)$$

and surface area to volume ratio (A/V) of the ideal pore is simply $2/r$. The value of dm can now be derived from the flow rate (F; m hr^{-1}) and the length of the segment (dx),

$$dm = dx \times \frac{dm}{dt} \times \frac{1}{F} \qquad (5\text{–}8)$$

where the length of dx (m) is dependent on the solution conditions. It is selected such that the solution would achieve equilibrium within 10^3 segments. In this first example we will consider a pore diameter of 200 μm (i.e., r = 100 μm) and a flow rate of 1 m a^{-1}. This necessitates that the length of $dx = 1.8 \times 10^{-9}$ m. The resulting change in saturation state with distance is presented in Figure 5–1. The calculation was replicated for 125 and 200 g L^{-1} TDS brines with similar initial conditions (i.e., $\Omega^*_{(in)} = 0.3$, 25 ºC, $pCO_{2(in)}$ = 1.0 bar) and are compared in Figure 5–1.

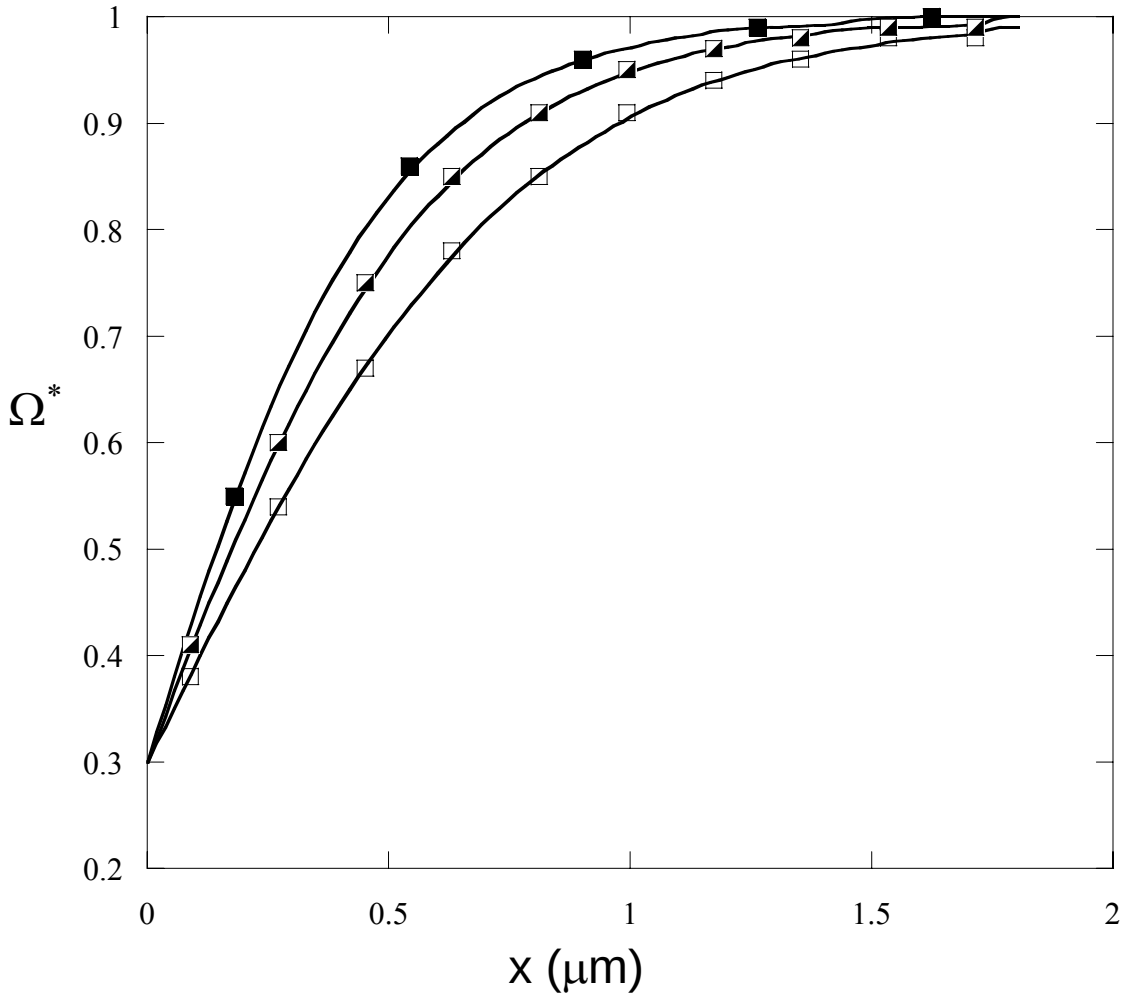

Figure 5–1. The change in apparent saturation state as a function of distance as a brine travels along an ideal solution channel composed of pure calcite with a radius of 100 μm. The initial conditions are $\Omega = 0.3$, 25 ºC, $pCO_2 = 1$ bar and a flow rate of 1 m a^{-1}. The example considers a 50 (open square), 125 (half full square) and 200 (full square) g L^{-1} Na-Ca-Mg-Cl brine.

The reaction front has been described in terms of second derivative, $\frac{d^2\Omega}{dx^2}$, and illustrated in Figure 5–2. Here the reaction front length (RFL) has been mathematically defined as the length at which the concavity maximum occurs in the change in saturation state (dΩ) as a function of travel distance (dx). The relative "sharpness" of the reaction front (RFM) is given by the magnitude of the $\frac{d^2\Omega}{dx^2}$ at its maximum. The saturation length is the length at which the solution achieves $\Omega > 0.999$ and effectively denotes equilibrium. Table 5–1 provides a summary of the parameters resulting from a series of initial conditions.

Table 5–1. Calculation results for a series of initial conditions that describe the reactive front and saturation length of a Na-Ca-Mg-Cl brine traveling though an ideal solution channel. The table summarizes the effects of concentration (TDS), pore radius (r), flow rate (F) and initial pCO_2. The saturation length is the length at which the solution achieves $\Omega > 0.999$. The reaction front length (RFL) and reaction front maximum (RFM) describe the relative "sharpness" of the reaction front.

Case	TDS ($g\ L^{-1}$)	r (μm)	F	$pCO_{2(in)}$	Saturation Length (mm)	RFL (mm)	RFM
1	50	100	1 m a^{-1}	1.0	$2.8x10^{-3}$	$0.46\ x10^{-3}$	$1.0x10^{12}$
1	125	100	1 m a^{-1}	1.0	$1.9x10^{-3}$	$0.30\ x10^{-3}$	$2.2\ x10^{12}$
1	200	100	1 m a^{-1}	1.0	$1.5x10^{-3}$	$0.23\ x10^{-3}$	$3.8\ x10^{12}$
2	50	50	1 m a^{-1}	1.0	$1.4x10^{-3}$	$0.23\ x10^{-3}$	$4.1x10^{12}$
2	125	50	1 m a^{-1}	1.0	$1.0x10^{-3}$	$0.15\ x10^{-3}$	$9.9\ x10^{12}$
2	200	50	1 m a^{-1}	1.0	$0.7x10^{-3}$	$0.11\ x10^{-3}$	$15.1\ x10^{12}$
3	50	50	3 m d^{-1}	1.0	36.2	6.0	$6.0x10^{3}$
3	125	50	3 m d^{-1}	1.0	25.2	3.9	$13.0x10^{3}$
3	200	50	3 m d^{-1}	1.0	19.5	3.0	$21.8\ x10^{3}$
4	50	50	3 m d^{-1}	0.25	31.0	6.3	$7.1x10^{3}$
4	125	50	3 m d^{-1}	0.25	33.2	5.7	$7.0x10^{3}$
4	200	50	3 m d^{-1}	0.25	32.3	5.1	$7.6x10^{3}$

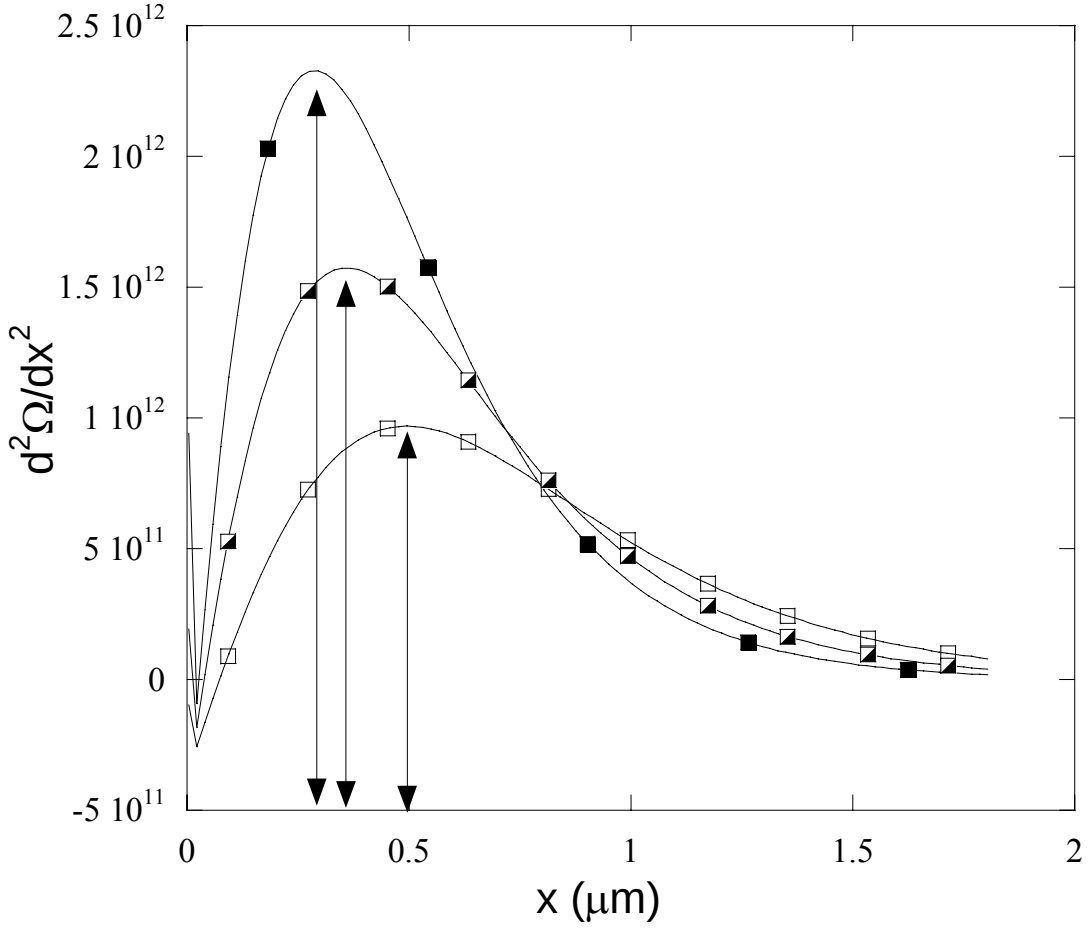

Figure 5–2. The saturation length. The saturation length is defined here as equivalent to the length at which maximum concavity occurs in Figure 5–1 and is calculated as the maximum in the second derivative $\frac{d^2\Omega}{dx^2}$ shown by the arrows.

5.3. Conclusion

These calculations reveal that, as a consequence of the high calcium concentrations, small carbonate carrying capacities result that manifest in very short saturation lengths. Even at high flow rates (3 m d^{-1}, cases 3 and 4) that might be expected in the vicinity of an injection well, the solutions achieve equilibrium in less than 40 mm. The reaction front is sharpest in the more concentrated brines but this is only true at higher pCO_2 where the compositional effect on the dissolution rate is more pronounced. At lower pCO_2, the reaction fronts are virtually the same amongst the brines (case 4).

These findings offer important insights into the relative importance of calcite dissolution kinetics with regard to carbonate transport in the subsurface. In these calcium-rich brines, thermodynamic rather than kinetic considerations may prove more critical in accurately modeling the transport processes since the rates are sufficiently rapid and the carbonate carrying capacities so small. It can be expected that at the higher temperature, pressure, and pCO_2 conditions of subsurface brines, reaction fronts would be even shaper and the saturation lengths even less. Thus, equilibrium can be reasonably assumed, but we lack models capable of accurately predicting it in these complex solutions.

CHAPTER VI

RESEARCH SUMMARY AND GENERAL CONCLUSIONS

Although the EQPITZER model reasonably (±10%) predicted equilibrium with respect to calcite at brine concentrations < 50 g L^{-1} TDS, with increasing brine concentration a systematic increase in the calculated saturation state was observed, achieving an apparent 2-fold supersaturation in the most calcium-rich brine (~ 1 m). There are several possible explanations for the discrepancy but the exact cause is unknown. It is possible the apparent increase in the equilibrium IAP is "real" and may represent an apparent increase in mineral solubility as a result of complex interaction between the mineral surface and these extremely concentrated solutions. Perhaps the simplest explanation, however, is that this apparent increase in IAP is an artifact of the Pitzer-based model used to derive the activity coefficient for the carbonate ion which is present in exceedingly small quantities in these calcium-rich solutions. A minor adjustment of the $CaCO_3^0$ stoichiometric association constant ($K^*_{CaCO_3^0}$) or activity coefficient ($\gamma_{CaCO_3^0}$) could correct for the error.

Surface reaction-controlled calcite dissolution rates in a series of synthetic Na-Ca-Mg-Cl brines across a range of CO_2 partial pressures (0.1 to 1.0 bar) and temperatures (25 to 82.5 °C) could be adequately modeled using the general equation ($R = k(1-\Omega)^n$) in which first-order kinetics are assumed (n = 1). The rate constant, k, was shown to be a function of temperature, pCO_2, ionic strength, and calcium and magnesium activity. It can be estimated from the multiple regression (MR) model:

$$k = \beta_0 + \beta_1(T) + \beta_2(pCO_2) + \beta_3(I) + \beta_4(a_{Ca^{2+}}) + \beta_5(a_{Mg^{2+}}).$$

Surprisingly, ionic strength showed a stronger effect on the rate of dissolution than did calcium or magnesium concentration. Magnesium showed only a minor inhibitory effect while calcium actually promoted the rate. The effect of ionic strength may be related to reduced water activity with increasing brine concentration. A reduced water activity would hinder the hydration of lattice-bond calcium ions thereby inhibiting the rate of dissolution. The MR model was fit to experimental dissolution rate data measured in brines typical for formation waters as predicted by Hanor (1994b) (50–200 g L^{-1} TDS) with regard to their calcium, magnesium and ionic strength. The model was also capable of predicting rates obtained in much more calcium-rich brines typical of the Gulf Coast basin formation waters. Care must be taken, however, in extrapolating the model to other solutions. Although the model was capable of predicting dissolution rates in brines containing close to 1 m calcium, caution is advised when applying the model to solutions beyond the domain of: $0.04 < Ca < 0.36$ m; $0.02 < Mg < 0.12$ m; $0.9 < I < 4.0$ m; $25 < T < 80.0$ °C; and $0.1 < pCO_2 < 1.0$ bars. Accurate prediction outside this domain demands the correlation between the rate constant and the factor remain linear, which is probably an unreasonable assumption in most cases.

When SO_4^{2-} was present, at concentrations typical for some subsurface formation waters, there was a strong inhibitory effect similar to that observed previously in seawater. Sulfate's effect was also very sensitive to calcium and magnesium concentration. Due to this relation, even though sulfate's presence in subsurface formation waters is generally less than that in seawater, at TDS concentrations greater

than 200 g L^{-1} (~0.01 m) its effect on the rate may be of similar magnitude to that measured in seawater.

A relatively high activation energy of 20.9 kJ mol^{-1} was calculated and no dependence on stirring rate was observed, consistent with surface reaction-controlled dissolution where transport processes are not rate limiting. When rates were normalized to the geometric surface area, no substrate effect was observed and predicted rates obtained using powdered calcite were in excellent agreement with rates obtained from crushed rhombs.

The findings of this research demonstrate that the reaction fronts in calcium-rich brines can be expected to be very sharp as a consequence of the small carbonate carrying capacities. Even at high flow rates (3 m d^{-1}) that might be expected in the vicinity of an injection well, the solutions achieve equilibrium in less than 40 mm. The reaction front is sharpest in the more concentrated brines, but this is only true at higher pCO_2 where the compositional effect on the dissolution rate is more pronounced.

These finding offer important insights into the relative importance of calcite dissolution kinetics with regard to carbonate transport in the subsurface. In these calcium-rich brines, thermodynamic rather than kinetic considerations may prove more critical in accurately modeling the transport processes since the rates are sufficiently rapid and the carbonate carrying capacities so small. Thus, equilibrium models of calcite reaction in the subsurface may be sufficient when such models are capable of accurate predictions in these complex solutions.

An important carbon mitigation strategy under consideration is CO_2 injection into geologic repositories. Possible formations that may serve as these repositories

include deep saline aquifers, depleted oil and gas reservoirs, and coal seems. Saline aquifers are the most abundant making them the most logical long-term storage reservoirs. However, before large scale implementation of these technologies can occur, key questions must be resolved with regards to the carbon mass exchange though interactions between the injected gas, formation minerals and the aquifer brines. Geochemical models must be devised describing the ultimate fate of the injected carbon and its impact on formation integrity. Modeling such processes requires the inclusion of rate kinetic terms such as those described in this study.

Simulations describing the change in mineral saturation in the vicinity of injection wells (e.g., Shiraki and Dunn, 2000) make use of general rate equations similar to the one modeled here and assume first-order kinetics (i.e. n =1) for mathematical simplicity. Considering the uncertainties with the other assumptions involved in these simple models, the assumption of first-order kinetics is probably reasonable in light of the findings of this study. In calcium-enriched solutions where the carbonate carrying capacity is greatly diminished, first-order kinetics do appear to be able to adequately describe the solution kinetics of calcite at least in the surface-controlled region.

REFERENCES

Akin G. W. and Lagerwerff J. V. (1965) Calcium carbonate equilibria in solutions open to the air. II. Enhanced solubility of $CaCO_3$ in the presence of Mg^{2+} and SO_4^{2-}. *Geochimica et Cosmochimica Acta* **29**(4), 353-360.

Alkattan M., Oelkers E. H., Dandurand J.-L., and Schott J. (1998) An experimental study of calcite and limestone dissolution rates as a function of pH from -1 to 3 and temperature from 25 to 80 °C. *Chemical Geology* **151**, 199-214.

Alkattan M., Oelkers E. H., Dandurand J.-L., and Schott J. (2002) An experimental study of calcite dissolution rates at acidic conditions and 25 °C in the presence of $NaPO_3$ and $MgCl_2$. *Chemical Geology* **190**(1-4), 291-302.

Arakaki T. and Mucci A. (1995) A continuous and mechanistic representation of calcite reaction-controlled kinetics in dilute solutions at 25 °C and 1 atm total pressure. *Aquatic Geochemistry* **1**(1), 105-30.

Arvidson R.S. and Mackenzie F.T. (1999) The dolomite problem: The control of precipitation kinetics by temperature and saturation state. *American Journal of Science* **299**, 257-288.

Berner R. A. (1967) Comparative dissolution characteristics of carbonate minerals in the presence and absence of aqueous magnesium ion. *American Journal of Science* **265,** 45-70.

Berner R.A. and Morse J.W. (1974) Dissolution kinetics of calcium carbonate in seawater: IV. Theory of calcite dissolution. *American Journal of Science* **274**, 108–134.

Bischoff J. L. (1968) Kinetics of calcite nucleation: Magnesium ion inhibition and ionic strength catalysis. *Journal of Geophysical Research* **73**(10), 3315-3322.

Brantley S. L. and Mellott N.P. (2000) Surface area and porosity of primary silicate minerals. *American Mineralogist* **85**(12), 1767-1783.

Brantley S. L. (2004) Reaction kinetics of primary rock-forming minerals under ambient conditions. In *Treatise on Geochemistry*. (eds. H. D. T. Holland and K. Karl) (pp. 73-117). Elsevier Ltd., Oxford, UK.

Brunauer S., Emmett P. H., and Teller E. (1938) Absorption of gases and multimolecular layers. *Journal of the American Chemical Society* **60**, 309-319.

Buhmann D. and Dreybrodt W. (1985a) The kinetics of calcite dissolution and precipitation in geologically relevant situations of karst areas : 1. Open system. *Chemical Geology* **48**(1-4), 189-211.

Buhmann D. and Dreybrodt W. (1985b) The kinetics of calcite dissolution and precipitation in geologically relevant situations of karst areas: 2. Closed system. *Chemical Geology* **53**(1-2), 109-124.

Buhmann D. and Dreybrodt W. (1987) Calcite dissolution kinetics in the system H2O-CO_2-$CaCO_3$ with participation of foreign ions. *Chemical Geology* **64**(1-2), 89-102.

Burton E. A. (1993) Controls on marine carbonate cement mineralogy: Review and reassessment. *Chemical Geology* **105**(1-3), 163-179.

Busenberg E. and Plummer L. N. (1986) A comparative study of the dissolution and crystal growth kinetics of calcite and aragonite. In *Studies in Diagenesis.,* (ed. F. A. Mumpton), *US Geol Survey Bull.* **1578**, 139-168

Case L. C. (1945) Exceptional Silurian brine near Bay City, Michigan. *Am. Assoc. Petrol. Geol. Bull.* **29**, 567-570.

Chatterjee S. and Price B. (1991) *Regression Analysis by Example*. Wiley, New York, 359 p.

Compton R. G. and Brown C. A. (1994) The inhibition of calcite dissolution/precipitation: Mg^{2+} cations. *Journal of Colloid and Interface Science* **165**, 445-449.

Coudrain-Ribstein A., Gouze P., and Marsily G. d. (1998) Temperature-carbon dioxide partial pressure trends in confined aquifers. *Chemical Geology* **145**, 73-79.

Dreybrodt W. (1981) Mixing corrosion in $CaCO_3$-CO_2-H_2O systems and its role in the karstification of limestone areas. *Chemical Geology* **32**, 221-236.

Freund R. J., and Littell R. C. (1986) *SAS System for Regression*. SAS Institute Inc., Cary, NC, 210 p.

Gunter W. D., Bachu S., Law D. H.-S., Marwaha V., Drysdale D. L., Macdonald D. E., and McCann T. J. (1996) Technical and economic feasibility of CO2 disposal in aquifers within the Alberta sedimentary basin, Canada. *Energy Conversion and Management* **37**(6-8), 1135-1142.

Gutjahr A., Dabringhaus H., and Lacmann R. (1996a) Studies of the growth and dissolution kinetics of the $CaCO_3$ polymorphs calcite and aragonite I. Growth and dissolution rates in water. *Journal of Crystal Growth* **158**(3), 296-309.

Gutjahr A., Dabringhaus H., and Lacmann R. (1996b) Studies of the growth and dissolution kinetics of the $CaCO_3$ polymorphs calcite and aragonite II. The influence of divalent cation additives on the growth and dissolution rates. *Journal of Crystal Growth* **158**(3), 310-315.

Hales B. and Emerson S. (1997) Evidence in support of first-order dissolution kinetics of calcite in seawater. *Earth and Planetary Science Letters* **148**(1-2), 317-327.

Hanor J. S. (1994a) Origin of saline fluids in sedimentary basins. In *Geofluids: Origin, Migration, and Evolution of Fluids in Sedimentary Basins.* (ed. J. Parnell), *Geol. Soc. Spec. Pub.* **78**, 151-174.

Hanor J. S. (1994b) Physical and chemical controls on the composition of waters in sedimentary basins. *Marine & Petroleum Geology* **11**(1), 31-45.

Hansson I. (1973) A new set of acidity constants for carbonic acid and boric acid in sea water. *Deep-Sea Research* **20**, 461-478.

He S. (1992). The carbonic acid system and solubility of calcium carbonate and sulfate in aqueous solutions over a wide range of solution compositions, temperature and pressure. Ph. D. dissertation, Texas A&M Univ.

He S. and Morse J. W. (1993) The carbonic acid system and calcite solubility in aqueous Na-K-Ca-Mg-Cl-SO4 solutions from 0 to 90 °C. *Geochimica et Cosmochimica Acta* **57**, 3533-3554.

Hendriks C. A. and Blok K. (1993) Underground storage of carbon dioxide. *Energy Conversion & Management* **34**(9-11), 949-957.

Hochella M. F. and Brown G.E. (1988) Aspects of silicate surface and bulk structure analysis using X-ray photoelectron sprectroscopy (XPS). *Geochimica et Cosmochimica Acta* **52**, 1641-1648.

Hodson M. E. (1998) Micropore surface area variation with grain size in unweathered alkali feldspars: Implications for surface roughness and dissolution studies. *Geochimica et Cosmochimica Acta* **62**, 3429-3435.

Hohl H., Sigg L., and Stumm W. (1980) Characterization of surface chemical properties of oxides in natural waters. In *Particulates in Water: Characterization, Fate, Effects, and Removal*. (eds. M. C. Kavanaugh and J. O. Leckie) (pp. 1-31). American Chemical Society, Washington, DC.

Jeschke A. A. and Dreybrodt W. (2002) Pitfalls in the determination of empirical dissolution rate equations of minerals from experimental data and a way out: An iterative procedure to find valid rate equations, applied to Ca-carbonates and -sulphates. *Chemical Geology* **192**(3-4), 183-194.

Kanel D. and Morse J. W. (1979) A simple technique for surface area determination. *J. Phys., Earth Sci. Instrum.* **12**, 272-237.

Kharaka Y. K. and Hanor J. S. (2004) Deep fluids in the continents: I. Sedimentary basins. In *Treatise on Geochemistry*. (eds. H. D. T. Holland and K. Karl) (pp. 499-540). Elsevier Ltd., Oxford, UK.

Knauss K. G., Wolery T. J., and Jackson K. J. (1990) A new approach to measuring pH in brines and other concentrated electrolytes. *Geochimica et Cosmochimica Acta* **54**, 1519-1523.

Koide H. G., Tazaki Y., Iijima M., Ito K., and Shindo Y. (1992) Subterranean containment and long-term storage of carbon dioxide in unused aquifers and in depleted natural gas reservoirs. *Energy Conversion & Management* **33**(5-8), 619-626.

Koide H. G., Tazaki Y., Noguchi Y., Iijima M., Ito K., and Shindo Y. (1993) Carbon dioxide injection into useless aquifers and recovery of natural gas dissolved in fossil water. *Energy Conversion & Management* **34**(9-11), 921-924.

Lasaga A. C. (1998) *Kinetic Theory in the Earth Sciences*. Princeton Universtity Press, Princeton, NJ, 811 p.

Lea A. S., Amonette J. E., Baer D. R., Liang Y., and Colton N. G. (2001) Microscopic effects of carbonate, manganese, and strontium ions on calcite dissolution. *Geochimica et Cosmochimica Acta* **65**(3), 369-379.

Lewis G. N. and Randall M. (1921) Activity coefficients of strong electrolytes. *J. Am. Chem. Soc.* **43**(1112).

Lippmann, F. (1973) *Sedimentary carbonate minerals*. Springer-Verlag, New York.

Millero F. J. and Schreiber D. R. (1982) Use of the ion pairing model to estimate activity coefficients of the ionic components of natural waters. *American Journal of Science* **282**(9), 1508-40.

Millero F. J., Milne P. J., and Thurmond V. L. (1984) The solubility of calcite, strontianite and witherite in NaCl solutions at 25 °C. *Geochimica et Cosmochimica Acta* **48**(5), 1141-1143.

Moldovanyi E. P. and Walter L. M. (1992) Regional trends in water chemistry, Smackover Formation, southwest Arkansas: geochemical and physical controls. *AAPG Bulletin* **76**(6), 864-894.

Morse, J. W. and Berner R. A. (1972) Dissolution kinetics of calcium carbonate in sea water. II. Kinetic origin for the lysocline. *American Journal of Science* **272**(9), 840-51.

Morse, J. W. (1973). The dissolution kinetics of calcite: A kinetic origin for the lysocline. Ph. D. dissertation, Yale Univ.

Morse J. W. (1974) Dissolution kinetics of calcium carbonate in sea water. V. Effects of natural inhibitors and the position of the chemical lysocline. *American Journal of Science* **274**(6), 638-47.

Morse J. W. (1983) The kinetics of calcium carbonate dissolution and precipitation. In *Carbonates: Mineralogy and Chemistry* (ed. R. J. Reeder) (pp. 227-264).Mineralogical Society of America, Washington, DC.

Morse J. W. and Mackenzie F. T. (1990) *Geochemistry of Sedimentary Carbonates*. Elsevier, Amsterdam, 707 p.

Morse J. W. and Mackenzie F. T. (1993) Geochemical constraints on $CaCO_3$ transport in subsurface sedimentary environments. *Chemical Geology* **105**, 181-196.

Morse J. W., Hanor J. S., and He S. (1997) The role of mixing and migration of basinal waters in carbonate mineral mass transport. In *Basin-Wide Diagenetic Patterns* (eds. I. P. Montanez, J. M. Gregg, and K. L. Shelton) (pp. 41-50). Society for Sedimentary Geology, Tulsa, Okla.

Morse J. W. and Arvidson R. S. (2002) The dissolution kinetics of major sedimentary carbonate minerals. *Earth-Science Reviews* **58**, 51-84.

Mucci A. and Morse J. W. (1984) The solubility of calcite in seawater solutions of various magnesium concentration, It = 0.697 m at 25 °C and one atmosphere total pressure. *Geochimica et Cosmochimica Acta* **48**(4), 815-822.

Mucci A., Canuel R., and Zhong S. (1989) The solubility of calcite and aragonite in sulfate-free seawater and the seeded growth kinetics and composition of the precipitates at 25 °C. *Chemical Geology* **74**(3-4), 309-320.

Murphy J. and Riley J. P. (1962) A modified single solution method for the determination of phosphate in natural waters. *Analytica Chimica Acta* **27**, 31-36.

Murray J. and Renard A. F. (1891) Report on deep-sea deposits based on the specimens collected during the voyage of H.M.S. Challenger in the years 1872 to 1876. 525 pp, Edinburg.

Nielsen A. E. and Toft J. M. (1984) Electrolyte crystal growth kinetics. *Journal of Crystal Growth* **67**(2), 278-88.

Philippi T. E. (1993) Multiple regression: Herbivory. In *Design and Analysis of Ecological Experiments* (eds. S. M. Scheiner and J. Gurevitch) (pp. 183-210). Oxford University Press, Oxford, NY.

Plummer L. N., Wigley T. M. L., and Parkhurst D. L. (1978) The kinetics of calcite dissolution in CO_2-water systems at 5 to 60 °C and 0.0 to 1.0 atm CO_2. *American Journal of Science* **278**, 179-216.

Plummer L. N., Parkhurst D. L., and Wigley T. M. L. (1979) Critical review of the kinetics of calcite dissolution and precipitation. *American Chemical Society*, 537-573.

Plummer L. N. and Busenberg E. (1982) The solubilities of calcite, aragonite, and vaterite in carbon dioxide-water solutions between 0 and 90 °C, and an evaluation of the aqueous model for the system calcium carbonate-carbon dioxide-water. *Geochimica et Cosmochimica Acta* **46**(6), 1011-40.

Pokrovsky O. S., Schott J., and Thomas F. (1999) Dolomite surface speciation and reactivity in aquatic systems. *Geochimica et Cosmochimica Acta* **63**(19-20), 3133-3143.

Pokrovsky O. S. and Schott J. (1999) Processes at the magnesium-bearing carbonates/solution interface. II. Kinetics and mechanism of magnesite dissolution. *Geochimica et Cosmochimica Acta* **63**(6), 881-897.

Pokrovsky O. S. and Schott J. (2002) Surface chemistry and dissolution kinetics of divalent metal carbonates. *Environmental Science & Technology* **36**, 426-432.

Pytkowicz R. M. and Hawley J. E. (1974) Bicarbonate and carbonate ion-pairs and a model of seawater at 25 °C. *Limnology and Oceanography* **19**(2), 223-234.

Salem M. R. (1994) Dissolution of calcite crystals in the presence of some metal ions. *Journal of Materials Science* **29**(24), 6463-6467.

Sass E., Morse J. W., and Millero F. J. (1983) Dependence of the calcite and aragonite thermodynamic solubility products on ionic models. *American Journal of Science* **283**, 218-229.

Schmalz R. F. (1967) Kinetics and diagenesis of carbonate sediments. *Journal of Sedimentary Petrology* **37**, 60-67.

Shiraki R. and Dunn T. L. (2000) Experimental study on water-rock interactions during CO2 flooding in the Tensleep Formation, Wyoming, USA. *Applied Geochemistry* **15**(3), 265-279

Sjöberg E. L. (1978) Kinetics and mechanism of calcite dissolutions in aqueous solutions at low temperature. *Stockholm Contr. Geology*. **32**, 1-96

Sjöberg E. L. and Rickard D. T. (1985) The effect of added dissolved calcium on calcite dissolution kinetics in aqueous solutions at 25 °C. *Chemical Geology* **49**(4), 405-413.

Terjesen S. G., Erga O., Thorsen G., and Ve A. (1961) II. Phase boundary processes as rate determining steps in the reaction between solids and liquids. The inhibitory action of metal ions on the formation calcium bicarbonate by the reaction of calcite with aqueous carbon dioxide. *Chemical Engineering Science* **74**, 277-288.

Van Cappellen P., Charlet L., Stumm W., and Wersin P. (1993) A surface complexation model of the carbonate mineral-aqueous solution interface. *Geochimica et Cosmochimica Acta* **57**(15), 3505-3518.

Weyl P. K. (1958) The solution kinetics of calcite. *J. Geol.* **66**, 163-176.

Weyl P. K. (1967) Solution behavior of carbonate materials in sea water. *Studies in tropical oceanography* **5**, 178-228.

White A. F., Blum A. E., Schulz M. S., Bullen T. D., Harden J. W., and Peterson M. L. (1996) Chemical weathering rates of a soil chronosequence on granitic alluvium: I. Quantification of mineralogical and surface area changes and calculation of primary silicate reaction rates. *Geochimica et Cosmochimica Acta* **60**(14), 2533-2550.

Wolf M., Breitkopf O., and Puk R. (1989) Solubility of calcite in different electrolytes at temperatures between 10 and 60 °C and at CO_2 partial pressures of about 1 kPa. *Chemical Geology* **76**(3-4), 291-301.

Zhang Y. and Dawe R. (1998) The kinetics of calcite precipitation from a high salinity water. *Applied Geochemistry* **13**, 177-184.

APPENDIX I

EQPITZER MODEL RESULTS FOR CALCITE SOLUBILITY EXPERIMENTS

In this appendix are presented the raw EQPITZER model results for the calcite solubility experiments.

Table I - 1. EQPITZER model output for calcite solubility experiments. All experiments were conducted at 25 °C and 1 bar. The term "I" and "O" refer to ionic strength and osmotic coefficient respectively. The model assumes unity γ_T for the ion pairs $CaCO_3^0$ and $MgCO_3^0$.

Experiment	Na	Mg	Ca	Cl	PCO2	H		MgOH		HCO3		CO3		OH		CO2		MgCO3	CaCO3	I	O	H2O	pH	Ω
#	γ_T	γ_T	γ_T	γ_T	molal	molal	γ_T	molal	γ_T	molal	γ_T	molal	γ_T	molal	γ_T	molal	γ_T	molal	molal	molal		Activity		
KSP_Brine1_1	0.635	0.224	0.208	0.689	0.52	1.28E-06	0.805	7.88E-09	0.964	0.0137	0.558	9.84E-06	0.036	2.52E-08	0.382	0.0148	1.19	1.39E-06	4.47E-06	0.9377	0.931	0.9722	5.988	0.96
KSP_Brine1_2	0.635	0.224	0.208	0.689	0.57	1.22E-06	0.804	8.38E-09	0.963	0.0158	0.558	1.19E-05	0.036	2.65E-08	0.380	0.0162	1.19	1.70E-06	5.39E-06	0.9383	0.931	0.9722	6.008	1.15
KSP_Brine1_3	0.634	0.223	0.208	0.690	0.61	1.28E-06	0.804	8.56E-09	0.961	0.0161	0.558	1.15E-05	0.035	2.58E-08	0.372	0.0173	1.19	1.77E-06	5.11E-06	0.9384	0.931	0.9722	5.987	1.09
KSP_Brine1_4	0.635	0.223	0.208	0.689	0.57	1.19E-06	0.802	8.83E-09	0.962	0.0163	0.559	1.24E-05	0.036	2.74E-08	0.378	0.0164	1.19	1.85E-06	5.57E-06	0.9243	0.930	0.9727	6.019	1.19
KSP_Brine2_1	0.634	0.302	0.243	0.755	0.51	1.45E-06	1.145	2.50E-08	0.778	0.0090	0.491	1.28E-05	0.010	3.80E-08	0.149	0.0110	1.57	2.17E-06	6.82E-06	2.4854	1.020	0.9242	5.779	1.46
KSP_Brine2_2	0.635	0.302	0.243	0.754	0.49	1.40E-06	1.145	2.52E-08	0.780	0.0089	0.492	1.31E-05	0.010	3.87E-08	0.151	0.0106	1.57	2.17E-06	7.00E-06	2.4820	1.020	0.9242	5.795	1.50
KSP_Brine2_3	0.634	0.301	0.242	0.755	0.45	1.32E-06	1.144	2.68E-08	0.779	0.0088	0.492	1.37E-05	0.010	4.12E-08	0.152	0.0098	1.57	2.28E-06	7.38E-06	2.4811	1.020	0.9243	5.822	1.58
KSP_Brine2_4	0.634	0.301	0.242	0.754	0.52	1.46E-06	1.142	2.34E-08	0.781	0.0091	0.492	1.26E-05	0.010	3.63E-08	0.155	0.0112	1.57	2.05E-06	6.79E-06	2.4716	1.019	0.9246	5.777	1.45
KSP_Brine2_1	0.688	0.520	0.353	0.919	0.53	1.61E-06	1.711	6.00E-08	0.546	0.0056	0.471	1.30E-05	0.003	6.95E-08	0.046	0.0088	2.04	2.30E-06	8.15E-06	4.1137	1.148	0.8691	5.561	1.74
KSP_Brine2_2	0.689	0.521	0.354	0.917	0.53	1.59E-06	1.711	6.11E-08	0.546	0.0056	0.471	1.33E-05	0.003	7.07E-08	0.046	0.0089	2.04	2.38E-06	8.30E-06	4.1093	1.148	0.8692	5.566	1.77
KSP_Brine2_3	0.690	0.527	0.357	0.918	0.54	1.60E-06	1.723	6.07E-08	0.545	0.0056	0.471	1.33E-05	0.003	7.01E-08	0.046	0.0089	2.04	2.35E-06	8.28E-06	4.1280	1.149	0.8684	5.560	1.77
KSP_Brine2_4	0.688	0.520	0.353	0.916	0.54	1.68E-06	1.708	5.70E-08	0.547	0.0055	0.471	1.23E-05	0.004	6.61E-08	0.047	0.0091	2.03	2.16E-06	7.67E-06	4.1014	1.147	0.8694	5.544	1.64
MgFree_1	0.710	0.460	0.362	0.725	0.97	7.01E-07	1.596	0.00E+00	0.780	0.0247	0.455	1.75E-05	0.027	1.50E-08	0.539	0.0165	1.86	0.00E+00	5.54E-06	3.0908	1.049	0.8909	5.951	1.18
MgFree_2	0.681	0.408	0.313	0.755	0.97	1.77E-06	1.448	0.00E+00	0.742	0.0107	0.476	9.24E-06	0.010	7.76E-09	0.459	0.0178	1.79	0.00E+00	6.37E-06	3.0456	1.052	0.8988	5.591	1.36
MgFree_3	0.531	0.194	0.131	0.991	0.97	3.92E-06	0.846	0.00E+00	0.520	0.0071	0.589	1.58E-05	0.004	1.57E-08	0.184	0.0214	1.49	0.00E+00	9.94E-06	2.9712	1.045	0.9414	5.479	2.13
MgFree_4	0.710	0.460	0.362	0.725	0.92	6.73E-07	1.596	0.00E+00	0.779	0.0255	0.455	1.90E-05	0.027	1.57E-08	0.539	0.0163	1.86	0.00E+00	6.07E-06	3.0921	1.049	0.8908	5.969	1.30
MgFree_5	0.681	0.408	0.313	0.755	0.92	1.87E-06	1.448	0.00E+00	0.742	0.0104	0.476	8.46E-06	0.010	7.35E-09	0.459	0.0181	1.79	0.00E+00	5.83E-06	3.0451	1.052	0.8988	5.568	1.25

APPENDIX II

MATLAB CALCITE DISSOLUTION RATE CALCULATION SOFTWARE

This appendix contains the MATLAB program written to derive the calcite dissolution rates from the experimental data and to empirically fit the rates as a first order function of the degree of disequilibrium. The output plots are also provided for each if the kinetic experiments.

```
% CALCITE DISSOLUION RATE PROGRAM
% version 18
% Dwight K Gledhill
% 9 October 2004
%   This program calculates dissolution rate from the derivative of a polynomial fit to TA-time data.  It corrects for changes in the
%             specific surface area and for changes in calcite mass as function of reaction extent.
%    Makes the simplifying assumption that calcium activity and the carbonate ion activity coefficient remain constant and that the
rate %       can be modeled with first order kinetics R=k(1-Omega).
%                imported variables:
%                  t   = experimental time data
%                  mv  = experimental millivolt data
%                  A   = experimental and extrapolated alkalinity (molal)
%                  pHp = EQPITZER pH
%                  CO  = EQPITZER calculated carbonate ion activity
%                  r = accepted surface roughness
%               input variables:
%                  pHs = EQPITZER pH of initial solution
%                  Es  = millivolt of initial solution
%                  S   = slope of electrode
%                  Calcite_initial = initial mass of calcite (g)
%                  Solvt = mass of solvent (kg)
%                  BET = specific area of calcite as determined using BET
%                  Alk_initial = initial alkalinity of solution (molal)
%                  cull = minimum acceptable dTA/dt (truncation threshold)%
%               declared variables:
%                  int =time interval between readings
%                  nr,nc = number of rows and columns in 'geometry'
%                  q = quarry to select different truncation threshold
%                  truc = truncation points defined from 'cull'
%_____________________________________________________________________________________________________
% Initializes the program
clear
close
q=1
[mv t] = textread('electrode.txt','%f %f',...;
   'headerlines',1);
[A pHp CO] = textread('EQPitzer.txt','%f %f %f',...;
   'headerlines',1);
load geometry.txt;
r=geometry(2,1);
%Obtain experimental inputs
pHs=input('pH of standard: ');
Es=input('Emf of standard: ');
S=input('Slope of electrode: ');
Calcite_initial=input('Calcite added(g): ');
Solvt=input('kg_solvt: ');
BET=input('BET specific surface area (m^2 g^-1):  ');
Alk_initial=input('Initial Alkalinity (molal): ');
%_____________________________________________________________________________________________________
_
%Relate pH to other species from EQPitzer calculations
X_pHp=[ones(size(pHp)) pHp pHp.^2];        %generates a nx3 matrix of  Pitzer pH data
X_A=[ones(size(A)) A A.^2];               %generates a nx3 matrix of batch Alk values
a=X_pHp\A;                              %solves for 2rd order polynomial coefficients for Alk f(pHp)
b=X_pHp\CO;                              %solves for 2rd order polynomial coefficients for CO f(pHp)
%Calibrate mv to pH
pH=pHs+((Es-mv)/S);                     %Converts fit mV data to pH
%Evaluates parameters from EQPitzer
TA=[ones(size(pH)) pH pH.^2]*a;           %evaluates alkalinity f(EQPitzer pH) model
CO_fit=[ones(size(pH)) pH pH.^2]*b;       %evaluates Carbonate activity f(EQPitzer pH) model
%_____________________________________________________________________________________________________
_
%Empirically fit TA-time data
c = polyfit(t,TA,6);
TA_fit = c(7) + (c(6)*t) + (c(5)*t.^2) + (c(4)*t.^3) + (c(3)*t.^4) + (c(2)*t.^5) + (c(1)*t.^6);
%_____________________________________________________________________________________________________
_%Calcite Loss
Alk = [TA_fit];
for i =Alk'
   Calcite(:,1)=(Calcite_initial)-(0.5*(Alk(:,1)-Alk_initial)*Solvt*100.09);
```

```
end
figure,plot(t,Calcite),axis([0 1 min(Calcite) max(Calcite)]),xlabel('hr'),ylabel('Calcite (g)'),saveas(1,'calcite.fig'), pause
%_____________________________________________________________________________________________________________
_
% Calculate surface area
Area_initial=(Calcite_initial*BET)/Solvt;
Area_corrected=(Calcite.*BET)/Solvt;
%_____________________________________________________________________________________________________________
_
%Obtain Dissolution Rate
RTA= c(6) + (c(5)*2*t) + (c(4)*3*t.^2) + (c(3)*4*t.^3) + (c(2)*5*t.^4) + (c(1)*6*t.^5); %dTA/dt
while q==1
   cull=input('input minimum acceptable dTA/dt: ');
   trunc = max(find(RTA>=cull))                                    % determines the truncation index for the dTA/dt data

   RC=(0.5*(RTA(1:trunc)))/Area_initial;                           %dCaCO3/dt uncorrected for calcite loss
   RCC=(0.5*(RTA(1:trunc)))./Area_corrected(1:trunc);              %dCaCO3/dt corrected for calcite loss
   RCCC=RCC;
   Rate = [RC(1:trunc) RCC(1:trunc) RCCC(1:trunc)]
%_____________________________________________________________________________________________________________
_   % Specific Surface Area Correction
   int = diff(t)  %time interval
   D = size(Rate);
   for j=1:3 %reiterates calculation 3 times
      row = 2; %initializes 'row'
      %calculate volume (m^3) of grain fraction
      volume(1,:) =((geometry(1,:)/6).^(3/2)) -Rate(1,3)*int(1,1)*(geometry(1,:))*0.00003693; %volume-(rate)(delta
time)(Area)(Vm)
      for i = Rate'
         volume(row,:) =real(volume(row-1,:) -Rate(row,3)*int(row,1)*6*(volume(row-1,:)).^(2/3)*0.00003693);
         row = row+1;
         if row > D(1,1), break, end
      end
      %Calculate Mass fraction
      d=2.71E6; %density of calcite (g/m^3)
      mass = real(d*volume(:,:));
      %calculate Area (m^2) of grain fraction
      area = real(6*volume(:,:).^(2/3));
      %normalizes individual Areas by total mass at each interval and multiplies by frequency
      total=sum(mass')';
      [nr,nc]=size(geometry)
      for i=1:nc
         norm(:,i) = real(area(:,i)./total);
      end
      %Calculates corrected Specific Surface Area (m^2/g)
      m=r*sum(norm')';
      SArea_corrected =(Calcite(1:trunc).*m(1:trunc))/Solvt;
      Rate(:,3)=(0.5*(RTA(1:trunc)))./SArea_corrected(1:trunc);
         j
   end
   RCCC = Rate(:,3);
%_____________________________________________________________________________________________________________
_
% Calculate Apparent saturations state
   LR = polyfit(RCCC,CO_fit(1:trunc),1);  %determines the intercept equivalent to apparent carbonate ion activity at steady-state
   Omega = CO_fit/(LR(2))            % LR(2) is the intercept
   disEQ=1-Omega(1:trunc)      % degree of apparent disequilibrium
   k=sum(RCCC.*disEQ)/sum(disEQ.^2)  %calculates the rate constant (k) for the first order rate equation Rate = k(1-Omega)
%_____________________________________________________________________________________________________________
_   % Plots
   close all
   plot(t(1:trunc),m(1:trunc));pause
   close all
   subplot(3,3,1),plot(t,mv),xlabel('time (hr)'),ylabel('mv'),pause
   subplot(3,3,2),plot(t,pH),xlabel('time (hr)'),ylabel('pH'),pause
   subplot(3,3,3),plot(pH,TA,'-',pHp,A,'x'),xlabel('pH'),ylabel('Alkalinity (molal)'),pause
   subplot(3,3,4),plot(pH,CO_fit,'-',pHp,CO,'.'),xlabel('pH'),ylabel('carbonate activity'),pause
   subplot(3,3,5),plot(t,TA_fit,'-',t,TA,'.'),xlabel('time (hr)'),ylabel('Alkalinity (molal)'),pause
   subplot(3,3,6),plot(t,RTA),xlabel('time (hr)'),ylabel('dTA/dt'),pause
```

```
   subplot(3,3,7),plot(t(1:trunc),RC(1:trunc),'x',t(1:trunc),RCC(1:trunc),'+',t(1:trunc),RCCC(1:trunc),'o'),xlabel('time
(hr)'),ylabel('moles m^-2 h^-1'),pause
   subplot(3,3,8),plot(RCCC(1:trunc),CO_fit(1:trunc)),xlabel('moles m^-2 h^-1'),ylabel('carbonate activity'),pause
   subplot(3,3,9),plot(Omega(1:trunc),RCCC(1:trunc)),xlabel('Apparent Omega'),ylabel('moles m^-2 h^-1'),pause
   q=input('rerun [Y=1/N=0]?')
end
%_____________________________________________________________________________________________________________
% Save output data
Rate = [RC(1:trunc) RCC(1:trunc) RCC(1:trunc) Omega(1:trunc)]
Calcite = [t(1:trunc) Calcite(1:trunc) m(1:trunc)]
Constants = [LR(2) k cull]
saveas(1,'plots.jpg')
save Rate.txt Rate -ascii -double       % calcite dissolution rate (uncorrected for changes in surface area, apparent saturation state
save Calcite.txt Calcite -ascii -double       %The effect of dissolution of calcite mass and specific surface area
save Constants.txt Constants -ascii -double  % apparent steady-state carbonate ion activity, rate constant (k)
```

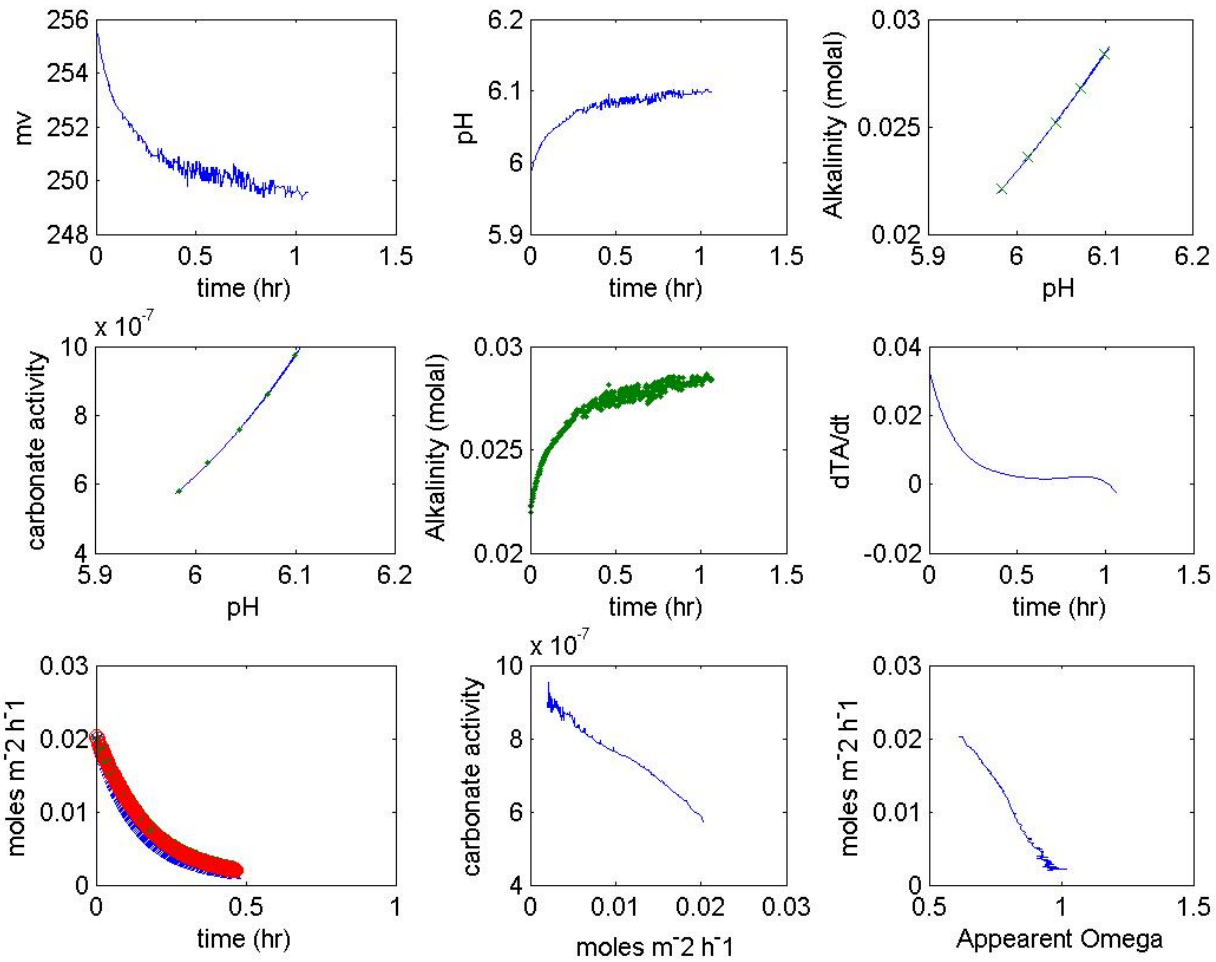

Appendix II–1. Experiment pseudo-seawater.

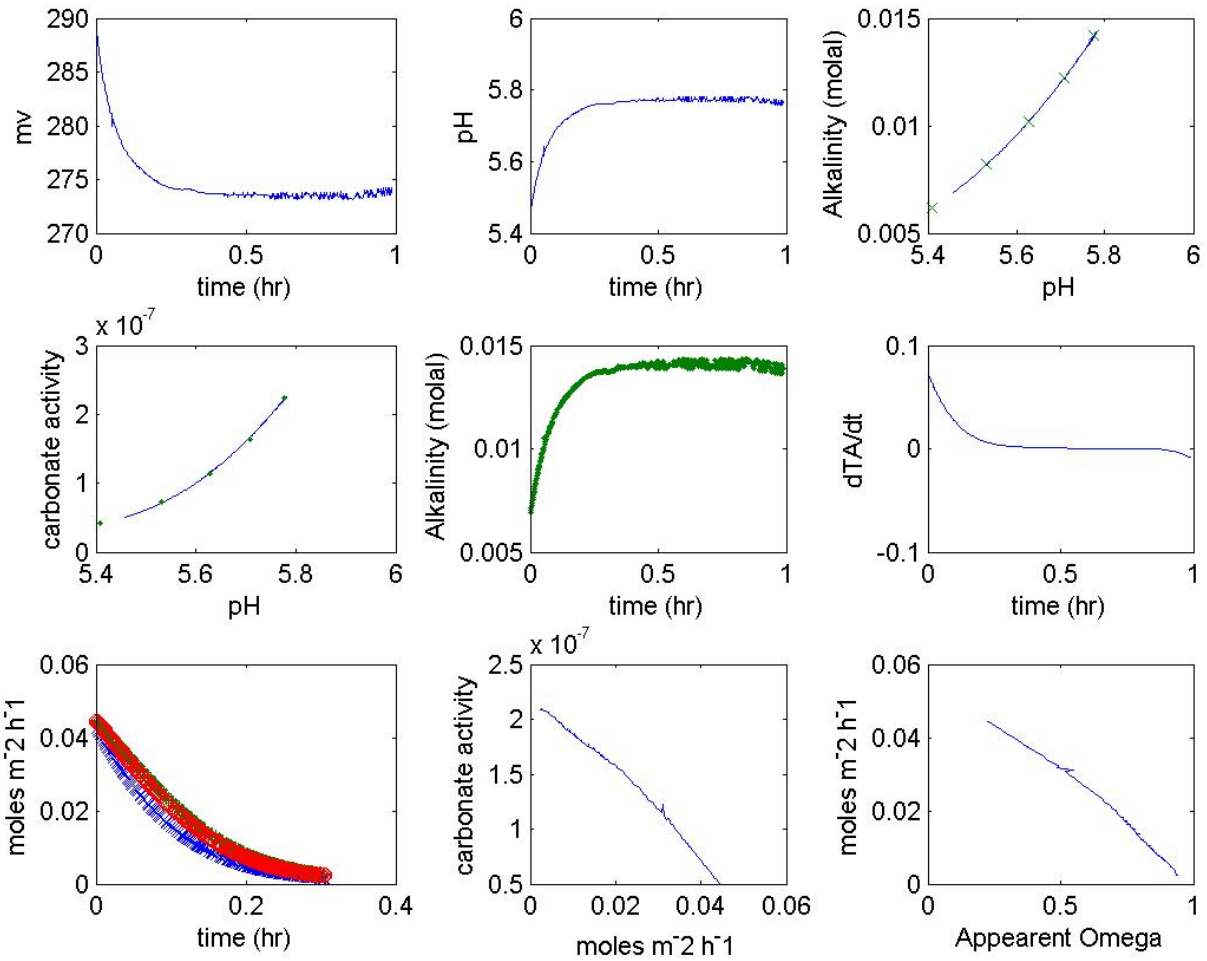

Appendix II–2. Experiment brine 1.

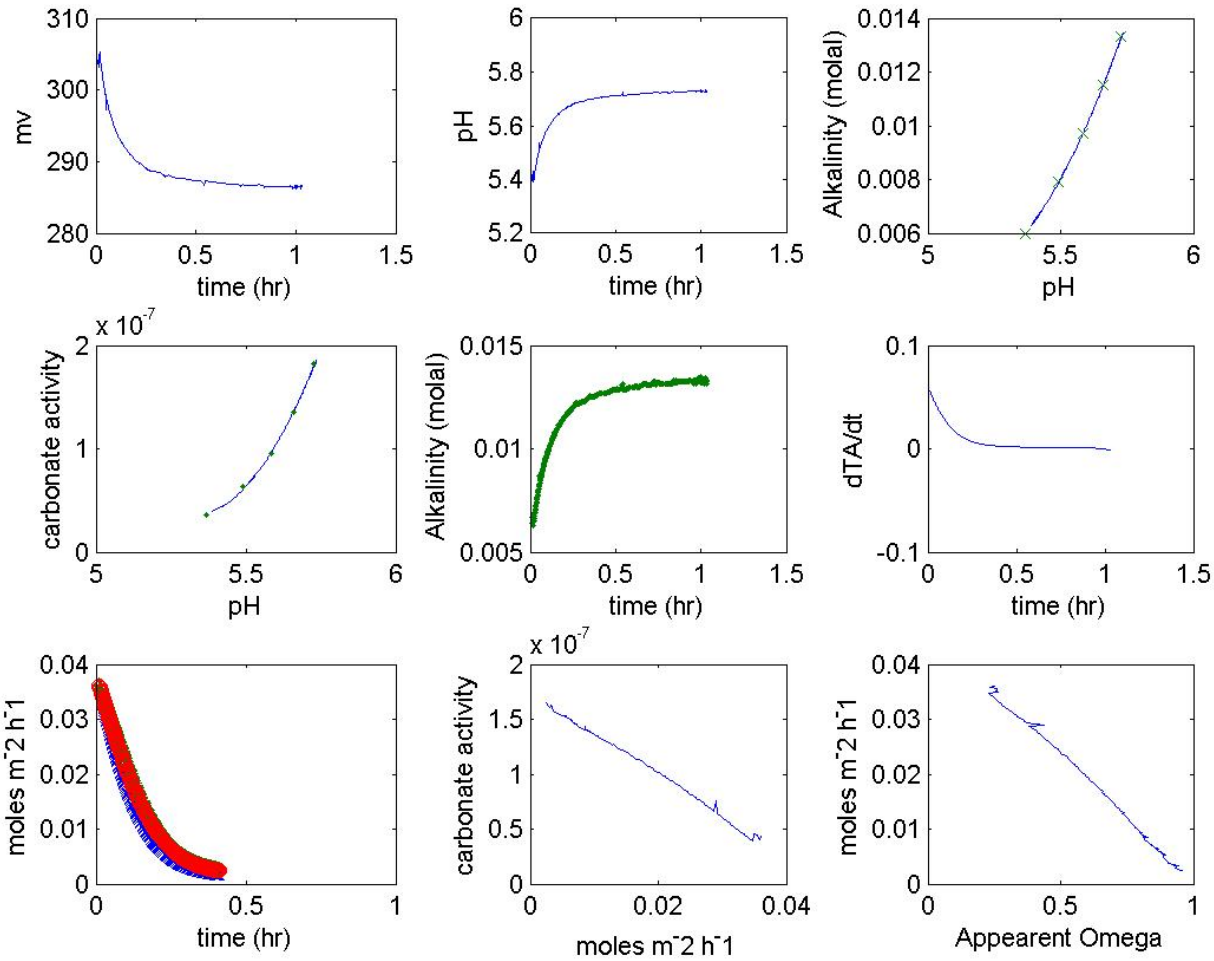

Appendix II–3. Experiment brine 2.

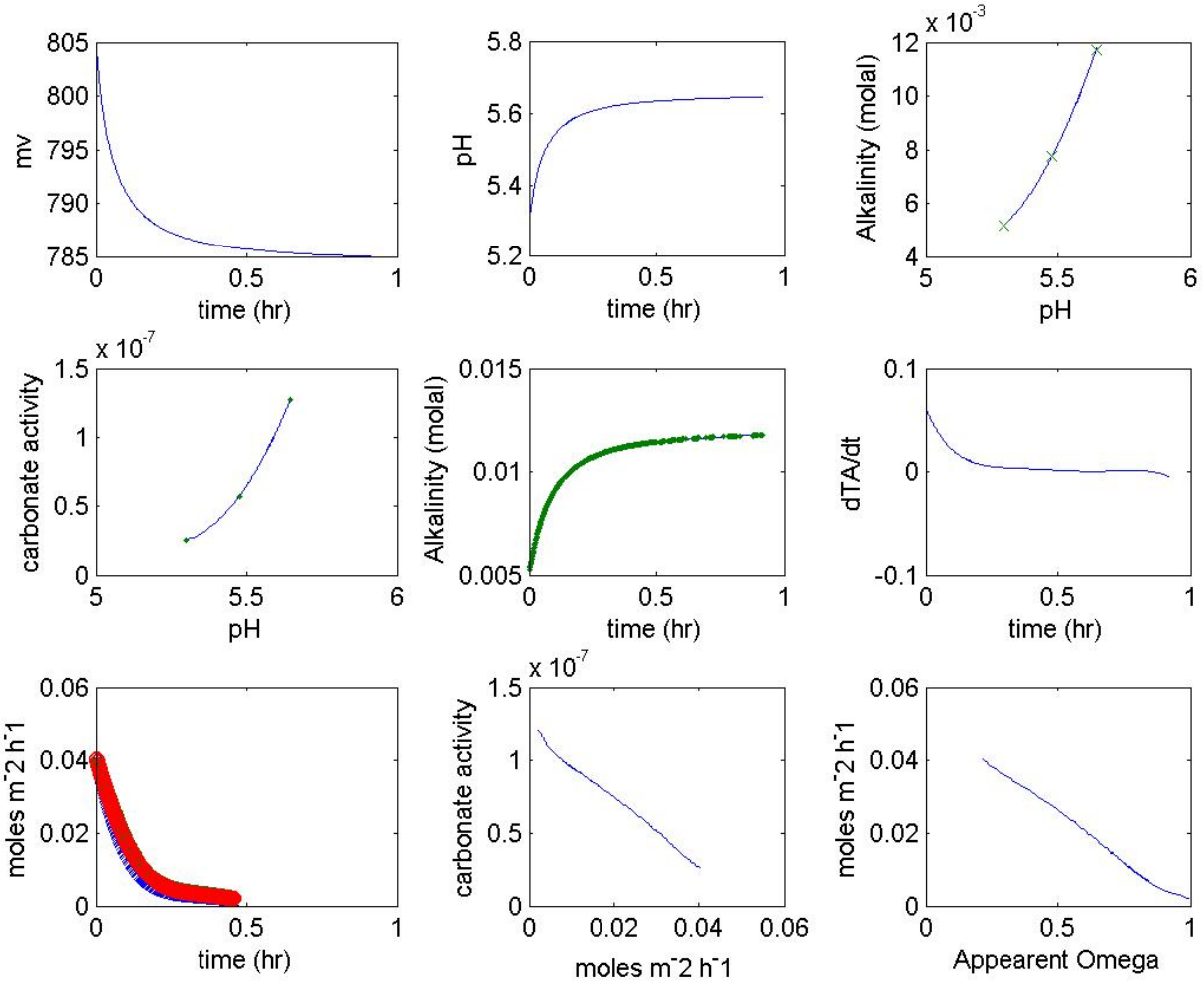

Appendix II–4. Experiment brine 3.

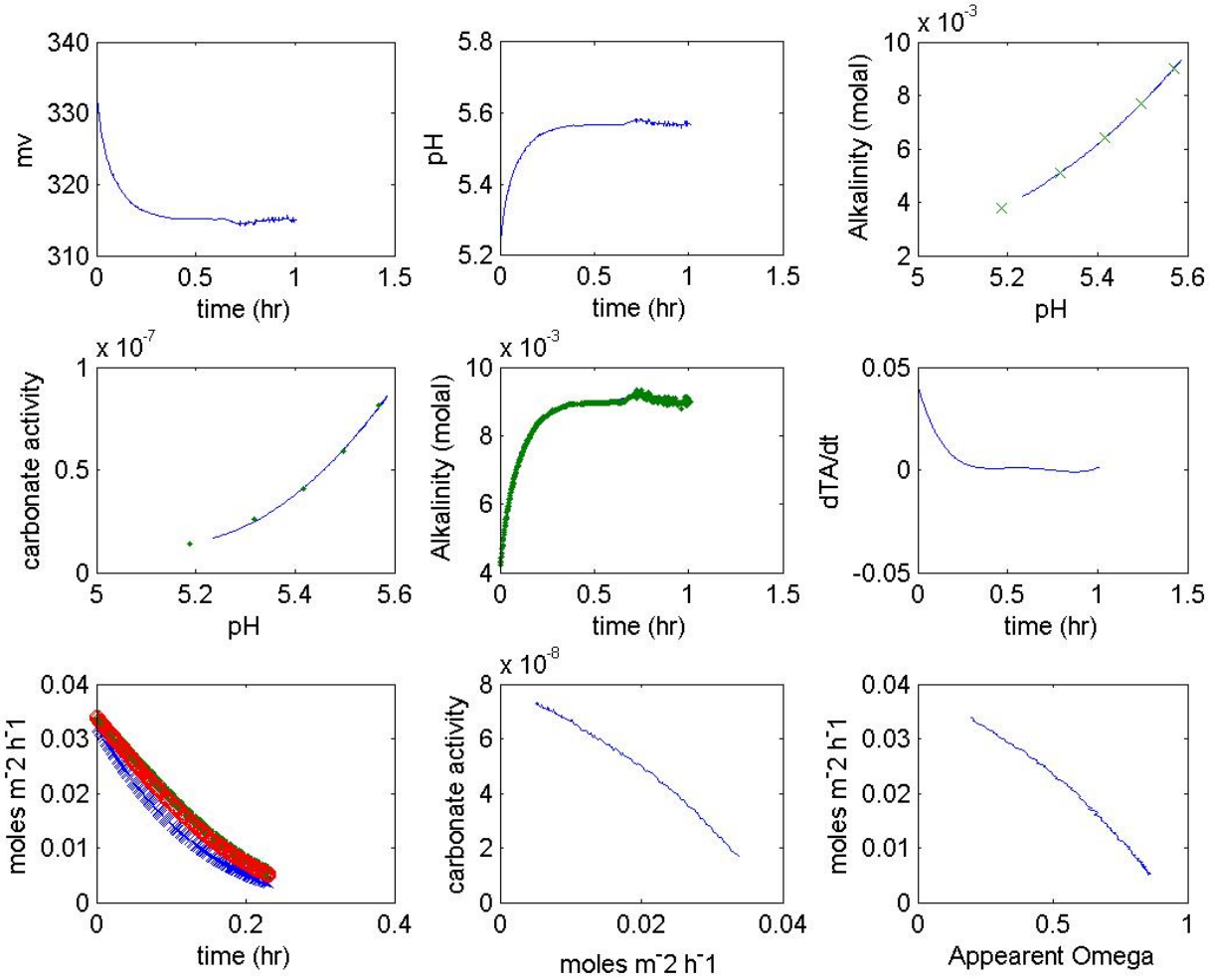

Appendix II–5. Experiment brine 4.

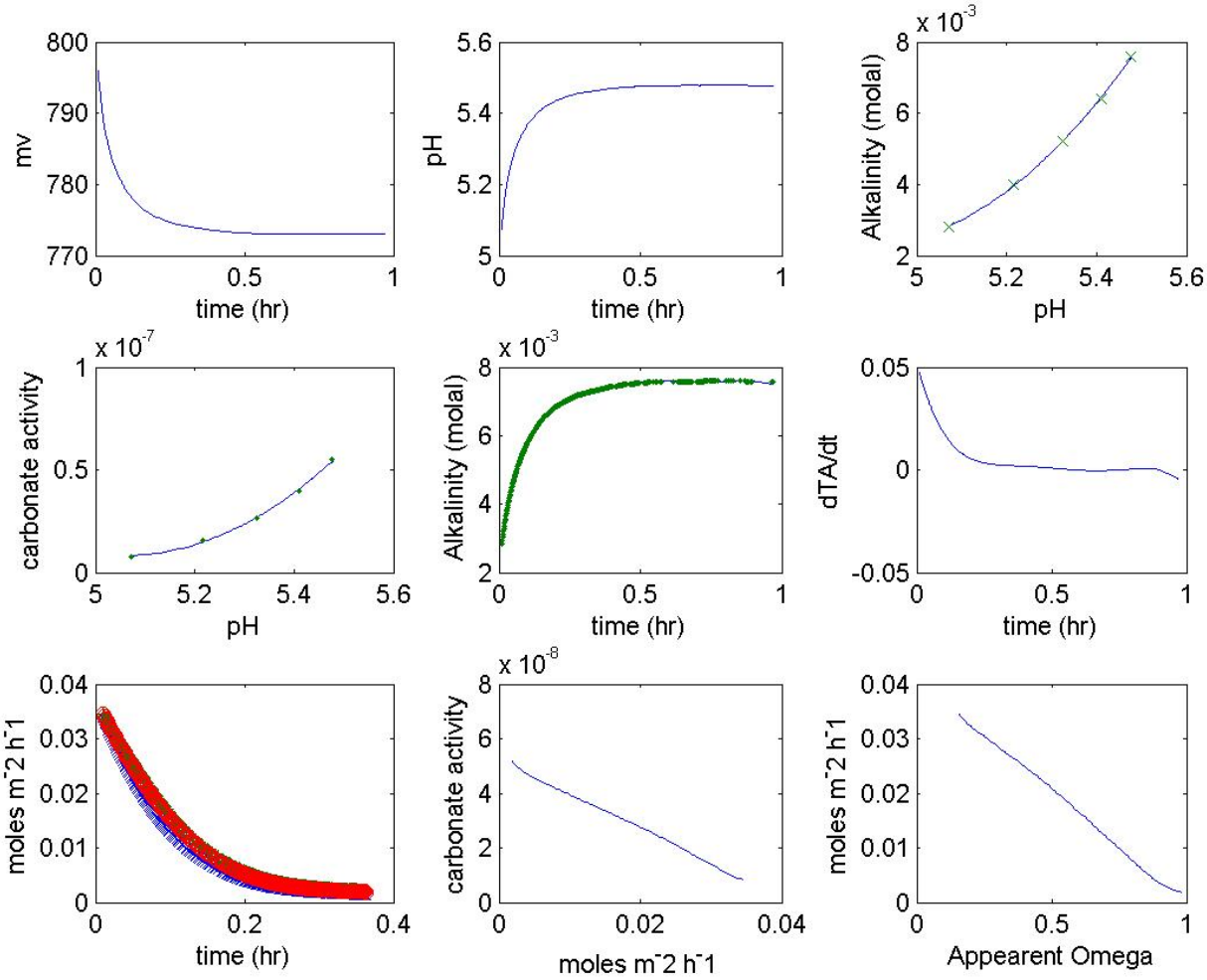

Appendix II–6. Experiment brine 5.

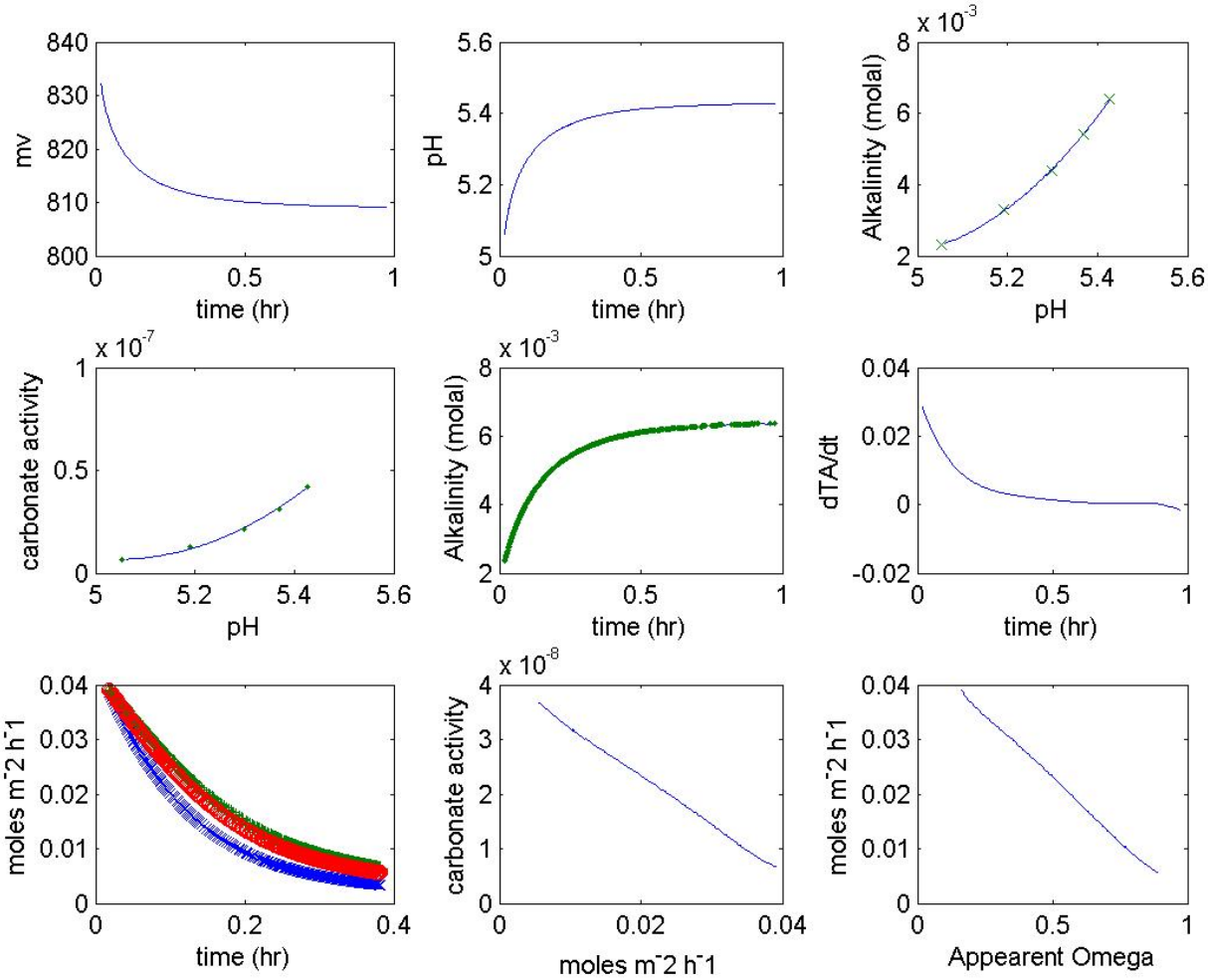

Appendix II–7. Experiment brine 6.

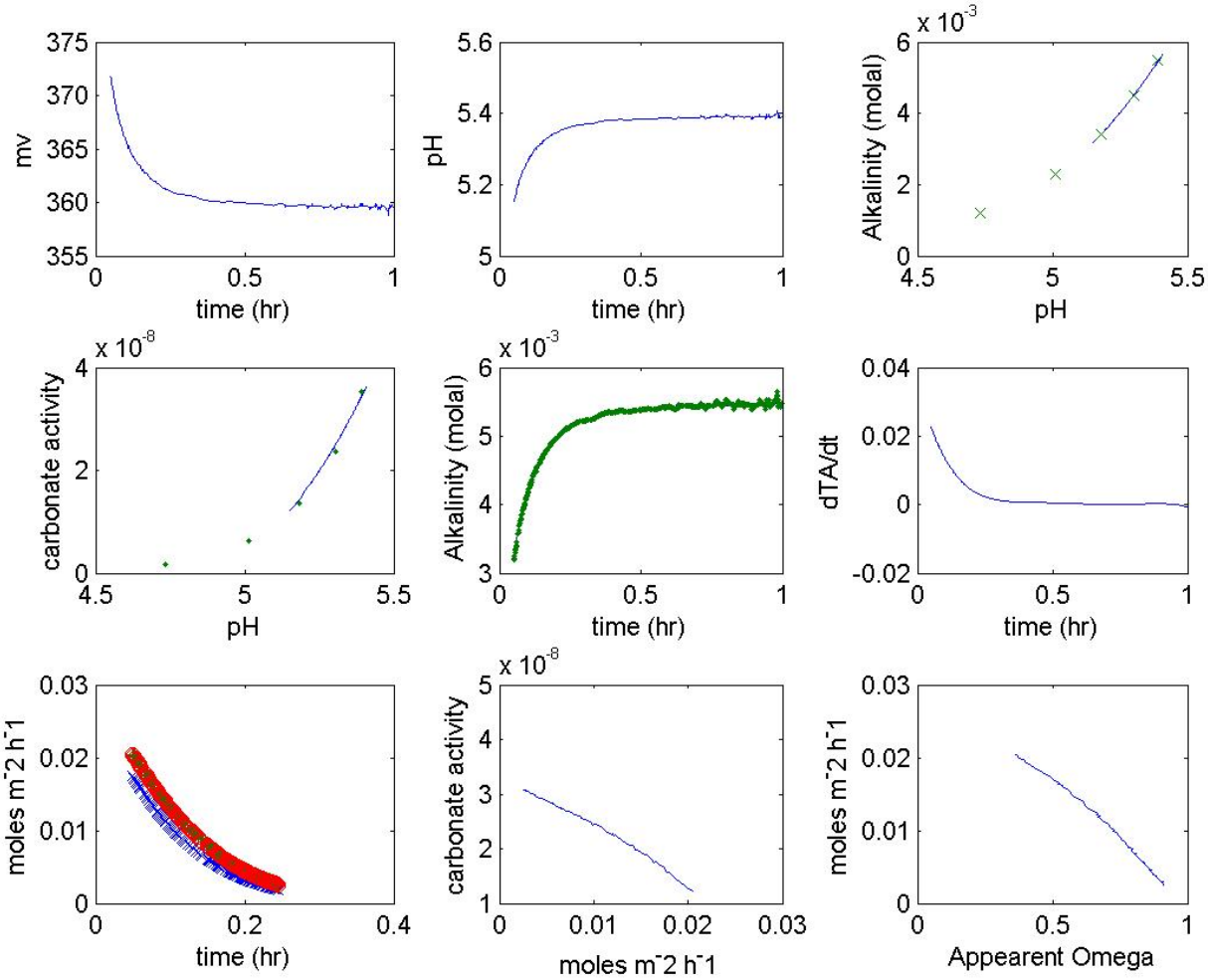

Appendix II–8. Experiment brine 7.

VITA

Dwight Kuehl Gledhill
NOAA/NESDIS E/OC53 SSMC1 5th floor
1315 East-West Highway, Silver Spring, MD 20910
dgledhill@NOAA.gov

Education

Ph.D. Oceanography, Texas A&M University, 2005

M.S. Oceanography, Texas A&M University, 2001

B.S. Environmental Earth Science, Eastern Connecticut State University, 1997.

Scholarly Papers Published or in Press

Gledhill D. K. and Morse J. K. (2004) Dissolution kinetics of calcite in NaCl-$CaCl_2$-$MgCl_2$ brines at 25 °C and 1 bar pCO2. *Aquatic Geochemistry* **10**, 171-190.

Morse J. W., Gledhill D.K. and Millero F.J. (2003) $CaCO_3$ precipitation kinetics in waters from the Great Bahama Bank: Implications for the relationship between bank hydrochemistry and whitings. *Aquatic Geochemistry* **67**, 2819-2826.

Morse J.W., Gledhill D.K., Sell K.S., and Arvidson R.S. (2002) Pyritization of iron in sediments from the continental slope of the northern Gulf of Mexico. *Aquatic Geochemistry* **8**, 3-13.

Morse J.W., Gledhill D.K., Sell K.S., and Arvidson R.S. (in press) Reaction kinetics of iron with sulfide in anoxic marine sediments from unique biologic environments. In *The Biogeochemistry of Iron Cycling in Natural Environments* (ed. C. Zhang and J.D. Coates), Kluwer Academic Press, New York.

Abstracts Presented

Gledhill D.K. and Morse J.W. (2004) Calcite dissolution kinetics and solubility in NaCl-$CaCl_2$-$MgCl_2$ brines up to 1 bar pCO2 and 80 °C. *Eos Trans.* AGU, **85**(47), Fall Meet. Suppl., Abstract V31A-1403.

Gledhill D.K. and Morse J.W. (2003) The kinetics of calcite dissolution in NaCl-$CaCl_2$-$MgCl_2$ brines at 1 bar pCO_2 and 25 °C. *GSA Abstracts with Programs*. The Geological Society of America, **35**(6), Annual Meet.

Morse J.W. and Gledhill D.K. (2003) Apparent Solubility of Bahama Bank Water Precipitate. Ocean Science Conference, New Orleans, LA.